

Oil & Natural Gas Technology

DOE Award No.: DE-FC26-NT0004654

Final Report

Instrumented Pipeline Initiative

Submitted by

Concurrent Technologies Corporation
100 CTC Drive
Johnstown, PA 15904

Principal Authors: Thomas J. Piro, Michael J. Team

Prepared for:
United States Department of Energy
National Energy Technology Laboratory

October 26, 2010



Office of Fossil Energy

Acknowledgment: “This material is based upon work supported by the Department of Energy under Award Number DE- NT-0004654.”

Disclaimer: “This report was prepared as an account of work sponsored by an agency of the United States Government. Neither the United States Government nor any agency thereof, nor any of their employees, makes any warranty, express or implied, or assumes any legal liability or responsibility for the accuracy, completeness, or usefulness of any information, apparatus, product, or process disclosed, or represents that its use would not infringe privately owned rights. Reference herein to any specific commercial product, process, or service by trade name, trademark, manufacturer, or otherwise does not necessarily constitute or imply its endorsement, recommendation, or favoring by the United States Government or any agency thereof. The views and opinions of authors expressed herein do not necessarily state or reflect those of the United States Government or any agency thereof.”

Abstract

This report summarizes technical progress achieved during the cooperative agreement between Concurrent Technologies Corporation (*CTC*) and U.S. Department of Energy to address the need for a low-cost monitoring and inspection sensor system as identified in the Department of Energy (DOE) National Gas Infrastructure Research & Development (R&D) Delivery Reliability Program Roadmap. The Instrumented Pipeline Initiative (IPI) achieved the objective by researching technologies for the monitoring of pipeline delivery integrity, through a ubiquitous network of sensors and controllers to detect and diagnose incipient defects, leaks, and failures. This report is organized by tasks as detailed in the Statement of Project Objectives (SOPO). The sections all state the objective and approach before detailing results of work.

TABLE OF CONTENTS

	Page
1.0 EXECUTIVE SUMMARY	1
2.0 REPORT ORGANIZATION	2
3.0 PROJECT EXECUTION	2
3.1 Task 1 – Project Management and Planning.....	2
3.1.1 Objective	2
3.1.2 Approach	3
3.1.3 Results	3
3.1.4 Summary	3
3.2 Task 2 – Technology Status Assessment (TSA) and Project Summary Updates	3
3.2.1 TSA Objective.....	3
3.2.2 TSA Approach.....	4
3.2.3 TSA Results.....	4
3.2.4 TSA Summary	9
3.2.5 Project Summary	9
3.3 Task 3 – Pipeline Wave Propagation Characteristics	9
3.3.1 Objective	9
3.3.2 Approach	9
3.3.3 Results	10
3.3.4 Summary	15
3.4 Task 4 – Development and Optimization of Active Sensing Devices.....	15
3.4.1 Objective	15
3.4.2 Approach	15
3.4.3 Results	16
3.4.4 Summary	17
3.5 Task 5 – System Engineering	17
3.5.1 Objective	17
3.5.2 Approach	18
3.5.3 Results	18
3.5.4 Summary	19
3.6 Task 6 – Extraction of Reference-Free Features.....	20
3.6.1 Objective	20
3.6.2 Approach	20
3.6.3 Results	20
3.6.4 Summary	25

3.7	Task 7 – Classification and Localization of Defects	25
3.7.1	Objective	25
3.7.2	Approach	26
3.7.3	Results	26
3.7.4	Summary	29
3.8	Task 8 – Proof of Concept Development and Implementation.....	29
3.8.1	Objective	29
3.8.2	Approach	29
3.8.3	Results	30
3.8.4	Summary	31
3.9	Task 9 – Technology Transition	31
3.9.1	Objective	31
3.9.2	Approach	32
3.9.3	Results	32
3.9.4	Summary	35
4.0	REFERENCES.....	35
	APPENDIX A: Peer Reviewed Technical Society Papers.....	1

LIST OF FIGURES

Figure 3-1. United States Natural Gas Transmission Pipelines	5
Figure 3-2. Excavation Damage/Outside Force ^[3]	6
Figure 3-4. Examples of Intelligent Mobile Sensing Devices	7
Figure 3-5. Standalone Inspection Systems and Instruments	7
Figure 3-6. Simulation Model of a Short Pipe	10
Figure 3-7. Time Plot Versus Frequency (Short Pipe)	11
Figure 3-8. Time Versus Frequency Plot (Short Pipe)	11
Figure 3-9. Simulation Model of a Long Pipe	12
Figure 3-10. Time Plot Versus Frequency (Long Pipe).....	12
Figure 3-11. Time Versus Frequency Plot (Long Pipe).....	13
Figure 3-12. Laboratory Test Configuration (Propagation Test).....	13
Figure 3-13. Received Signal (Propagation Test).....	14
Figure 3-14. Pipe Illumination.....	14
Figure 3-15. Attenuation in Air and Soil Embedment.....	15
Figure 3-16. PZT and MFC Compared.....	16
Figure 3-17. Laboratory Transducer Experiment	16
Figure 3-18. Transducer Response Comparison.....	17
Figure 3-19. Conceptual System Diagram.....	18
Figure 3-20. Transmit Signal (TRA Step #1)	21
Figure 3-21. Receive Signal (TRA Step #2).....	21
Figure 3-22. Time Reverse Signal (TRA Step #3)	21
Figure 3-23. Transmit Time Reversed Signal Back to the Transmitter (TRA Step #4)	22
Figure 3-24. Received Focused Signal (TRA Step #5).....	22
Figure 3-25. Difference Signal	23
Figure 3-26. Normalized Time Reversed Difference Signal	23
Figure 3-27. Focused Signal Due to Change Detection.....	23
Figure 3-28. Lateral Defect.....	24
Figure 3-29. Longitudinal Defect	24
Figure 3-30. Corrosion-Like Defect	25
Figure 3-31(a). Direct Subtraction Figure 3-31(b). Time Reversal	26
Figure 3-32. Time Reversal Beamforming Imaging (Echoing / Defect Localization)	27
Figure 3-33. Cognitive Sensor Consensus Algorithm	27
Figure 3-34. Bayes M-ary Detection Procedure with Time Reversal.....	28
Figure 3-35. Defect Model used for Classification Studies.....	28
Figure 3-36. Increasing Probability of Classification	28
Figure 3-37. Laboratory Test Equipment (Photograph)	31

LIST OF TABLES

Table 3-1. Inspection Technologies Benefits and Inadequacies	8
Table 3-2. Trade Study	19
Table 3-3. Power Requirement Assessment	19
Table 3-4. IPI Simulation and Modeling Development System	30
Table 3-5. Laboratory Test Equipment (Configuration).....	31

1.0 EXECUTIVE SUMMARY

The objective of the Instrumented Pipeline Initiative (IPI) was to address sensor system needs for low-cost monitoring and inspection as identified in the Department of Energy (DOE) National Gas Infrastructure Research & Development (R&D) Delivery Reliability Program Roadmap. This initiative achieved the objective by researching technologies for the monitoring of pipeline delivery integrity, through a ubiquitous network of sensors and controllers to detect and diagnose incipient defects, leaks, and failures. This activity supports the National Energy Technology Laboratory (NETL) Strategic Center for Natural Gas and Oil (SCNGO).

Recent fires in San Bruno California, suspected to be caused by a ruptured natural gas transmission line, support maturing the technologies developed during this project. There is a documented need for the ability to identify weaknesses in the Nation's pipeline infrastructure.

Concurrent Technologies Corporation (*CTC*) successfully developed enabling technologies for a network of sensors and performed laboratory testing to quantify the ability to provide integrity monitoring of our nation's natural gas pipeline delivery, which consists of a network of more than 1.4 million miles of aging transmission and distribution pipelines and bulk gas storage reservoirs. *CTC* executed the IPI through a research, development, and testing program to develop prototype sensor/controller networks for the uninterrupted supervision of pipeline systems to detect, identify, and prevent at an early stage, material defects, pipe faults, gas leakages, or major damage. Various types of pipe materials and construction were analyzed during this R&D effort.

The goal of this project was to develop a new sensing and continuous monitoring system. The system may also be used as an inspection method. Nine specific tasks detail the activities were used to execute this project. The tasks included:

- Task 1 – Project Management and Planning
- Task 2 – Technology Status Assessment and Project Summary Updates
- Task 3 – Pipeline Wave Propagation Characteristics
- Task 4 – Development and Optimization of Active Sensing Devices
- Task 5 – System Engineering
- Task 6 – Extraction of Reference-free Features
- Task 7 – Classification and Localization of Defects
- Task 8 – Proof of Concept Development and Implementation
- Task 9 – Technology Transition

CTC performed these activities to assess the available technologies for pipeline integrity monitoring leading to defect detection and location. The initial technology assessment supported the need for this effort to further research new methods that develop a low-cost continuous monitoring system. Promising results surfaced as a result of the project team's investigation of ultrasonic wave propagation as a plausible technology for development and optimization of active sensing and a means to classify and locate defects. A low-cost piezoelectric material was selected as an effective sensor that can easily implemented for this application. An excitation waveform was selected that maximizes the time reversal acoustic technique. This technique was proven effective in detecting various defects including lateral, longitudinal, and simulated corrosion. Laboratory simulations demonstrated that time reversal focusing can improve defect localization.

Electrical power consumption was analyzed for the sensor systems to support economic feasibility and sensor system and power selection. The selected technologies and system components were implemented in a proof of concept demonstrator to validate operation and performance under typical pipeline conditions. A technology transition plan was completed as part of the project final report. The technology transition plan identified future research required to mature and implement the technology based on the outcomes of this project. Future efforts should refine time reversal acoustics as well mature defect classification and localization. There is also potential for further development in area such as intelligent pipe, machine learning and experimentation in pipeline environments.

In addition to above technical tasking, *CTC* facilitated all logistics including contractual, schedule, budget, and management needs for all activities. *CTC* teamed with Carnegie Mellon University (CMU) on this effort.

2.0 REPORT ORGANIZATION

This report is organized by tasks as detailed in the Statement of Project Objectives (SOPO). The sections all state the objective and approach before detailing results of work. The sections focus on the results and minimize long discussions of theory, with each section ended with a summary. The interested reader can refer to many of the attached Appendix A, Peer Reviewed Technical Society Papers for detailed theories and background information.

3.0 PROJECT EXECUTION

The goal of this project was to develop a new pipeline sensing and continuous monitoring system that may also be used as an inspection method. Nine specific tasks detail the activities used to execute this project. Many of the tasks were sequential tasks and relied on the outcome or decision of the prior task to enable research and development of technologies.

3.1 Task 1 – Project Management and Planning

3.1.1 Objective

This task details the *CTC* management of this project to ensure that technical requirements, schedule, and program budget were met. Due to the expected dynamic nature of this effort, the project tasking and schedule were maintained in a program management plan (PMP) and updated as necessary to reflect up to date agreements between *CTC* and the government.

3.1.2 Approach

Project management was composed of:

- Designation of a Project Manager and Technical Lead
- Development and maintenance of a PMP that maintained tasking, schedule, and project organization information
- Deliverable review and approval
- Organization and conducting of technical interchange meetings, subcontractor meetings, project review meetings, and milestone demonstrations as agreed upon with the government
- Coordination of project resources
- Development of Reports.

3.1.3 Results

A subcontractor kickoff meeting was held on August 6, 2008. A kickoff meeting was held at the DOE NETL facility on September 4, 2008. The PMP was developed and submitted and delivered on August 20, 2008. Throughout the project, *CTC* worked together with the DOE Project Officer to modify and update the PMP. Meetings were held on a weekly schedule with combined meetings held about 1-2 times per month between *CTC* and CMU. Quarterly progress reports were submitted to DOE that documented key accomplishments during that period. All quarterly reports were delivered on or before scheduled due date. A midpoint review was held on April 14, 2009 at CMU that included attendance from *CTC*, CMU, and DOE. A 6 month No Cost Time Extension (NCTE) was granted by DOE on January 26, 2010 that extended the project end date to July 31, 2010. Two project summary and demonstration meetings were conducted at the DOE NETL facility in Morgantown, West Virginia on November 13, 2009 and July 14, 2010 respectively.

3.1.4 Summary

All project management and planning objectives were completed and all documents were delivered on or prior to the scheduled due date. Updates to the PMP, schedule and scope were addresses with the Contracting Officer Representative (COR).

3.2 Task 2 – Technology Status Assessment (TSA) and Project Summary Updates

3.2.1 TSA Objective

In order to minimize or prevent duplication of efforts, a TSA was performed at the start of this project. This assessment included both positive and negative aspects of each technology. In addition to the TSA, the project summary document was reviewed and updated as part of this task.

3.2.2 TSA Approach

The team communicated with various natural gas pipeline utilities and industry representatives, in particular those from Pennsylvania, and collected public information from government agencies, research institutions, and industry. The report presents the benefits and shortcomings of existing technology and compares each sensor system to the low-cost, in-situ, time-reversal based, continuous monitoring of distributed pipelines proposed by this project. The report also outlines opportunities for the development of future sensor technologies for pipeline monitoring applications. The purpose of the TSA was to:

- Identify benefits and inadequacies of current technology
- Determine required new technology and research
- Identify barriers the research will overcome
- Define the impact new technology will have on the gas supply industry.

As noted previously, the goal of the IPI Project was to develop a distributed autonomous sensor system capable of continuously and automatically monitoring natural gas pipelines. The TSA illustrated that the IPI distributed sensor concept differs substantially from many existing systems and technologies that primarily focus on pipeline inspection.

3.2.3 TSA Results

3.2.3.1 Summary of Existing Industry/Sector

Natural gas pipelines are critical infrastructures that gather, transport, and distribute natural gas for many of our day-to-day needs and activities. Natural gas pipeline companies monitor, control, and manage the natural gas that enters the pipeline from the producers and processors and delivers this gas to the consumers via the local distribution companies. The United States natural gas pipeline network is a highly integrated transmission and distribution grid. A 2007 report authored by the Energy Information Administration (EIA) of the DOE shows that there are more than 305,000 miles of large diameter (61% exceeding 16" diameter) natural gas transmission pipelines in the United States ^[1] as shown in Figure 3-1.

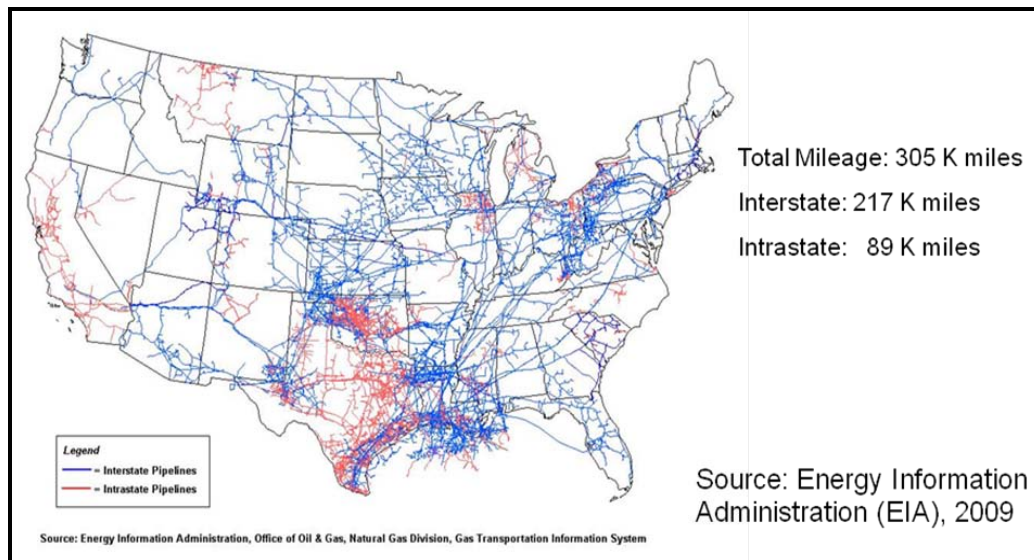


Figure 3-1. United States Natural Gas Transmission Pipelines

There are three major types of pipelines: the gathering pipelines, the transmission pipelines, and the distribution pipelines. The gathering pipelines transport raw natural gas from the wellhead to the processing plant, often operating under significantly lower pressure than the transmission lines and using pipes with diameters of 4 inches to 12 inches. The transmission system consists of interstate and intrastate pipelines with diameters ranging from 6 inches to 48 inches at pressures anywhere from 200 to 1500 pounds per square inch (psi). The distribution pipelines deliver natural gas to retail customers. The diameter of most distribution pipelines are small, ranging in size from 1 to 6 inches in diameter. Most pipes in service are made of bare steel or coated steel. In addition to steel pipes, more than 500,000 miles of buried polyethylene (PE) plastic natural gas pipelines have been installed over the past 40 years in the United States^[2]. The corrosion resistance properties and ease of installation have significantly stimulated demand for PE pipes.

According to the Department of Transportation (DOT) Office of Pipeline Safety, the majority of damage is caused by excavation as seen in Figure 3-2. Not all excavation damage is reported or even noticed at the time of the incident. Often a minor scratch or dent will corrode and the damage will not be evident until much later.

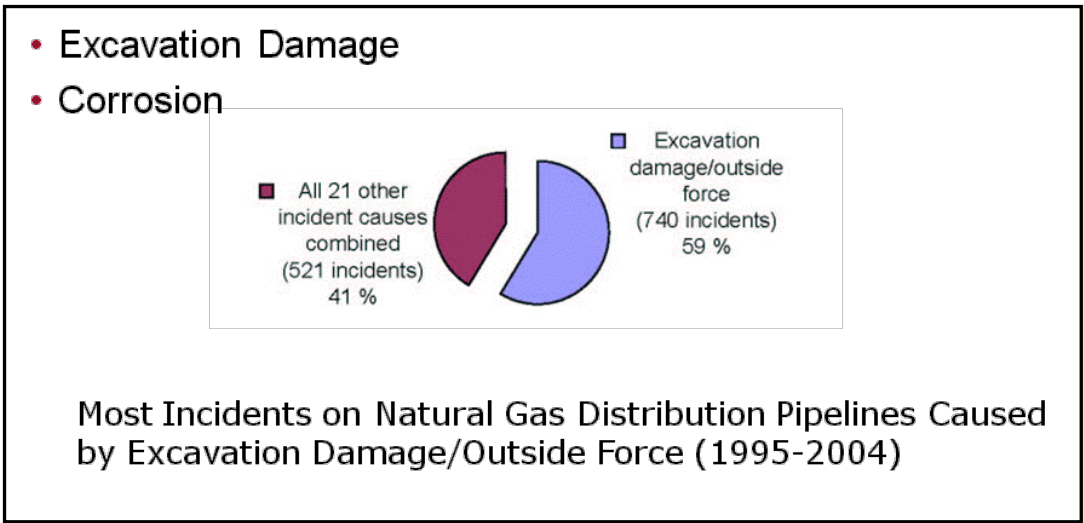


Figure 3-2. Excavation Damage/Outside Force ^[3]

In addition to excavation damage, typical corrosion can take the form of pitting, channel style, general stress, and weld stress as shown in Figure 3-3.



Figure 3-3. Corrosion Examples

3.2.3.2 Typical Inspection Technologies/Tools

Over the years, engineers have developed many pipeline inspection tools and the technologies for inspection of pipeline safety and integrity. There are three types of basic tools or platforms for pipeline inspection: intelligent mobile sensing devices, standalone inspection systems, instruments, and resident pipeline sensors.

3.2.3.2.1 Intelligent Mobile Sensing Devices

Intelligent mobile sensing devices are pigs, crawlers, and the Explorer^[4] type robots. Pigs, also called pipeline inspection gauges, are intelligent robotic devices that are propelled down pipelines to inspect the interior part of pipes. Pigs can inspect the conditions of the pipeline wall and perform pipeline internal cleaning as shown in Figure 3-4. Although pigs are standard inspection tools for large diameter pipelines, they are limited by unpiggable pipelines due to over- or under-sized valves, radius or mitered bends.



Figure 3-4. Examples of Intelligent Mobile Sensing Devices

3.2.3.2.2 Standalone inspection and systems and instruments

Standalone inspection systems and instruments, for example, General Electric's (GE) automated sensor systems utilizing phased array ultrasonic technology are mounted on the outer surface of pipelines and use ultrasonic or electromagnetic waves to detect corrosion and defects at a given point in time and space. Examples of standalone inspection systems are shown in Figure 3-5.

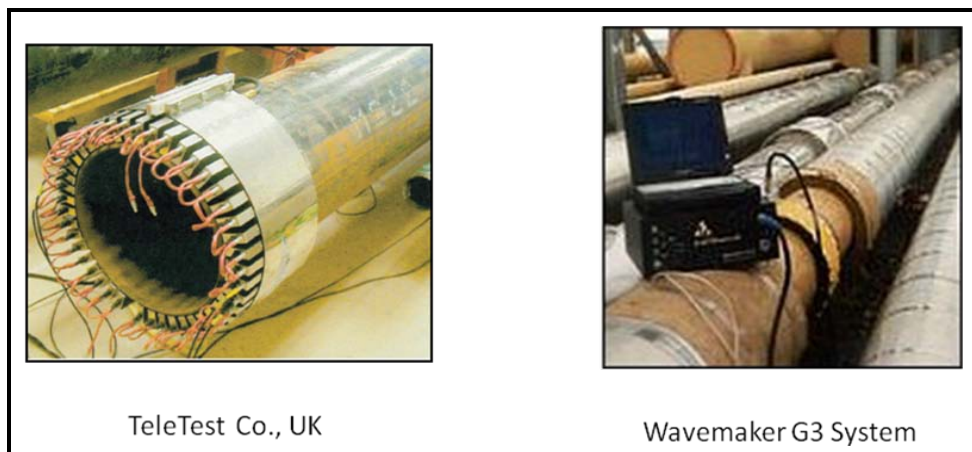


Figure 3-5. Standalone Inspection Systems and Instruments

3.2.3.2.3 Resident Pipeline Sensors

Limited research has been conducted on using a distributed network system of sensors, deployed along pipelines, for inspection and monitoring. As outlined in the SOPO this technology is the focus of the research covered under this effort

3.2.3.3 Benefits and Inadequacies of Current Technology

Each tool or platform can utilize various techniques to achieve the goal of inspection and monitoring. This technology survey, although not exhaustive, summarizes the following four major technologies:

- Magnetic flux leakage (MFL),
- Remote field eddy current,
- Ultrasonic guided wave technologies, and
- Remote sensing techniques.

The benefits and inadequacies of the four inspection technologies are listed in Table 3.1.

Table 3-1. Inspection Technologies Benefits and Inadequacies

Technologies	Basic Principles	Benefits	Inadequacies
Magnetic Flux Leakage (MFL) ^[5]	MFL uses a powerful magnet to magnetize the steel pipe. At areas where there is corrosion or missing metal, the magnetic field that “leaks” from the pipe is detected.	MFL can detect metal-loss defects in pipelines with good confidence. An MFL tool can characterize the depth, shape, and length of a metal-loss region.	Many MFL inspection systems use extremely high magnetic intensities. Very narrow axially oriented defects, such as cracks and seam corrosion are rarely detected using current MFL technology and only work on metal pipe.
Remote Field Eddy Current (RFET) ^[6]	Eddy-current testing uses electromagnetic induction to detect flaws in conductive metal pipelines.	Can operate at large lift-off distance from the pipe surface. Reasonable wall thickness measurements. Sensitive to many pipeline defects.	It works only for metal pipes. Depth of penetration is limited. Signal levels are small. Significant excitation power is needed.
Ultrasonic Guided Wave ^[7]	Acoustic waves travel long distances on the surface of pipelines, detect and locate corrosion or defects by measuring the elapsed time between the reflections.	No need for a liquid coupling; Ability to traverse valves and other internal pipe obstructions; can use piezoelectric sensors or magnetostrictive sensors. Most accurate technology for wall thickness	It is not able to scan a long range axial distance of a pipe from a single transducer position.
Remote Sensing Technologies ^[8]	Uses aerial and satellite remote sensing integrated with GIS technologies to assist pipeline risk assessment and inspection.	Capable of wide area pipeline infrastructure change mapping and inspection and pipeline emergency assessment and management.	This technology is not adequate for detection and inspection of corrosion defects. Does not detect before a substantial leak.

In addition to the aforementioned four major technologies, there are many variations of such inspection methodologies and sensing techniques, for example, electromagnetic acoustic transducer (EMAT) ^[9], permanent magnet eddy current ^[10], multi-purpose deformation sensor ^[11], dual magnetization MFL ^[12], and magnetostrictive sensor technique ^[13]. Furthermore, natural gas companies and research institutions aspire to develop inspection techniques for plastic pipelines ^[14-15]. In this technology assessment, the team focused on the monitoring and inspection technologies for steel pipes.

The TSA concluded no past DOE or DOT efforts explored time reversal-based techniques for pipeline inspection and continuous monitoring. Although some past DOE or DOT awards have considered using acoustic sensors for pipeline monitoring and experimenting with guided wave propagation in the wall of a pipe, they do not fully characterize the wave propagation nor do they address the problem of how to organize and deploy sensors as a network and validate the

network performance. In contrast with existing technologies, an inspection platform will be developed based on a network of active sensing and actuating devices to continuously monitor pipelines.

The main distinguishing feature of the IPI research and solution is the automatic, continuous monitoring of the state of the pipelines and the pipeline infrastructure. Further, this sensing and monitoring solution can be used to detect defects in areas where conventional inspection technologies cannot be implemented, for example, with unpiggable pipelines. The deployment of active sensors provides the opportunity to localize defects with high accuracy and to characterize their nature and type, improving the detection of real defects and reducing the rate of false alarms. Based on the concept of time reversal acoustics (TRA), the method will improve the ability to detect and localize damage for further assessment.

3.2.4 TSA Summary

The TSA was authored and delivered as a draft report on September 19, 2008. After receiving and incorporating NETL feedback, the Final TSA Report was delivered on September 30, 2008. After discovering new and relevant information, the TSA was updated and delivered on February 20, 2009.

3.2.5 Project Summary

Additionally, a project summary was developed by NETL. Per the SOPO, this document was reviewed and comments were provided quarterly by CTC.

3.3 Task 3 – Pipeline Wave Propagation Characteristics

3.3.1 Objective

The objective of this task was to conduct experimental research to understand wave propagation characteristics in pipes and the effects of various materials and environment loading. After completion of this task, the team determined the effectiveness of wave propagation techniques in pipeline systems as a continuous monitoring and/or inspection method. The wave propagation method that provided the optimum signal response was selected for use in follow on tasks.

3.3.2 Approach

The approach utilized a combination of computer simulation and laboratory testing. Computer simulation was used to conduct numerous experiments that would be very time consuming in the laboratory. The laboratory experiments were used for validation of simulations and to test theories outside the capabilities of simulation tools.

Unlike traditional ultrasonic inspection techniques, the proposed TRA technique benefits from multiple modes, multiple signal paths, and wave dispersion. Initial tests and simulations were performed to assess and understand the excitation of the pipeline.

3.3.3 Results

Using the laboratory described later in Task 8 that includes simulation and modeling tools as well as a proof of concept test system, tests were performed to determine the effectiveness of multimode, multipath, and dispersive wave propagation in pipes for time reversal acoustics. As part of the evaluation process, simulations were performed to assess optimum frequency excitation. Additional tests were performed to assess the ability of a single small transmitter to fully illuminate the circumference of the pipe.

3.3.3.1 PZFlex simulation to determine frequency response of the pipe

Using PZFlex simulations it was determined that a wideband sinc pulse excites a broadband response in the pipe. This broadband pulse was used in laboratory tests to validate the simulations. Two simulations are highlighted in this section that includes a short pipe model and a long pipe model.

The short pipe model was configured as a 1.5 meter (m) long pipe with the dimensions shown in Figure 3-6.

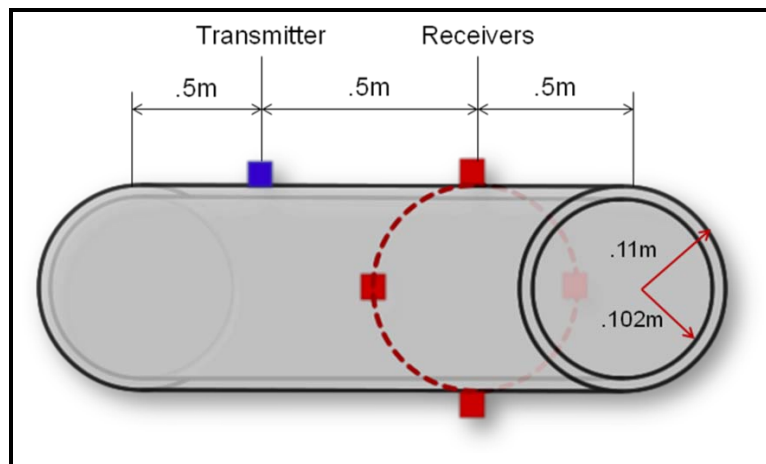


Figure 3-6. Simulation Model of a Short Pipe

The simulation results in Figure 3-7 and Figure 3-8 clearly show the dispersive, multimode, multipath propagation of this excitation. This is particularly evident in the received signal, time versus voltage graph in the lower left of Figure 3-7. The multiple peaks correspond to multiple paths and modes, and the spreading of the time pulse corresponds to the dispersion of the signal.

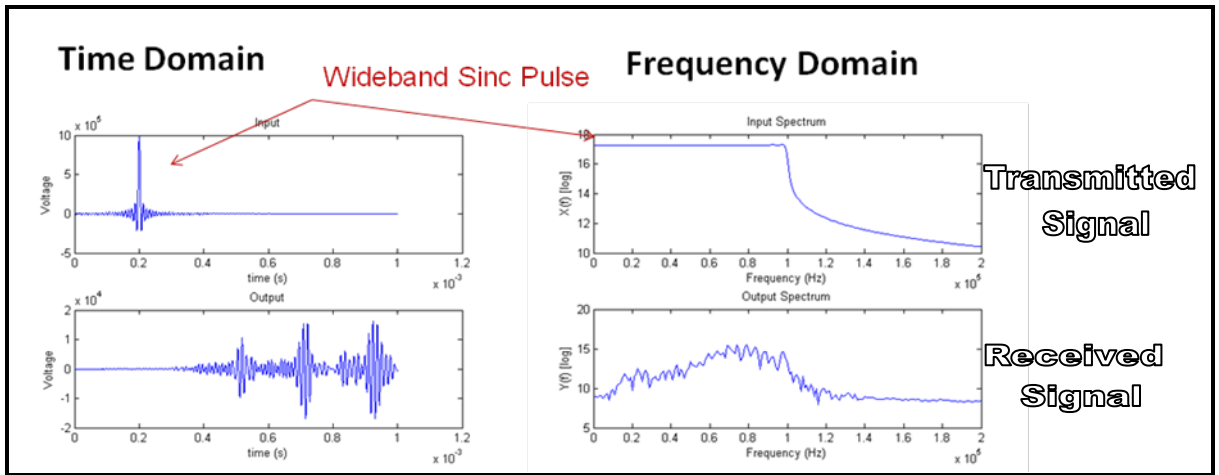


Figure 3-7. Time Plot Versus Frequency (Short Pipe)

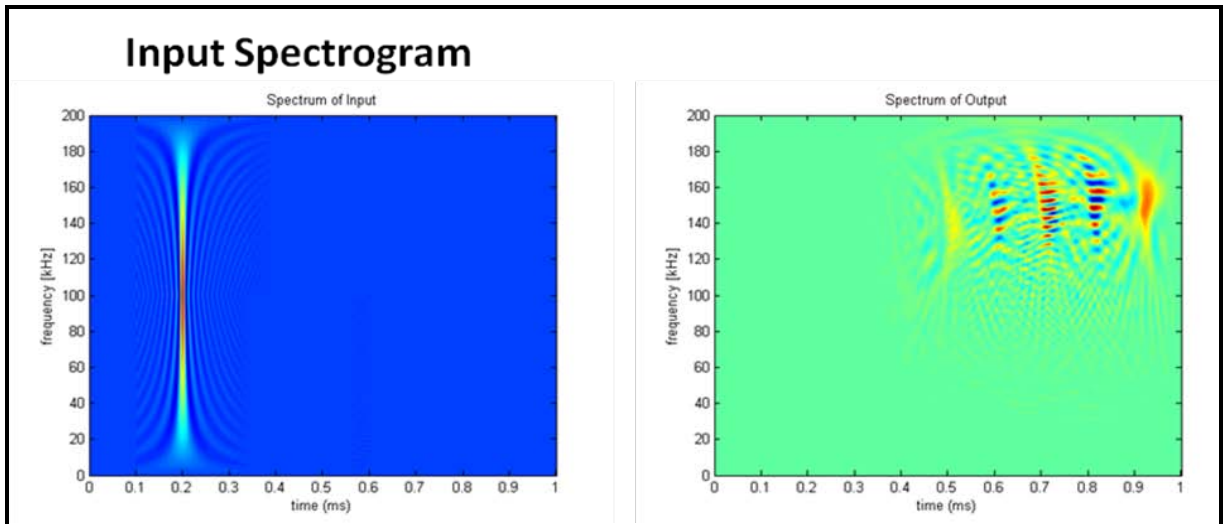


Figure 3-8. Time Versus Frequency Plot (Short Pipe)

Figure 3-9 details the configuration of a long pipe simulation including the model dimensions.

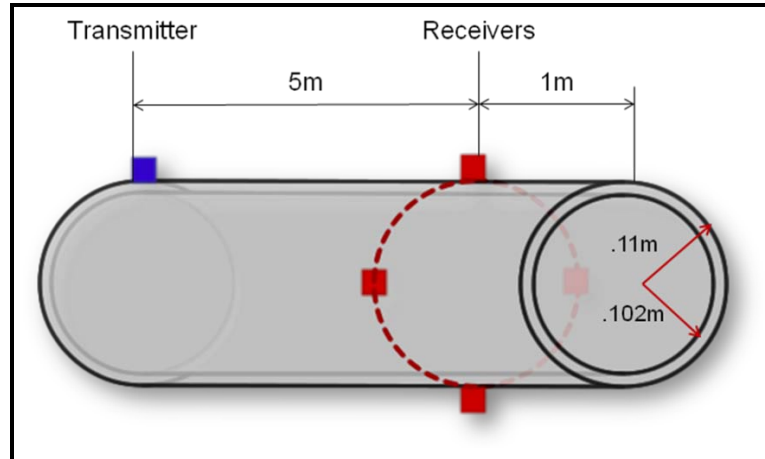


Figure 3-9. Simulation Model of a Long Pipe

Figure 3-10 and Figure 3-11 show the simulation results of the long pipe. The simulation results more drastically illustrate the dispersive, multimode, and multipath propagation when compared to the short pipe.

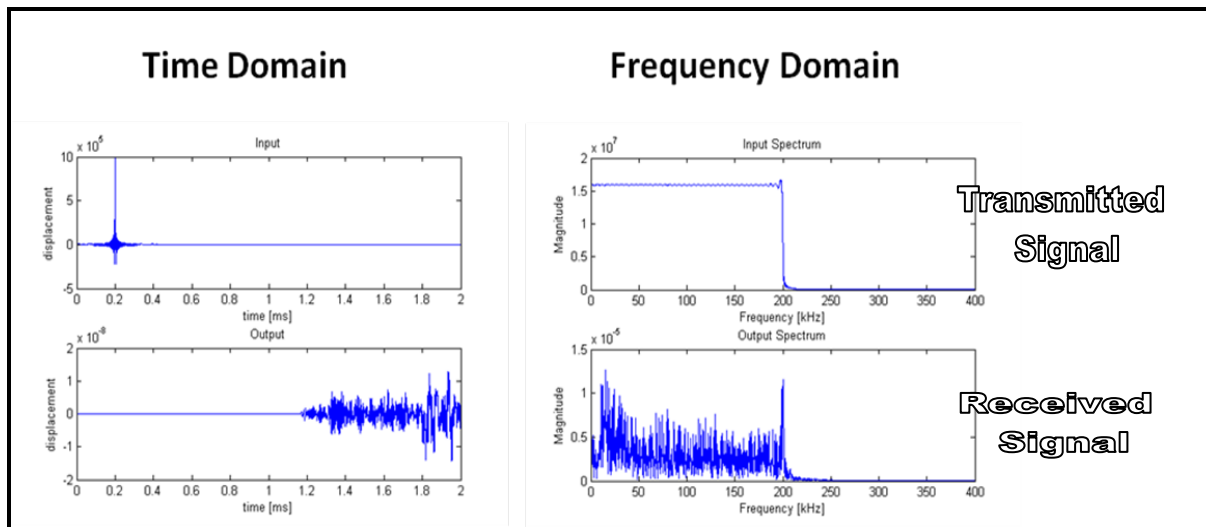


Figure 3-10. Time Plot Versus Frequency (Long Pipe)

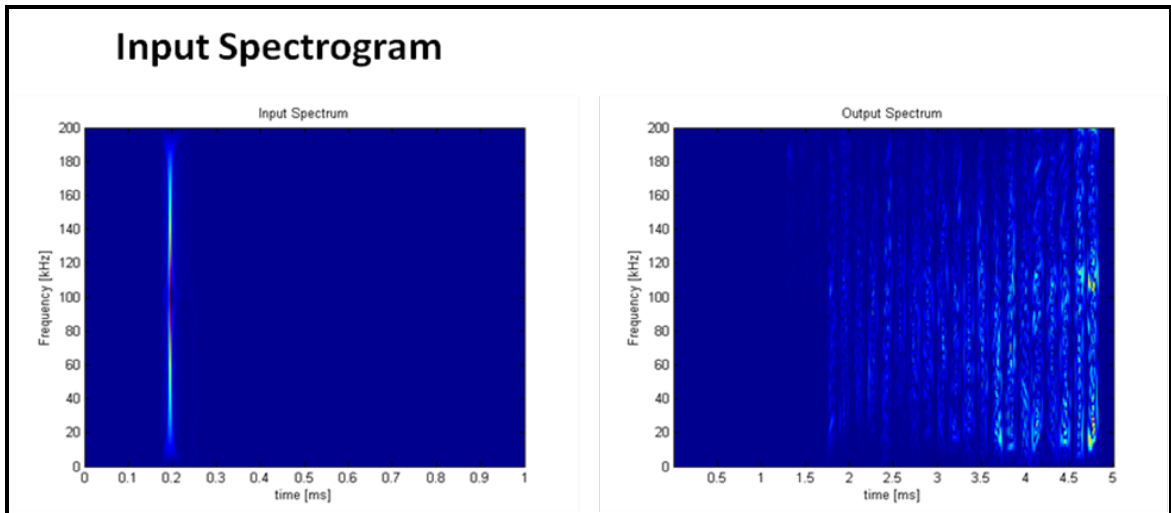


Figure 3-11. Time Versus Frequency Plot (Long Pipe)

Multimode, multipath, dispersive propagation test
 Calculations and PZFlex simulation models were used to determine optimal frequencies for wave propagation. These simulations resulted in a selection of a wideband frequency excitation from 75 kilohertz (kHz)-150 kHz being used in following experiments. This broadband pulse was generated using a sinc pulse. To confirm the simulations a laboratory test was performed on a steel pipe with the following conditions shown in Figure 3-12:

Length = 3050 millimeters (mm)

Outside Diameter = 60.3mm

Wall Thickness = 3.6mm

Transmitter/Receiver = Lead Zirconate Titanate (PZT) wafers spaced 1200mm apart
 (6mm x 12mm x 1mm)

Excitation = 10V using wideband sync pulse (less than 0.04 millisecond (ms) in duration).

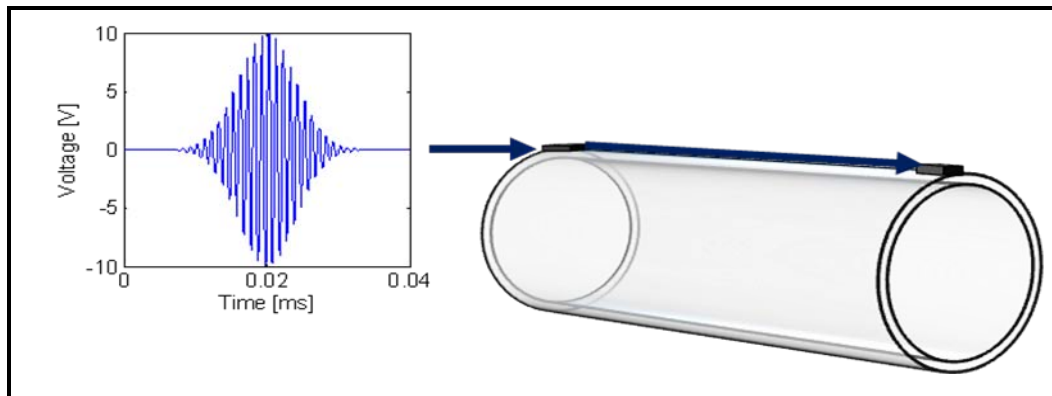


Figure 3-12. Laboratory Test Configuration (Propagation Test)

The received signal was collected and recorded for a duration of 2 ms. The received signal shown in Figure 3-13, clearly shows the presence of multiple modes and paths in addition to dispersion. The laboratory results confirm the simulated results and calculations that predicted the presence of many modes, and paths. The dispersive medium is also evident in the spreading of the pulse.

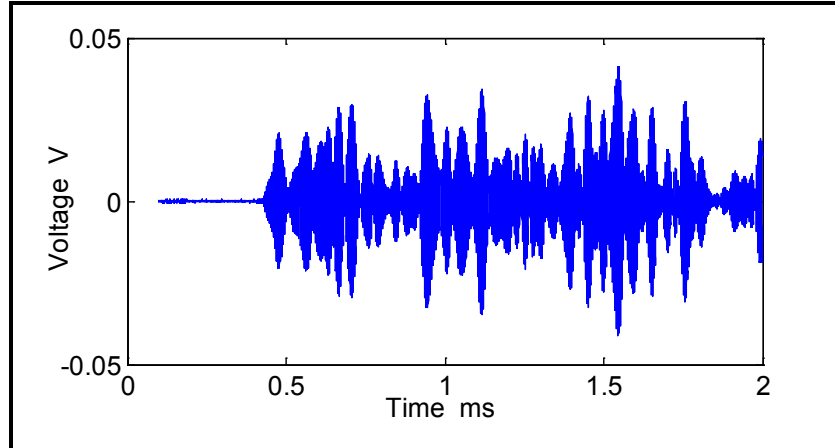


Figure 3-13. Received Signal (Propagation Test)

Pipe Illumination Test

In order to assess the effectiveness of a small (6mm x 12mm x 1mm) PZT transducer to fully illuminate a pipe, an acoustic probe was used to measure illumination of the pipe. Figure 3-14 shows the result of recorded signals at eight equally spaced positions around the circumference of the pipe. As is evident in the results, a single transducer fully illuminates the entire circumference of the pipe.

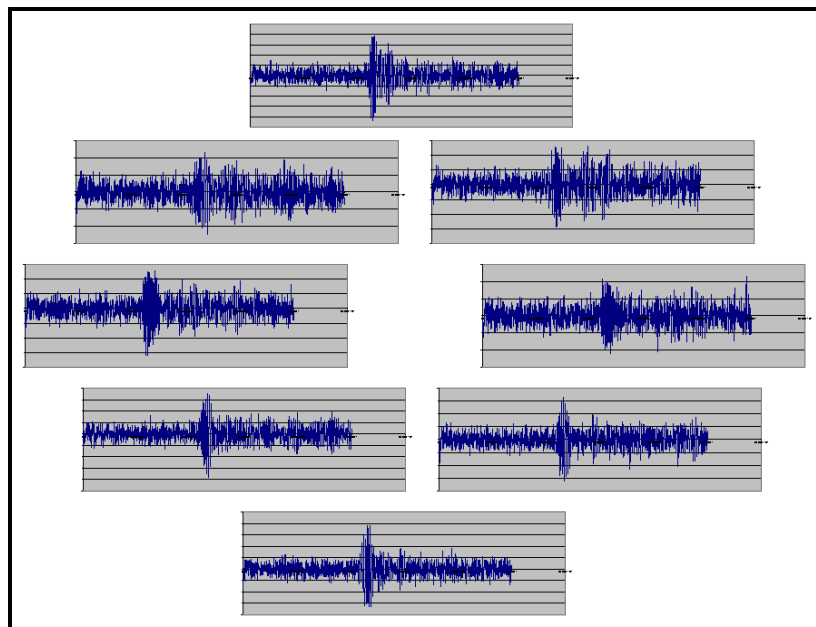


Figure 3-14. Pipe Illumination

Attenuation Tests in Air and Soil Embedment

To test and understand attenuation of the acoustic wave in air and soil embedment, experiments were performed on a 3m pipe. Figure 3-15 shows a 0.55 decibel/meter (dB/m) attenuation of the signal when the pipe is in air and 1.4 dB/m when in sand embedment. This change in attenuation corresponds to a 21 dB drop in signal at 38m and 15m respectively.

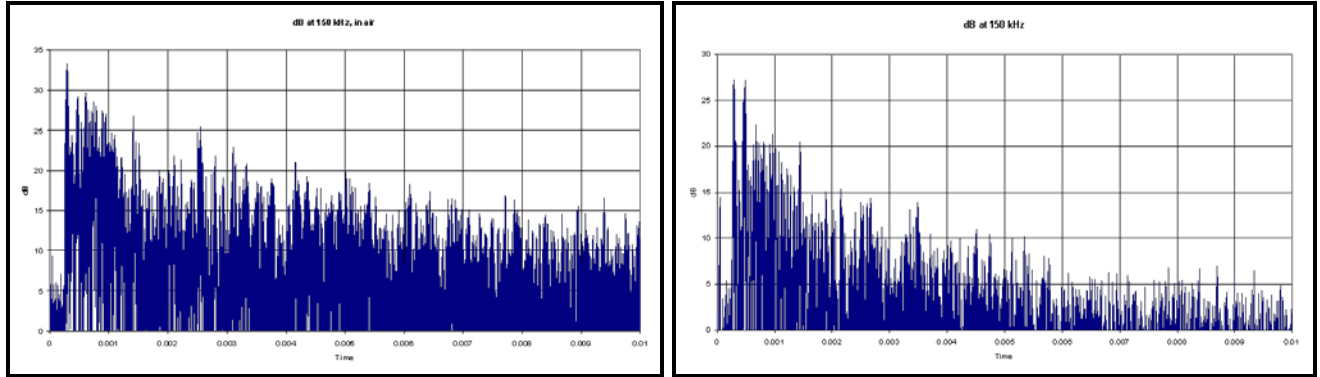


Figure 3-15. Attenuation in Air and Soil Embedment

3.3.4 Summary

The simulations and laboratory experiments have shown distinct dispersive wave propagation. The simulations and tests also show multimode and multipath propagation is present. Long distance propagation, simulated physically by reflecting waves off open pipe ends, was demonstrated and attenuation in air and in sand embedment was quantified. Finally, it was shown that a small, low cost PZT transducer with dimensions 6mm x 12mm x 1mm can effectively excite rich propagation modes for use in the following tasks.

3.4 Task 4 – Development and Optimization of Active Sensing Devices

3.4.1 Objective

The objective of Task 4 was to investigate and determine the optimal type, size and spacing of the active sensing devices and the effective configuration along the circumference of the piping system. Active sensing devices were tested on surfaces of pipeline systems, investigating both inside and outside surface attachments. This task employed active sensing devices such as PZT piezoelectric devices and other technologies to accomplish simultaneous actuation and sensing.

3.4.2 Approach

The approach utilized a combination of computer simulation and laboratory testing. Computer simulation was used to conduct numerous experiments that would be very time consuming in the laboratory. The laboratory experiments were used for validation of simulations and to test theories outside the capabilities of simulation tools.

In this task, Macro Fiber Composite (MFC) transducers were compared to PZT transducers for excitation of acoustic waves in pipes. In addition, the feasibility of employing array transducers

was explored. Arrayed transducers will most likely be necessary for localization and classification.

3.4.3 Results

Piezoelectric materials produce a coupling between the mechanical stress and the electrical field. This coupling can be used to excite acoustic waves on pipes and also to sense and receive propagating waves. MFC transducers were considered for pipeline applications because they easily conform to the curved surface; however other comparisons of the PZT and MFC transducers show that PZT transducers have many favorable features over the MFC transducers. Figure 3-16 compares PZT and MFC transducers.

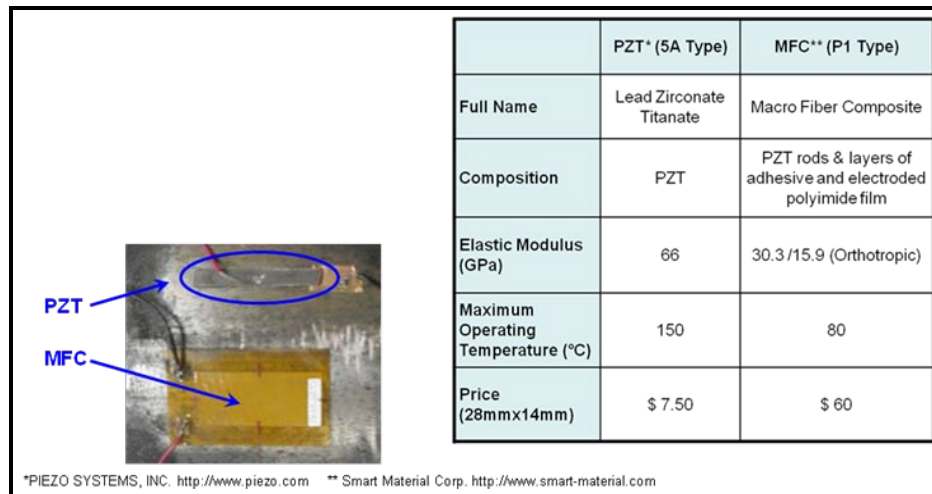


Figure 3-16. PZT and MFC Compared

Testing and simulations were performed to aid in selection of the transducer. Since initial simulations indicated PZT transducers may be more effective, a laboratory experiment was performed. The setup as shown in Figure 3-17 was used to validate the simulations. The MFC (P1) transducer was 28mm x 14mm and the PZT transducer was 28mm x 3.5mm in length and width respectively. A narrow band toneburst with excitation voltage of 10V was swept across the frequency range of 20 kHz – 550 kHz to assess the frequency response and efficiency of the transducer/pipeline system.



Figure 3-17. Laboratory Transducer Experiment

The response comparison shown in Figure 3-18 was used to select PZT transducers as the material of choice for the following tasks.

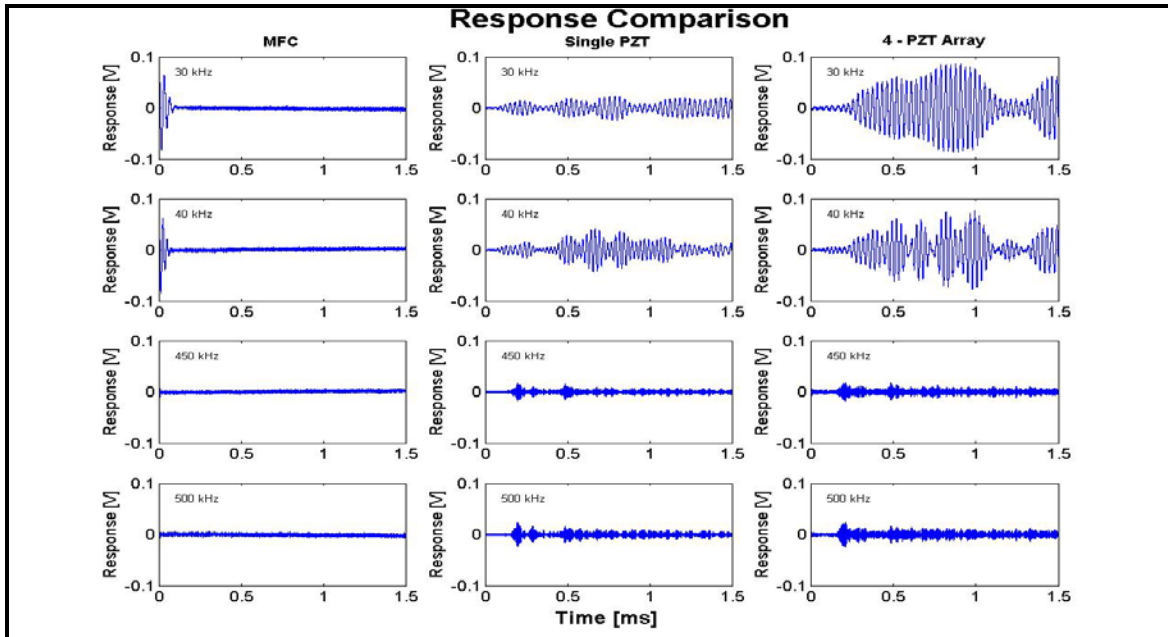


Figure 3-18. Transducer Response Comparison

The response comparisons show that the PZT transducer captures more signal than the MFC transducers at most frequencies. In addition, a PZT array is also shown in this comparison. The array is effective as well and will be useful for localization and classification.

3.4.4 Summary

In summary, a single PZT transducer is an efficient and cost-effective transducer for steel pipes. A multiple transducer array may prove to be effective for localization and classification. MFC transducers are less suitable for steel pipes because they provide significantly weaker ultrasonic emissions.

3.5 Task 5 – System Engineering

3.5.1 Objective

The objective of this task was to identify all of the components that are required for the sensor system and determine the power and data bandwidth requirements for the continuous monitoring and/or inspection system. This task was performed in parallel with several of the other tasks. The IPI team reviewed the power requirements for the continuous monitoring/inspection system and quantified any limitations. The team determined data bandwidth for the system and computing requirements for the system and determined the computing power required to execute algorithms.

At the conclusion of this task, the IPI Team developed and provided a proof of concept design package consisting of conceptual schematics and specifications.

3.5.2 Approach

The concepts and lessons learned throughout Tasks 3, 4, 6, and 7 were applied to the system design. The result was implemented in a proof of concept system, expanded with an extended proof of concept system and finally a path was defined for an implementable and independent monitoring system.

3.5.3 Results

The main systems components of a laboratory or implementable systems are the following:

- PZT Piezoelectric Sensors
- Signal Generator
- Analog to Digital (A/D) Converters
- Communication Network
- Data processor

Supporting system components are: batteries and charging circuits, drivers, Direct Current to Direct Current (DC/DC) converters and potentially energy harvesting circuits.

The laboratory system is effectively a one (1) node system and is detailed in Task 8 (Proof of Concept System). In order to extend this system to longer pipeline tests, a multiple node system must be created. Each node of the systems would have to communicate to a networked or distributed processor. A conceptual diagram as shown in Figure 3-19, would allow nodes to be separated long distances in order to assess long distance propagation in real environments.

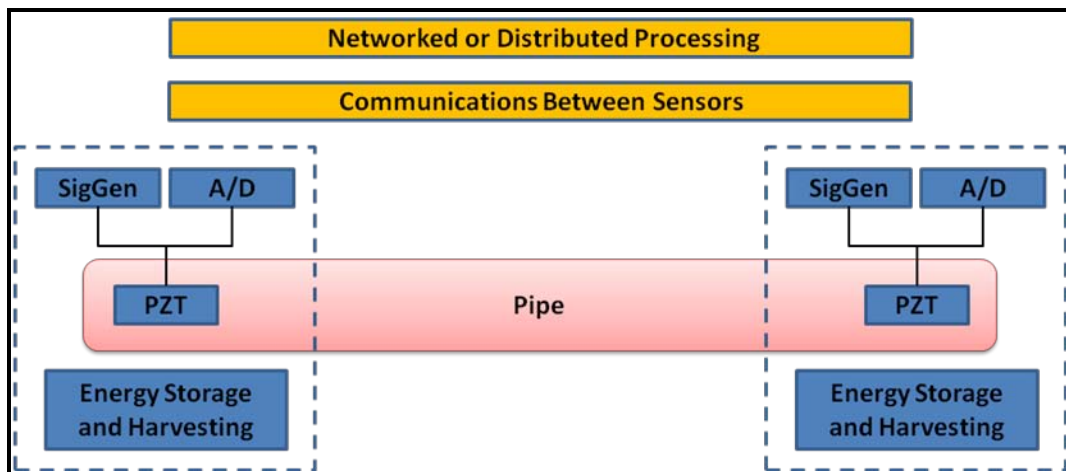


Figure 3-19. Conceptual System Diagram

Sensor Location Trade Study

It is theorized that the PZT transducers would be equally effective on the inside or outside of the pipeline; therefore the ultimate selection is based on realistic applications of the PZT and associated circuitry. A trade study determined the positives and negatives for internal versus

external pipe applications. Ultimately this choice would need to be reanalyzed for specific applications. The trade study is summarized in Table 3-2:

Table 3-2. Trade Study

Trade Study Internal vs. External	Internal Pipe	External Pipe
Positives	Could possibly use flow and pressure for energy harvesting. Sensors are in a more controlled environment.	Reduced intrinsic safety concerns. Better access for existing pipeline installations.
Negatives	Intrinsic Safety Concerns. Might hinder PIG operations. Difficult to access for existing pipeline installations.	No access to gas flow for energy harvesting. Potentially intrusive to surface activity. Sensors are open to external environment conditions.

Power Requirement Assessment

Using the information derived to date, the following power requirements and limitations are estimated for an implementable system. A preliminary estimate of 6.5 Watt hours per day (Wh/day) (as shown in Table 3-3) can be used for a realistic prediction of the power requirement for each node. If further testing proved advantageous for increased power transducers, this estimate would be updated accordingly.

Table 3-3. Power Requirement Assessment

Energy Budget:				
Component	Power Required (mW)	Notes	On Time / Day (hours)	Energy Consumed / Day (W*h)
PZT Transducer Ring	8800	16 PZT's operated at 10V RMS	0.04	0.35
PZT Drive Circuitry	3771	70% efficiency	0.04	0.15
A/D Converter	800	14 bit, 105 MS/sec	0.40	0.32
	75	Standby	23.60	1.77
Signal Processor	294	16-bit microcontroller, 40 MIPS	2.00	0.59
	80	16-bit microcontroller, idle	22.00	1.76
RF Transceiver	76	Transmit, 250 kbps	4.00	0.30
	63	Receive, 250 kbps	20.00	1.26
Total Energy Consumed Per Day (W*h):				6.50

If the power requirements of a node remain near the 6.5Wh daily estimate, it may be possible to power the nodes with a battery and energy harvesting systems.

3.5.4 Summary

System components are identified and are present in the laboratory and the conceptual systems. A single node based sensor concept has been identified and the laboratory proof of concept system is based on this single node concept. In addition, a multiple node system has been identified for long distance testing. A preliminary power budget has been defined based on a 10V excitation of the PZT transducers. This budget is subject to change when a fully implementable system is defined.

3.6 Task 6 – Extraction of Reference-Free Features

3.6.1 Objective

The objective of this task was to determine if TRA is an acceptable method for defect detection. Various pipeline configurations were tested to review the shape of the reconstructed TRA signal. The IPI team examined the deviation of the reconstructed signal from the known input signal, identifying the damage. The IPI team also studied the objective of achieving change detection that would be fully reference-free, using TRA for different types of defects, but concluded that reference-free flaw detection is not a practical objective in the near term. At the conclusion of this task, the team determined that TRA defect extraction techniques are effective with the identification of defects in pipeline systems implementing the sensors recommended in the earlier phases of this project.

If the TRA defect extraction techniques studied proved to be ineffective in pipeline systems, the IPI team would have further researched other techniques identified in the TSA.

3.6.2 Approach

The approach utilized a combination of computer simulation and laboratory testing. Computer simulation was used to conduct numerous experiments that would be very time consuming in the laboratory. The laboratory experiments were used for validation of simulations and to test theories outside the capabilities of simulation tools.

Various pipeline configurations were tested in the laboratory and simulation environment. The effectiveness of TRA was assessed for effectiveness of defect detection.

3.6.3 Results

The TRA solution effectively focuses energy for use in determining changes to pipeline, including damage. This technique focuses the energy of all of the modes, paths, and dispersion at one point in time and space. This focused signal can then be used to characterize the pipe medium and the damage within it. Specifically time reversal focusing simplifies the response without a cost to signal strength, coherently focuses energy from dispersion, modes, and paths, and focusing occurs regardless of frequency or bandwidth.

The time reversal focusing is performed using the following steps. These steps perform the TRA medium characterization process.

Step #1 (Figure 3-20): Transmit the excitation signal. This signal is a short sinc pulse with a broad frequency bandwidth.

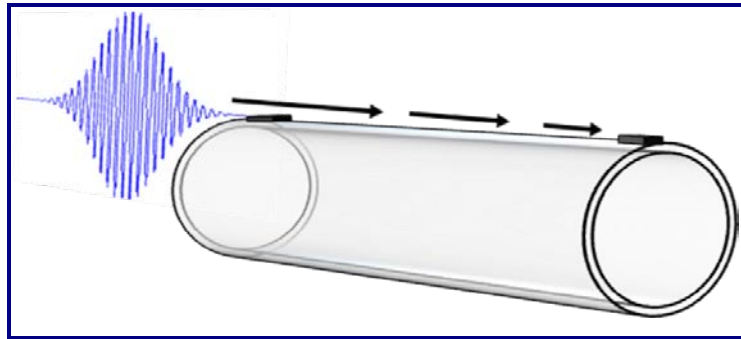


Figure 3-20. Transmit Signal (TRA Step #1)

Step #2 (Figure 3-21): Receive the signal at the receive transducer. This signal is complex and broadband. The received signal displays the signature of the dispersive multipath and multimode wave propagation present in the pipe.

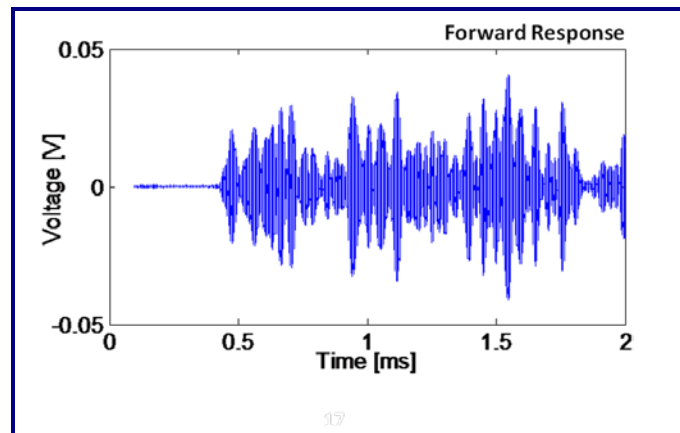


Figure 3-21. Receive Signal (TRA Step #2)

Step #3 (Figure 3-22): Normalize and time reverse the received signal. The signal is normalized so that it contains the same amount of energy as the original excitation. The time reversal can be achieved by using a first-in, last-out register.

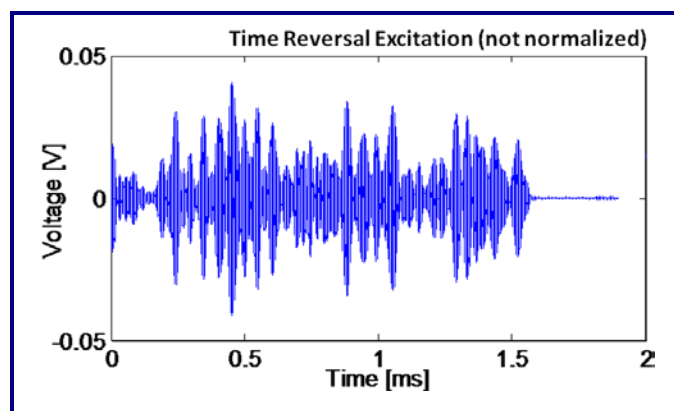


Figure 3-22. Time Reverse Signal (TRA Step #3)

Step #4 (Figure 3-23): Transmit the time reversed signal backward into the medium.

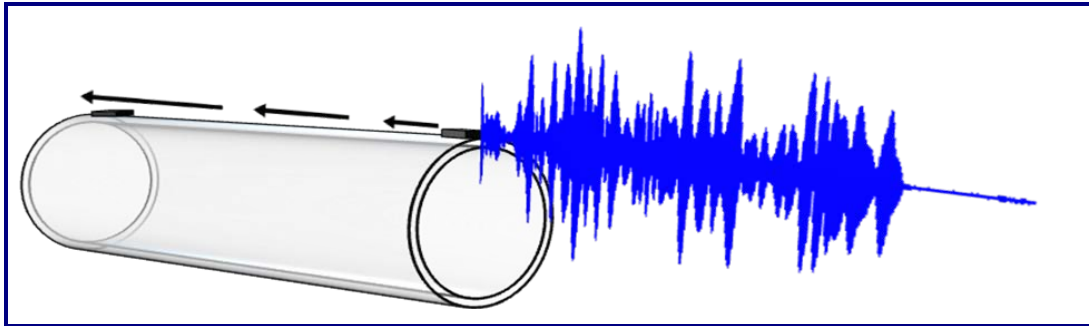


Figure 3-23. Transmit Time Reversed Signal Back to the Transmitter (TRA Step #4)

Step #5 (Figure 3-24): Receive the signal back at the original transducer after having been transmitted back through the complex media. This signal will focus. The peak is evident in the plot below.

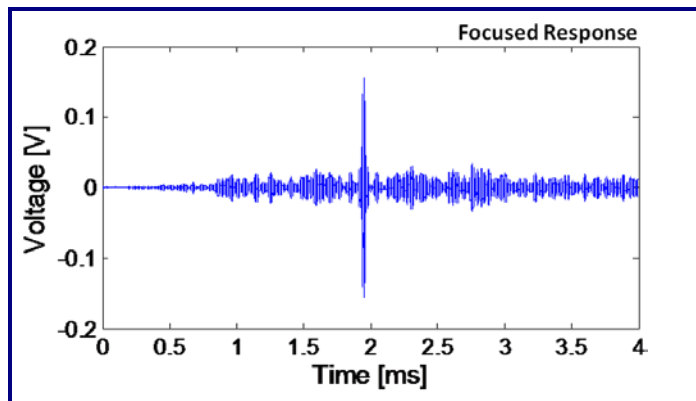


Figure 3-24. Received Focused Signal (TRA Step #5)

When compared to other acoustic test methods, dispersion, multimode, multipath effects are a burden to signal analysis and transducer design. The time reversal focusing technique benefits from the dispersion, multimode and the multipath effects. In general, the more complexity of the propagation environment, the greater the focusing effect.

After the medium is characterized, the defect detection is performed with slight modifications to the process described above. Rather than transmitting the received signal back to the initial transducer (as in steps 3 and 4), a difference signal is created by using the original characterization signal and the newer test signal. The difference signal may look similar to Figure 3-25 depending on the change.

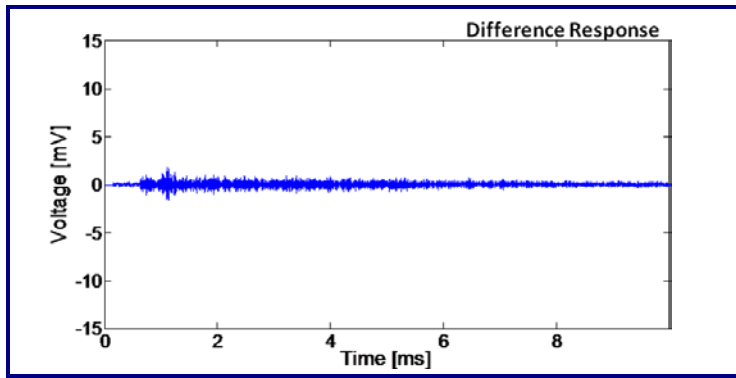


Figure 3-25. Difference Signal

The difference signal is time reversed, normalized and sent back to the original transducer. A representative normalized signal is shown in Figure 3-26.

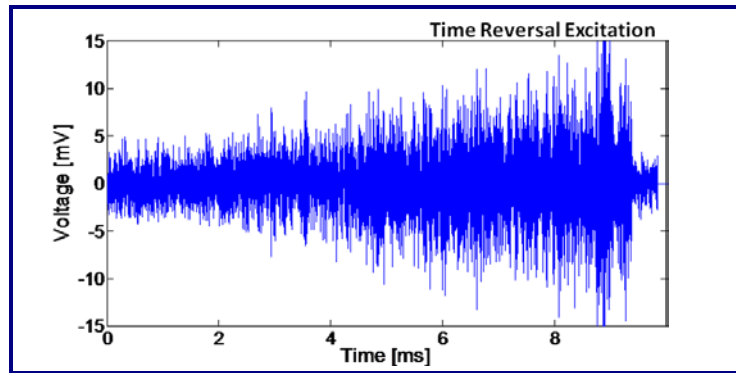


Figure 3-26. Normalized Time Reversed Difference Signal

The change detection is evident in the focused response in Figure 3-27.

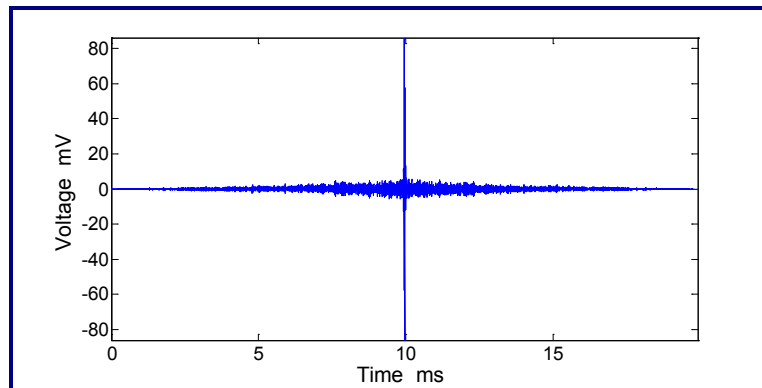


Figure 3-27. Focused Signal Due to Change Detection

Test results of various defects and configurations

The time reversal focusing technique was testing on lateral defects, longitudinal defects, & corrosion like defects. The results of these tests are summarized.

Lateral Defect

Lateral defects shown in Figure 3-28 created with a hacksaw, were tested and are the results showing that time reversal focusing is quite effective at detecting damage from a longitudinal effect.

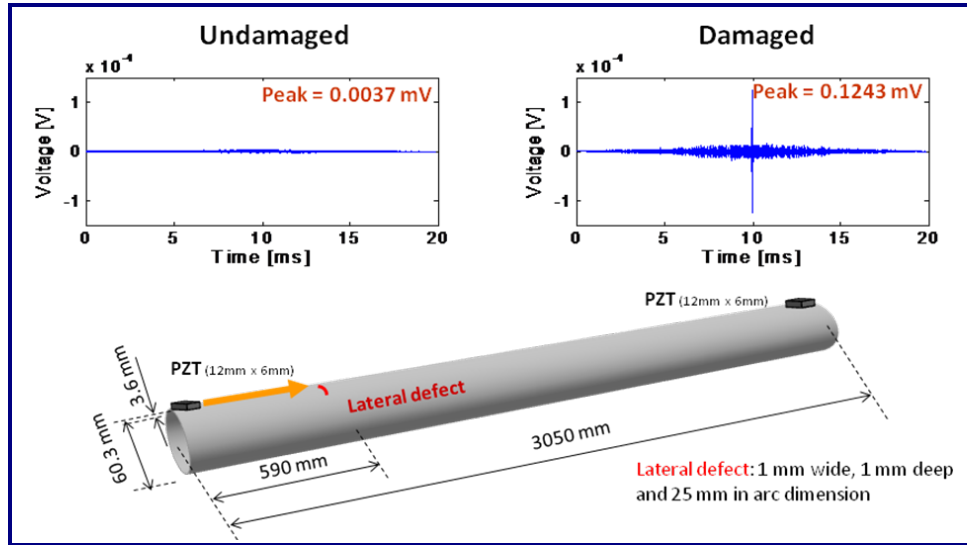


Figure 3-28. Lateral Defect

Longitudinal Defect

Longitudinal defects shown in Figure 3-29, created with a grinder, were tested and are the results show that time reversal focusing is quite effective at detecting damage from a longitudinal effect.

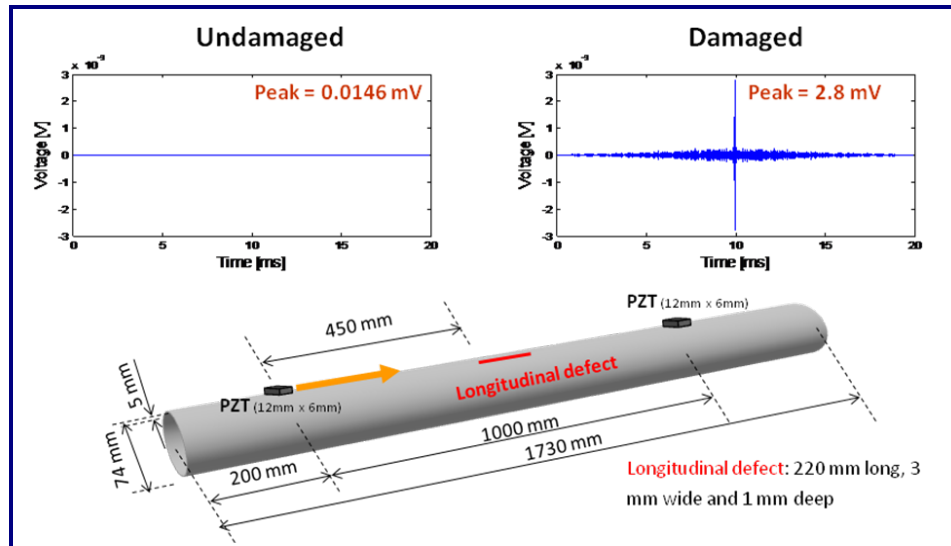


Figure 3-29. Longitudinal Defect

Corrosion-Like Defect

A corrosion-like defect shown in Figure 3-30 was created by using a grinder to remove a small oval of approximately 20mm major axis, 15mm minor axis, and 1mm deep. This defect was tested and the results show that time reversal focusing is quite effective at detecting corrosion-like defects.

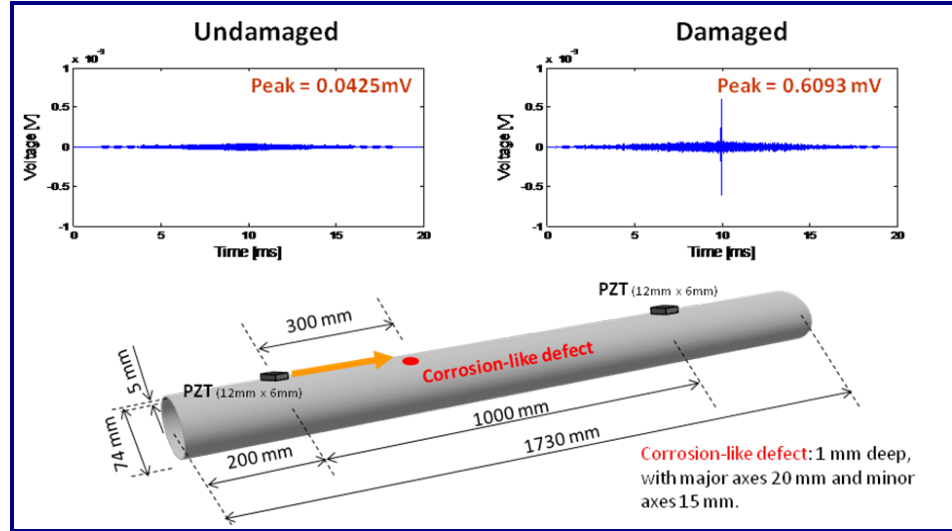


Figure 3-30. Corrosion-Like Defect

3.6.4 Summary

In summary, TRA using ultrasonic sensors proved to be highly effective for the detection of defects in a multimodal and dispersive steel pipe environment. The time reversal focusing technique compresses modes temporally and spatially and enhances signal-to-noise ratio. The change focusing relaxes the restriction of excitation from narrow band and low frequency to allow broadband and wide band frequencies. Modes do not need to be analyzed individually since all modes are focused into one signal peak. Due to the focusing this technique enables higher detection ability and is effective with detection of varied and small defects.

3.7 Task 7 – Classification and Localization of Defects

3.7.1 Objective

The work performed under this task intended to study the characterization (classification) of structural damage types by their signature waveforms. The work performed under this task intended also to study the localization (the position on the pipe) of structural damage. The IPI team performed experiments on a time reversal classification algorithm to evaluate its functionality for classification, and performed related experiments on localization.

If TRA classification and localization techniques studied had been determined to be ineffective in pipeline systems, the IPI team would have analyzed other techniques identified in the TSA.

3.7.2 Approach

As in other tasks, this approach utilized a combination of computer simulation and laboratory testing. Computer simulations were used to conduct numerous experiments that would be very time consuming in the laboratory. The laboratory experiments were used for validation of simulations and to test theories outside the capabilities of simulation tools.

3.7.3 Results

Localization

Using MathWorks MATLAB[®] simulations, localization techniques were studied. An 8-transducer array was used on each side of the simulated pipe and various localization and imaging techniques were studied. The following simulation result, shown in Figure 3-31(a), shows the output of direct subtraction and is common with traditional beamforming and imaging techniques. When time reversal is added to the calculations, a time reversal beamforming result can be generated. The time reversal beamforming result is shown in Figure 3-31(b). This result takes advantage of the focusing of energy as described throughout this document. The result shows a clearer and sharper image that will certainly be useful for localization applications.

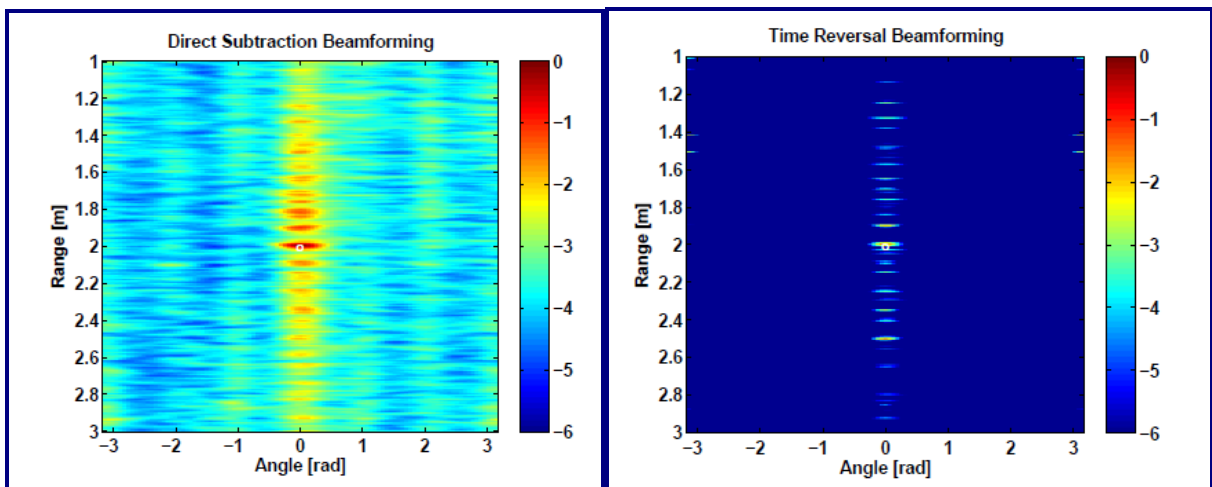


Figure 3-31(a). Direct Subtraction

Figure 3-31(b). Time Reversal

Time reversal beamforming technique was developed and simulated by the IPI team as a defect localization method. In this following MATLAB[®] simulation, Figure 3-32, 8 transducers were used on each side of a pipe. While there is echoing evident in the result, it is clear that this technique can locate damage.

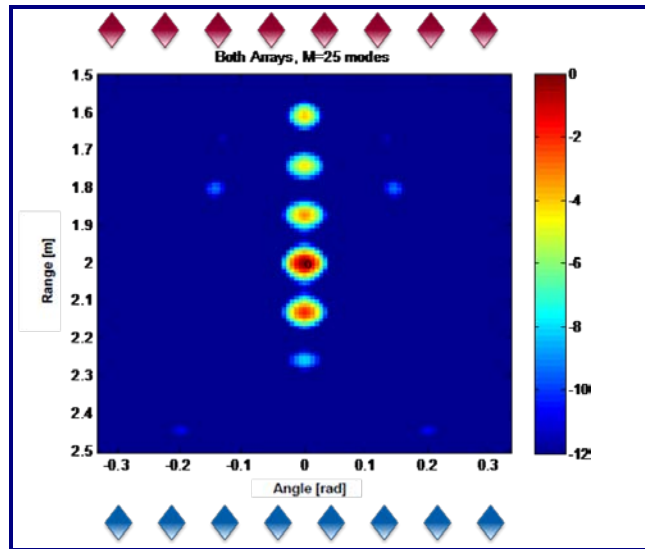


Figure 3-32. Time Reversal Beamforming Imaging (Echoing / Defect Localization)

Classification

In order to classify defects into categories, a sequential Bayesian classifier was studied. PZFlex-generated data was used exclusively for these experiments. Machine learning (using as SVM [support vector machine] implementation) was also investigated as a way to perform classification. In general, effective cognitive sensor networks are adaptive and utilize feedback to alter behavior. The cognitive sensor networks used multiple independent measurements and sensor fused or consensus algorithm to classify (Figure 3-33).

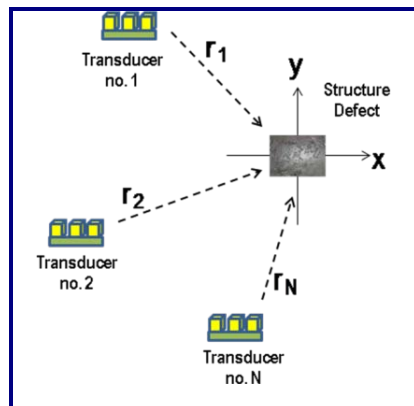


Figure 3-33. Cognitive Sensor Consensus Algorithm

The Bayes M-ary detection shown in Figure 3-34 uses the following decision procedure with time reversal focusing techniques applied.

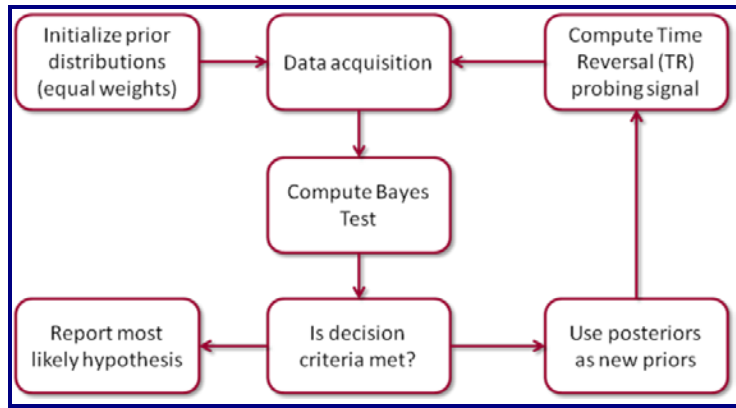


Figure 3-34. Bayes M-ary Detection Procedure with Time Reversal

To test technique the following PZFlex model and simulation were used to compare and classify the following defects: a hole, interior corrosion, exterior corrosion, and a saw cut. The model is detailed in Figure 3-35.

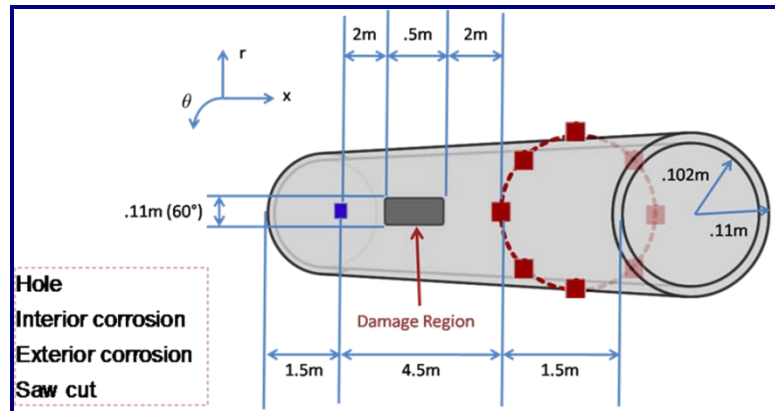


Figure 3-35. Defect Model used for Classification Studies

As can be shown in Figure 3-36, the output of the experiment, increased probability of detection occurs as the average energy per transmission is increased. The second graph shows that multiple pulses can be used as an alternative to increased power per pulse.

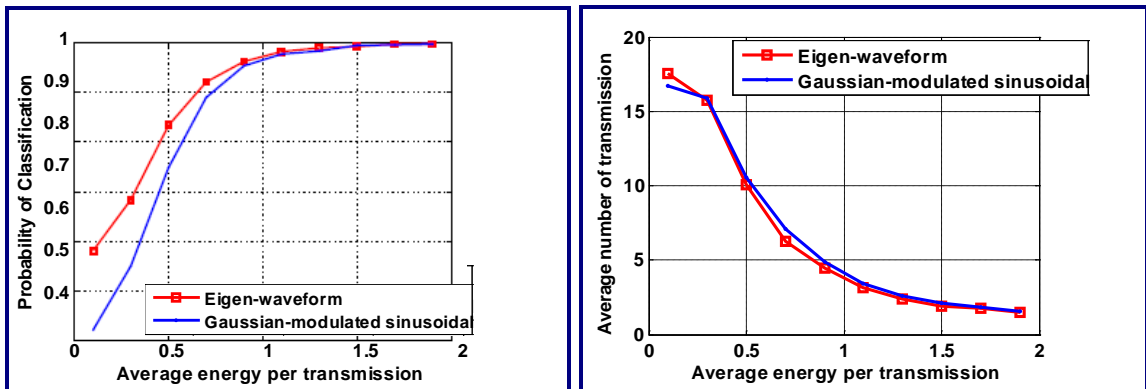


Figure 3-36. Increasing Probability of Classification

All validation was conducted on purely simulated data. A more robust conclusion could be made if experimental data could be collected and analyzed.

Machine learning may prove valuable for classification of defects. Machine learning seeks to develop theories and computer systems for representing; classifying, clustering, and recognizing; reasoning under uncertainty; predicting; and reacting to change.

Machine learning follows a simple structure:

Initialization:

- Determine the structure of the classifier – What data features will be used?
- Feed the system training data of known classes
- System tunes decision parameters based on training data.

Test:

- Using the initialization data, when presented with a test the systems will determine the most probable class.
- While Bayesian Networks were studied, there are several other machine learning tools including: K-means clustering, support vector machines, artificial neural networks, genetic algorithms, and others.

3.7.4 Summary

Time reversal beamforming produces tighter focusing of energy therefore providing a sharper image of defect location. The time reversal beamforming technique provides greater resolution, therefore enabling the possibility of imaging multiple defects. This technique reduces clutter and therefore should perform better under noisy conditions.

Bayesian networks were investigated to classify defects. Using simulated data, the algorithms show promise as a classifier. Additional testing using laboratory data is required to draw further conclusions. In general, additional machine learning techniques should be studied in order to maximize the effectiveness of the classifier.

3.8 Task 8 – Proof of Concept Development and Implementation

3.8.1 Objective

The objective of this task was to ensure that the sensor system can be effectively deployed in an operational environment and to develop and test a proof of concept continuous monitoring/inspection system. Initial testing was performed on the sensor system to validate the performance of the proof of concept system. Strengths and weaknesses were documented for different applications of the system.

3.8.2 Approach

In order to simulate acoustic wave propagation in pipelines, the Advanced Infrastructure Systems (AIS) Laboratory established in the Department of Civil and Environmental Engineering at CMU, was used as a test bed site for this project. The intent of the AIS lab was to support

research in sensors and sensing for supporting the AIS mission of proactive data-driven infrastructure construction and maintenance. The lab contains a variety of test equipment such as high-speed data acquisition systems, arbitrary signal generators, signal amplifiers, power amplifiers, multiplexers and an oscilloscope. The lab also contains scientific engineering software such as LabVIEW, MATLAB®, ABAQUS, and COMSOL. Currently, the lab is supporting research sponsored by the NETL, National Science Foundation, Transportation Research Board, Bombardier, Inc. Bosch, Physical Acoustics Corporation, Yooshin Corporation, and Pennsylvania Infrastructure Technology Alliance.

A proof of concept test system was specified, procured, and built with National Instruments (NI) hardware. Computer simulation tools were identified and procured in order to support modeling and simulation of acoustic wave propagation. An extended proof of concept system was identified to allow future long distance testing.

In addition, CTC consulted with gas pipeline industry representatives throughout the duration of the project. The goal was to obtain industry input throughout this project to ensure the system is usable. CTC sought guidance on the implementation of the sensor system at a natural gas representative testing area.

3.8.3 Results

The simulation was accomplished using two Dell® workstations using PZFlex acoustic simulation software. MATLAB® was also used for data processing and large array calculations, localization and imaging.

The computers used for modeling and simulations were configured as detailed in Table 3-4.

Table 3-4. IPI Simulation and Modeling Development System

IPI Development System	
Equipment	Description
Dell Precision T7400 Workstation	Intel Xeon E5405 Quad Core Processor
	Windows XP Pro - 32 bit
	4GB DDR2 667MHZ FDB SDRAM
	250GB SATA Hard Drive
PZFlex Professional	Virtual Prototyping Software

Much of the laboratory experiments were performed using bench-top hardware based on NI. The hardware used a NI chassis with a waveform generator card, a digital to analog converter card, and a multiplexer card.

The specific configuration of the NI equipment as shown in Figure 3-37 including model numbers details shown in Table 3-5.

Table 3-5. Laboratory Test Equipment (Configuration)

National Instruments Test Bench	
Equipment	Description
Chasis	PXI-1031-4-slot 3U
Controller	PXI-8106-Core 2 Duo 2.16 GHz
AWG	PXI-5421-100 Ms/Sec
Digitizer	PXI-5122-2 ch., 14-bit, 100MHz
Multiplexer	PXI-2530-High Density
Terminal Block	TB-2631
Coaxial Cable	SMB112 Double Shielded SMB BNC
LabVIEW	Measurement and Automotive Software

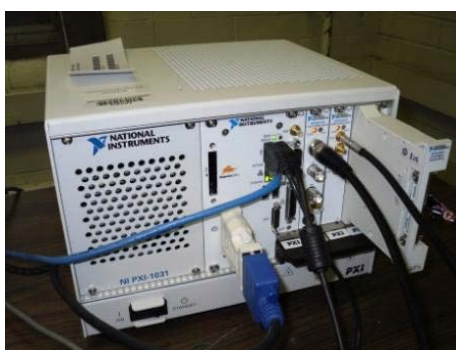


Figure 3-37. Laboratory Test Equipment (Photograph)

While there are many options for an extended proof of concept system, a preferred system would use an additional and identically equipped NI Test Bench. The hardware could be networked (wired or wireless) for long distance testing. As an added feature, the additional test bench could serve as a backup in the event of damage.

3.8.4 Summary

A proof of concept systems was designed, procured and built with NI hardware. The laboratory equipment was used for nearly all laboratory experiments on this project. An extended proof of concept system was developed that extends this single node system to a multi-node system. The additional nodes are copies of the single node to allow substitution in the case of damage. Computer hardware and simulation tools were identified, procured and configured using two Dell workstations and PZFlex simulation software.

3.9 Task 9 – Technology Transition

3.9.1 Objective

IPI team documented the technical challenges that the sensor research and validation overcame and address the potential impacts on the target markets. IPI team continued consulting with pipeline application experts to review the technology transition needs.

3.9.2 Approach

Technology transition planning was based upon the results and progress of the initial research phases. The goal for this phase of the research was to perform initial technology transition research and to determine the necessary extended transition plan for future phases based on the outcomes of the research.

3.9.3 Results

The following identifies the basic steps required to achieve successful technology transition beyond the scope of this effort.

3.9.3.1 General TRA refinement

There is a need to continue to investigate and improve Time Reversal Acoustics-based methods for detecting the presence of faults and failures in buried pipes. In this effort, TRA using ultrasonic sensors proved to be highly effective for the detection of defects in a multimodal and dispersive steel pipe environment. Refining these methods will provide improved system performance and design systems to operate in varying, unpredictable environments.

There is a need to continue to investigate waveguide propagation and the design of signals for defect detection. Waves that propagate in pipes are typically dispersive and multimodal. For example, there exist longitudinal modes, torsional modes, and flexural modes in pipes. This multimode phenomenon in pipe wave propagation limits the application of waves in conventional methods for defect detection. In contrast with conventional detection methods, the strength of TRA-based detection lies in its ability to benefit from the multiple modes and propagation paths as well as waveform dispersion, and to allow the coherent transmission of signals between transducers. The signal excitations used in TRA are not limited to using only low frequency and small bandwidth. Simulation and experimental results have shown that TRA improves, over other conventional methods, the spatial and temporal focusing of waves through inhomogeneous mediums. TRA focusing leads to a higher signal-to-noise ratio in detection; it manifests itself as a strong peak at the receiver when a defect is present. This peak clearly indicates a change in the pipe. The observed peak is the result of a change in the pipe transfer function induced by the defect. As the damage in the pipe increases, so does the size of the time reversal peak. Many questions remain to be answered; for example, the robustness of the TRA detection algorithm to changing temperatures, gas pressure, and the baseline data. The sensitivity of the TR algorithm can be extensively tested using the finite element simulation software, PZFlex, by changing the material properties, bonding conditions, and sensor characteristics that are caused by these variations in the temperature, gas pressure, and other environmental factors. There is a need to investigate adaptive TRA methods for detecting defects in both colored noise and non-stationary noise. These factors are useful in development of a robust detection method, which is invariant to common complicating influences found in a real-world environment.

General Classification and Localization

There is a need to continue to research and refine the ability of TRA to classify and localize flaws that have developed in pipes. Defect classification and localization are two important problems in pipeline monitoring. There is a need to investigate localization of defects, in order to provide knowledge to the user about the location of potential pipe failures and enable the user to excavate the appropriate sections of pipe.

- Defect classification: Investigate how pipeline defects can be identified by their characteristic responses to given excitation modes. These unique responses are often referred to as signature waveforms. Damage classification can be formulated as a problem of signature representation and identification. A good representation of signatures greatly simplifies the design of the classifier. Time-frequency representations and wavelet analysis are promising candidates for defect classification. Time-frequency representations describe defect signatures by linear combination of basic functions or atoms chosen from a complete dictionary. Each dictionary is a set of time-shifted, frequency-shifted, and time-scaled atoms that are normalized to have unit energy. By comparing the coefficients of a defect signal and those of the signatures stored in a database, it is possible to classify the defect using distance measures. When time reversal is used, it is anticipated that the mode representation can be simplified because of the focusing effect due to time reversal.
- Defect localization: Use sparsely deployed transducers along a pipeline to locate the defects. Further investigate the use of two clusters of sensors on a section of a pipe in a multi-static configuration. By calculating the reflectivity map of the pipe of interest, it should be possible to identify the location of the defect on the pipe. In addition to localization of failures, investigate methods to determine the magnitude of defects within the pipe and which class of failure is experienced. In this effort, the team developed rudimentary methods using time-reversal acoustics for measuring the relative magnitude of the failures. There is a need to expand upon these methods in order to provide a metric or scale to determine the magnitude of damage in the pipe and the probability of failure in a certain time period. This will allow the pipeline administrator to better gauge the risks.

Machine Learning

The transducer network deployed along a pipe will provide a large amount of sensor data in real time. A major focus of machine learning research is to automatically learn to recognize complex patterns and make intelligent decisions based on data. One of the key challenges in the design of a reliable damage detection and classification system is the ability to account for the variability inherent in sensor data. This variability might arise due to material properties, geometry variation, sensor characteristics, debonding issues, measurement noise, or other environmental factors such as temperature. Sensor data variability results in high false alarms. There is a need to develop machine learning techniques for detection, classification, and localization to minimize false alarms. In investigation of classification techniques, it is required to consider two different goals. The first is classification of damage types, such as corrosion and stress failures, and the second is adaptation of the sensors to time-varying environmental conditions in order to minimize false alarms. The implementation of machine learning techniques will assist these research goals, and may include SVMs and Pattern Recognition (PR) algorithms. These techniques can be used to identify different classes of failure using known training data. Machine learning methods can also be used to help sensors adapt and adjust to individual varying environments over time.

Intelligent Pipe

There is a need to investigate practical methods for integration or embedded placement of sensors within the pipeline. These investigations would include different methods for placement of the sensors, above and below the corrosion-resistant coatings of existing pipe sections and potential methods for directly manufacturing embedded sensors in new pipes. Also, the need exists to investigate, through simulations and experiments, different arrangements of sensor arrays, and how those arrangements affect performance.

Extended Proof of Concept System

In order to demonstrate the effectiveness of TRA fault detection, the purchase the necessary components to construct an expanded proof of concept system is required. This system would be capable of monitoring a section of pipe and generating a warning whenever faults in the pipe exceed a specified threshold. Appropriate threshold levels will be determined to ensure that failures are detected with a very high probability, while false alarms are minimized, and the system will be configured accordingly. In order to optimize power use, there is a need to explore the relationship between the power used to excite waves, the distance of useful wave propagation, and the probability of false alarm across that length.

Additionally the investigation into the development of an intelligent pipeline system for distributed monitoring of a natural gas pipeline would be of value. Due to the great size of a natural gas pipe network, strategies where local data must be transmitted to a centralized processing unit are costly to implement and may be weakened by a single point of failure. Distributed strategies allow for a more robust, easier to implement system. However, there are significant challenges involved with processing the enormous amounts of data collected by large-scale sensor networks. There is a need to develop efficient algorithms that minimize sensor resource requirements (i.e. power consumption, bandwidth, or storage) as well as the time to distribute the local information. An effort to investigate the prospect of using local communication between sensors in order to assess the probability of failure across the entire pipeline, and to determine an appropriate communication strategy to relay failure decisions to the user is also worthy of additional research. The proof of concept system could utilize data collected from field tests to determine appropriate threshold levels and will include several sets of sensors to test the network communication schema.

Environmental

Uncontrolled environmental effects play a large role in wave propagation in real world scenarios. Changes in temperature will compress and contract steel pipes and affect how waves travel across them by altering the wave speed. Water, dirt, or materials that surround the pipe will suppress and absorb specific wave modes. Pressure loading, such as vehicles traveling above a pipeline, will also distort the steel slightly and affect the traveling waves. There is a need investigate how these environmental effects affect wave propagation. This knowledge is essential for developing robust algorithms and methods for detecting, locating, and classifying defects. The environmental effects will be studied and tested using models and simulation techniques and verified through experimental observation. This task will involve modeling, testing, and documenting environmental loading on pipes, the effects of pressure, liquid, road vibrations and other effects. Use of finite element methods to simulate a pipe sample with different corrosion conditions, crack lengths, and piezoelectric sensor signals would provide valuable information. Physics-based modeling could be used to analyze various environmental

loading conditions. The use of PZFlex simulation software to provide design guidelines for defect detection, classification, and localization under a variety of conditions could also yield promising results. In addition, lab experiments to test various loading condition and to verify simulation models would need to continue.

Pipeline Configurations

In addition to environmental conditions, pipeline specifics such as coupling, joints, and welds also affect wave propagation. At welds, new metals are introduced into the pipe, often with different material properties than that of the pipe itself. This welded area will scatter waves and generate new wave modes. However, the degree to which these affects occur is unknown. Similarly, the propagation of waves across joints is important to the distribution of energy in each section of the pipe. Thus, there is a need to investigate how welds and pipe configurations affect wave propagation in order to optimize sensor placement and TRA signal processing algorithms.

3.9.4 Summary

The technical challenges that the sensor research and validation overcame were addressed in this report and the attachments. Technology transition planning was conducted based on the results and progress made throughout this effort. As detailed in the results above, technology transition research and extended transition planning for future phases were executed based on the outcomes of the research.

4.0 REFERENCES

1. U.S. Department of Energy (DOE) Energy Information Administration (EIA), available online http://www.eia.doe.gov/pub/oil_gas/natural_gas/analysis_publications/ngpipeline/mileage.html
2. Techlines, U.S. Department of Energy (DOE) Office of Fossil Energy, available online at <http://www.fossil.energy.gov/news/techlines/index.html>
3. American Gas Association, available on line at <http://www.aga.org/Kc/aboutnaturalgas/consumerinfo/CausesofNGPipelineAccidents.htm>
4. DOE-Funded Pipeline Robot Revolutionizes Inspection Process - Explorer II Demonstrates Huge Potential for Hard-to-Reach Gas Line Inspections, NETL Publications News Release, December 04, 2007, available online at http://www.netl.doe.gov/publications/press/2007/071204-Pipeline_Robot_Revolutionizes_Inspection_Process.html
5. J. B. Nestleroth, T. A. Bubenik, and Harvey Haines, *Magnetic Flux Leakage (MFL) Technology for Natural Gas Pipeline Inspection*. Topical Report, November 1992, available through the National Technical Information Center.
6. Remote Field Eddy Current Technology for Inspecting “Unpiggable” Pipelines, available online at <http://www.gastechnology.org/>
7. Ultrasonic Technology for Gas Pipeline Inspection, available online at <http://www.gastechnology.org/>
8. W. E. Roper and S. Dutta, Remote Sensing and GIS Applications for Pipeline Security Assessment, available online at <http://gis.esri.com/library/userconf/proc05/papers/pap1762.pdf>
9. M. Hirao and H. Ogi, *An SH-wave EMAT technique for gas pipeline inspection*, NDT&E International, Vol. 32, pp 127-132, 1999.

10. *Innovative Sensors for Pipeline Crawlers to Assess Pipeline Defects and Conditions*, Oil & Natural Gas Projects Transmission, Distribution, & Refining (DE-FC26-03NT41881), available online at http://www.netl.doe.gov/technologies/oil-gas/NaturalGas/Projects_n/TDS/TD/T&D_A_41881Crawlers.html
11. *Multi-purpose Acoustic Sensor*, Los Alamos National Laboratory (LA-UR-02-5703), available online at <http://www.netl.doe.gov/publications/proceedings/02/naturalgas/5-3.pdf>
12. *Dual Field MFL Pig May Provide Best of Both Worlds*, *Pipeline & Gas Journal*, Oct, 2005
13. H. Kwun, J. J. Hanley, and A. E. Holt, *Detection of Corrosion in Pipe Using Magnetostrictive Sensor Technique*, *Nondestructive evaluation of aging maritime*, SPIE, Vol. 2459, pp. 140-148, 1995.
14. *Brittle-like cracking in plastic pipe for gas service*, Special Investigation Report, National Transportation Safety Board, Washington D.C. 20594, available online at <http://www.nts.gov/Publicatn/1998/SIR9801.pdf>
15. *Capacitive Sensor for Polyethylene Pipe Inspection*, National Energy Technology Laboratory (NETL).

APPENDIX A:
Peer Reviewed Technical Society Papers



Published Papers

Preliminary studies on the dispersion of signals produced by permanently installed MFC transducers for pipeline monitoring

A. Agrawal¹, J. Harley¹, Y. Ying¹, J.H. Garrett Jr.¹, H. Sohn², L. Soibelman¹
¹Carnegie Mellon University, USA, ²Korea Advanced Institute of Science and Technology, South Korea
lucio@andrew.cmu.edu

Abstract. The paper provides an initial study of the dispersion and attenuation of signals produced by permanently installed Macro Fiber Composite (MFC) transducers on pipelines for monitoring these pipelines. Important issues that have been investigated include the dispersion characteristics of the different wave propagation modes on a pipe generated by the MFC patches. These issues have been investigated by comparing results from experiments and simulations. Developing an accurate numerical simulation is important for predicting the potential of new defect detection techniques before investing the resources involved in performing extensive physical experiments and prototyping.

Using finite element simulations, guided wave propagation in a hollow cylinder has been shown to be comparable with results from an equivalent experimental setup. In addition, the use of an alternate transducer-structure interaction model has been shown to be effective in modeling guided wave propagation in hollow cylinders. The results show a positive correlation between the guided wave modes observed and theoretical dispersion characteristics.

1 Introduction

There has been an increasing demand for using Structural Health Monitoring (SHM) and nondestructive testing (NDT) techniques for the purpose of monitoring damage in civil infrastructure as well as aerospace and mechanical systems. In order to build reliable monitoring systems, many SHM and NDT techniques have been developed and tested for different types of structures [1-4]. Among these techniques, the active sensing technique based on piezoelectric transducers has been widely used for monitoring plate-like structures such as aircraft panels and steel girders [5,6]. Since the 1960s, a particular type of guided wave known as a Lamb wave has been studied in great detail for the nondestructive testing of plate-like structures [5, 7, 8]. Lamb waves are one type of guided waves that exist in thin plate-like structures, and are constrained by two free surfaces [9]. For the purpose of application to NDT and SHM, Lamb waves have been a topic of study because they can propagate over considerable distances and cover large areas of thin plates with little attenuation.

Recently, there has been significant interest in monitoring thousands of miles of pipelines transporting oil and natural gas. Gas pipeline accidents have become a common problem associated with damaged pipes [11,12]. A significant effort has been made towards understanding guided wave propagations in hollow cylinders, such as pipes, and other complex structures [13-17]. Guided waves are useful for detecting corrosion, cracks, notches, delamination in composites, etc. because of the sensitivity of these waves to surface and internal damage and the ability to propagate over long distances [18,19]. However, guided wave propagation in hollow cylinders is complicated due to the presence of multiple modes at each frequency and its dispersion characteristics [5].

This paper focuses on (1) developing numerical simulations using the commercial finite element software PZFlex [24] for the theoretical model developed by Raghavan and Cesnik [20]; (2) demonstration of the agreement of these finite element simulations with an

experimental analysis done using MFC transducers for exciting and sensing guided waves in pipelines; and (3) establishing the capability of the finite element simulations as well as the experimental data to represent the conventional guided wave dispersion curves obtained using the open source software PCDISP [25].

2 Theory

Guided waves are mechanical waves that have wavelengths of the same order of magnitude as the thickness of a structure such, as a flat plate and a hollow cylinder, having a thin cross-section. They occur in an infinite number of discrete modes, each travelling at a different speed, with the speed in turn being a complex function of frequency [22]. These modes occur when longitudinal and shear wave reflections constructively interfere and energy propagates through the thickness of the structure [22].

Chree has discussed the propagation of harmonic waves in an infinitely long cylindrical rod on the basis of the linear theory of elasticity [23]. Several researchers have tried to study these waves propagating in a hollow cylinder, under the restriction of axial symmetry of motion [13-15]. Gazis has extended this study to the most general type of harmonic waves in a hollow circular cylinder of an infinite length [16] and has obtained a characteristic equation, within the framework of the linear theory of elasticity, for the eigenmodes of an isotropic continuous medium that is bounded by two concentric cylindrical surfaces.

Guided waves in hollow cylinders are similar to those in flat plates. In hollow cylinders, however, the propagation of guided waves becomes much more complicated than in flat plates, due to the different geometry and boundary conditions. Therefore, guided waves in a plate can propagate infinitely far from the actuator location, but guided waves in a hollow cylinder can repeatedly propagate around the cylinder's continuous circumference.

There exist three fundamental classes of guided wave modes in hollow cylinders. These are

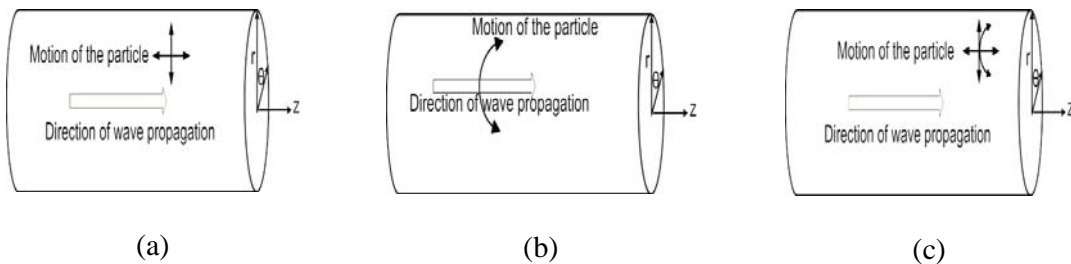


Figure 1: (a) Longitudinal, (b) Torsional, (c) Flexural guided wave modes

the longitudinal, torsion and flexural modes as shown in Figure 1. In addition to these three modes, there exist a class of circumferential modes in which the waves propagate along the circumference of the cylinder. The nomenclature for the three types of modes present in hollow cylindrical waveguides have been outlined by Silk and Bainton [17] and then modified by Demma, et al. [18] for their software, DISPERSE. The three types of modes are the longitudinal modes $L(0,n)$, the torsional modes $T(0,n)$ and the flexural modes $F(m,n)$. In this notation, m represents the harmonic number of circumferential variation and n is an index counter [17]. The longitudinal and torsion modes are axisymmetric with respect to the cylinder's axis, but the flexural modes are not.

As the radius of the cylinder tends to infinity, the guided wave modes in the hollow cylinder correspond to guided wave and horizontal shear waves in the flat plate. One difficulty with guided wave techniques, in general, is that the modes are dispersive, meaning that the group speed of the modes varies with changing driving frequency. Thus, the shape of the propagating wave changes with distance making the interpretation of results difficult [17].

Raghavan and Cesnik [20] determined theoretical expressions for the response of a hollow cylinder to axisymmetric loading starting with the governing equations of motion from elasticity. The boundary conditions were modified to include the effect of excitation by piezoelectric actuators as shown in Figure 2. The advantage of this approach lies in the fact that it reduces the computation time as compared to a multi-physics model in which piezoelectricity of the transducers needs to be modelled, thereby increasing computation time.

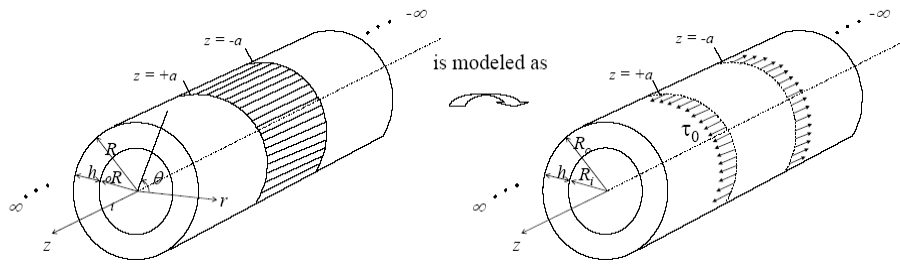
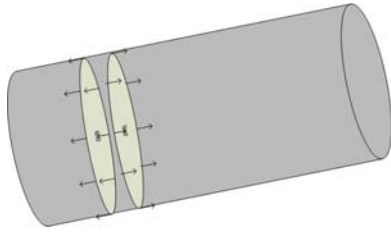


Figure 2: Configuration of surface bonded piezoelectric actuators on a hollow cylinder and the modeled representation [20]

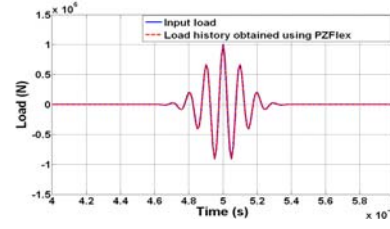
In this study, the numerical simulations were performed using the above model. In addition to that, the results from the simulations were compared to the experimental data, thereby providing experimental validation for the transducer-structure interaction model. The experiments have been described in Section 4 of the paper.

3 Numerical Simulations of Guided Wave Propagation

The numerical simulations for this study were carried out using PZFlex, the finite element simulation software program designed to analyze the response of continuous media subjected to dynamic or static loads. Table 1 describes the configuration of the numerical simulations. The dimensions of the hollow cylinder were chosen to be the same as that of the pipe specimen that was used in the experiments, which have been described in Section 4. Figure 3 shows the axisymmetric loading being applied on the hollow cylinder. In order to study the different phenomena associated with guided wave propagation, numerical simulations were done at excitation frequencies of 100, 130, 150 and 170 kHz. . This range was chosen such that the guided wave modes were not highly dispersive, meaning that the group speed of these modes varied little with changes in the driving frequency. If the guided wave modes are highly dispersive in the region of excitation, the large range of excited group speeds would make it difficult for us to observe the different modes distinctly. The finite element mesh was refined until convergence was observed. By doing so, the reliability of the finite element simulations can be increased by removing the possibility of an inappropriate mesh size. Figure 4 shows the mode separation obtained using PZFlex as well as from experiments.



(a)



(b)

Figure 3: (a) Loading on the hollow cylinder, (b) Loading function

Table 1: Description of numerical simulations

Material	Steel
Density	7890 kg/m ³
Pressure wave velocity C_p	5790 kg/m ³
Shear wave velocity C_s	3100 m/s
Inner radius r_i	0.102 m
Outer radius r_o	0.11 m
Length	1.5 m
Damping	No damping
Sampling rate	6.81 MS/s
Element type	4 noded quadrilateral
Mesh size (z-axis x thickness x circumference)	0.00125m x 0.0011m x 1 degree

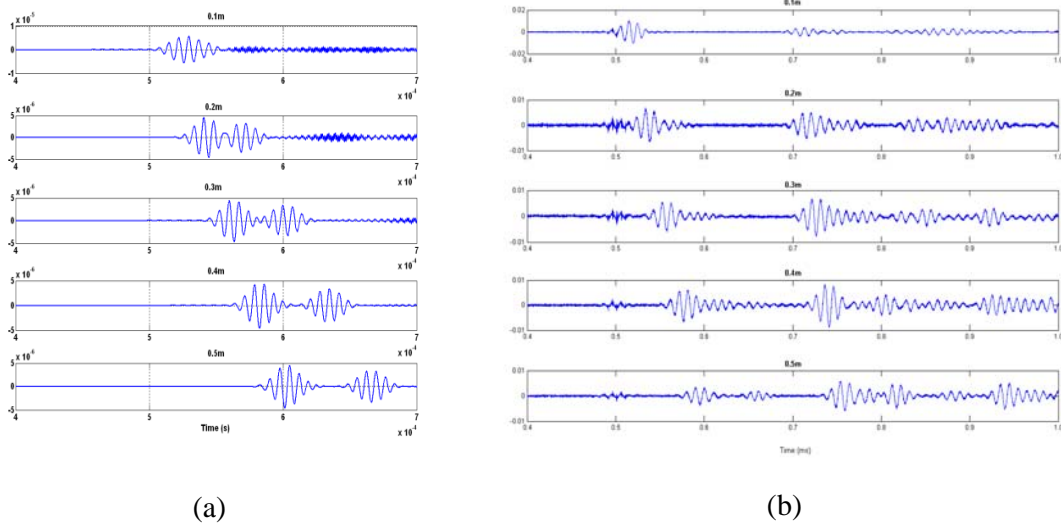


Figure 4: (a) Mode separation in simulation (b) Mode Separation in experiment

The PZFlex simulations were used to determine the group speeds of the L(0,1) and L(0,2) modes, which were compared to the theoretical dispersion curves obtained using the software PCDISP [26]. The comparison has been shown in Figure 5. The group speeds of these two modes obtained using these two different methods were observed to be similar.

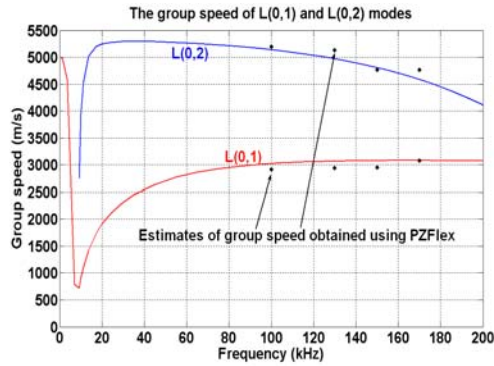


Figure 5: Theoretical group speed vs PZFlex results

The axisymmetric loading was then modified to non-axisymmetric loading, by reducing the axisymmetric line loads all around the circumference to arcs with dimensions corresponding to that of the MFC transducers, representing a single MFC transducer attached to the hollow cylinder.

4 Experimental Analysis

Numerical simulations give us the ability to predict the guided wave modes in hollow cylinders without the need of doing experiments. However, before we can do that, it is necessary to compare the numerical simulations with experiments. The experimental study

was carried out using a carbon steel hollow cylindrical specimen. Figure 6 shows the dimensions of the pipeline specimen and the placement of the MFC transducers on the specimen. The inner radius of the specimen was 0.102m and the outer radius was 0.11m. The specimen was 1.5m in length and was large enough such that the guided waves could be examined without being concerned with reflections from the boundaries of the hollow cylinder. In this study, MFC transducers made by Smart Materials Inc. [21] were attached to the hollow cylinder using the cyanoacrylate adhesive for the purpose of generating and sensing guided waves. The advantage of using MFC transducers is their flexibility, allowing them to be placed onto the unaltered surface of a pipe. Fig. 5 shows the schematic diagram of the dimensions and arrangement of the MFC transducers on the pipe specimen, with one exciting transducer and four sensing transducers at angular positions of 0°, 90°, 180° and 270° relative to the exciting transducers. The MFC transducers used in this study are of P1 type, made of PZT5H2 type of PZT material and measuring 28mm x 14mm. The orientation of the PZT fibers is along the longitudinal direction, thereby mainly producing excitation in that direction.

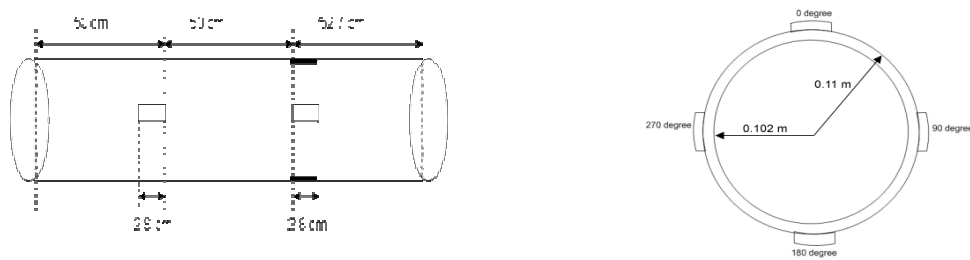
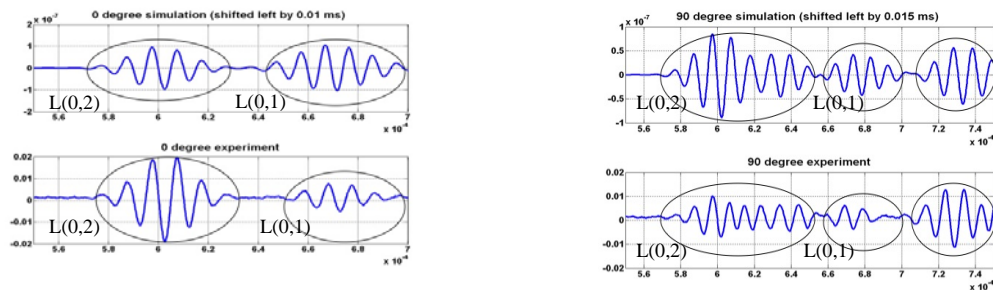


Figure 6: The dimensions of the specimen

The experimental results which show the output voltage signal at the four MFC transducers were compared with the results from the numerical simulations. Figure 7 illustrates that the numerical simulations match closely with the experiment results with respect to the modes generated as well as the group speed of each mode at each of the transducer located at 0, 90, 180 and 270 degrees as shown in Figure 6. The response in the experiments is in form of the voltage generated in the transducers due to the mechanical vibrations due to the propagating guided waves. For the numerical simulations, the response is in form of the strain induced across a patch on the outer surface of the hollow cylinder, with dimensions and location same as that of the transducer in the experimental specimen. Since the voltage in the transducers is directly proportional to the strain, it is possible to compare the guided wave modes generated as well as their propagation speeds.



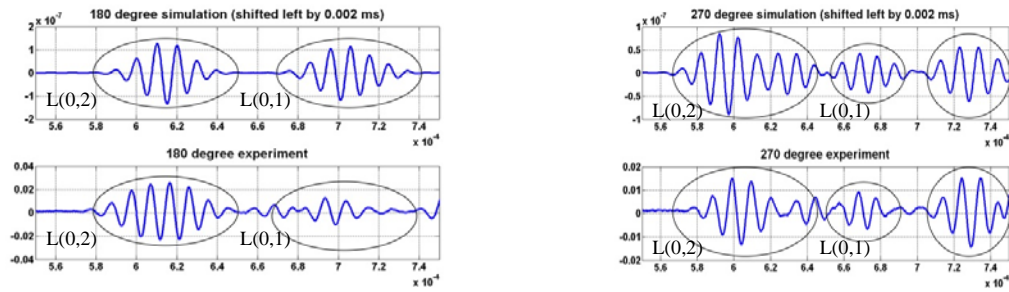


Figure 7: Numerical simulations vs Experimental results

5 Conclusions

In addition to demonstrating the applicability of MFC transducers for exciting and sensing guided waves in pipelines, this paper provides numerical validation of the theoretical transducer-structure interaction model described by Raghavan and Cesnik [20] which uses an alternate loading model for representing the piezoelectric transducers. The simulation results were compared with the experiments and the correlation observed between the numerical simulations and experiments provides experimental validation for the theoretical model.

Through validation of a the theoretical model in [20], this model can be used to estimate the performance of damage detection techniques prior to the need to do tedious and time consuming experiments in the initial stages of investigation. The use of an equivalent loading model in place of modelling MFC transducers helps to simplify the modelling effort as well as make the implementation of numerical simulations more efficient since the introduction of electromechanical elements in simulations is expected to increase the implementation time.

References

1. Sohn H, Park H W, Law K H and Farrar C R (2007). Damage Detection in Composite Plates by Using an Enhanced Time Reversal Method *Journal of Aerospace Engineering*, ASCE
2. Kim S D, In C W, Cronin K E, Sohn H and Harries K (2007). A Reference-Free NDT Technique for Debonding Detection in CFRP Strengthened RC Structures *Journal of Structural Engineering*, ASCE
3. Giurgiutiu V (2003). Embedded NDE with Piezoelectric Wafer Active Sensors in Aerospace Applications *Journal of Materials*
4. Giurgiutiu V and Zagari A (2005). Damage Detection in Thin Plates and Aerospace Structures with the Electro-Mechanical Impedance Method. *Structural Health Monitoring* 4(2) 99-118
5. Sohn H, Park G, Wait J, Limback N and Farrar C R (2004). Wavelet-Based Active Sensing for Delamination Detection in Composite Structures. *Smart Materials and Structures* 13 153-160
6. Wang C H, Rose J T and Chang F K (2004). A Synthetic Time-Reversal Imaging Method for Structural Health Monitoring *Smart Materials and Structures* 13(2) 415-423
7. Moulin E, Assaad J, Delebarre C, Kaczmarek H and Balageas D (1997). Piezoelectric Transducer Embedded in a Composite Plate: Application to Lamb Wave Generation. *Journal of Applied Physics* 82(5) 2049-2055 74

8. C.A. Paget, S. Grondel, K. Levin and C. Delebarre (2003). Damage Assessment in Composites by Lamb Waves and Wavelet Coefficients. *Smart Materials and Structures* 12(3) 393-402
9. I. Viktorov (1967). *Rayleigh and Lamb Waves*, Plenum Press, New York
10. Graff K F (1991). *Wave Motion in Elastic Solids* (New York: Dover Publications)
11. National Transportation Safety Board (2001). Natural Gas Pipeline and Fire near Carlsbad, New Mexico, August 19, 2000 Pipeline Accident Report NTSB/PAR-03/01, 1-57, Washington, D.C
12. National Transportation Safety Board (1999). Pipeline Rupture and Subsequent Fire in Bellingham, Washington, June 10, 1999 Pipeline Accident Report NTSB/Par-02/02, 1-79, Washington, D.C.
13. Ghosh J (1924). Longitudinal Vibrations of a Hollow Cylinder *Bulletin of Calcutta Math. Soc.* 14 31-40
14. McFadden J A (1954). Radial vibrations of thick-walled hollow cylinders *Journal of the Acoustical Society of America* 26 714-715
15. Herrmann G and Mirsky I (1956). Three-Dimensional and Shell-Theory Analysis of Axially Symmetric Motions of Cylinders *Transactions of the American Society of Mechanical Engineers* 18 563-568
16. Gazis D C (1959). Three-Dimensional Investigation of the Propagation of Waves in Hollow Circular Cylinders *Journal of the Acoustical Society of America* 31 568-578 75
17. Silk M G and Bainton K F (1979). The propagation in metal tubing of ultrasonic wave modes equivalent to Lamb waves *Ultrasonics* 27 11-19
18. Demma A, Cawley P, Lowe M, Roosenbrand A G (2003). The reflection of the fundamental torsional mode from cracks and notches in pipes *Journal of Acoustic Society of America* 114 611-625
19. Lowe M J S, Alleyne D N, Cawley P (1998). Defect Detection in Pipes Using Guided Waves *Ultrasonics* 36 147 154
20. Raghavan A and Cesnik C E S (2007). 3-D Elasticity-Based Modeling of Anisotropic Piezocomposite Transducers for Guided Wave Structural Health Monitoring *Journal of Vibration and Acoustics* (A special edition on Structural Health Monitoring)
21. www.smart-material.com
22. Rose J L (1999). *Ultrasonic Waves in Solid Media* (UK: Cambridge University Press)
23. Chree C (1889). The Equations of an Isotropic Elastic Solid in Polar and Cylindrical Coordinates, Their Solutions and Applications *Transactions of Cambridge Philosophical Society* 14 250
24. Weidlinger Associates (2006). *Flex User's Manual*
25. Seco F, Martin J M, Jimenez A, Pons J L, Ceres R (2002). PCDISP: A Tool for the Simulation of Wave Propagation in Cylindrical Waveguides 9th International Congress on Sound and Vibration, Orlando, Florida

Title: *Focusing of Ultrasonic Waves in Cylindrical Shells using Time Reversal*
for Proceedings of the **7th International Workshop on Structural Health
Monitoring 2009**

Authors: Joel Harley
Nicholas O'Donoghue
Joe States
Yujie Ying
James Garrett
Yuanwei Jin
José M.F. Moura
Irving Oppenheim
Lucio Soibelman

ABSTRACT

This paper investigates time reversal focusing techniques for the development of low-power, long-range, structural health monitoring applications for pipelines. We analytically examine time reversal's ability to compensate for unwanted multi-modal and dispersive behavior that are characteristic of guided waves travelling through pipes. We then develop a method to illuminate changes caused by structural damage using time reversal focusing as a pitch-catch operation. Using experimental and finite element simulation results with two transducers, we demonstrate these concepts and show that time reversal focusing provides a clear, interpretable metric for the characterization of damage in a pipe.

INTRODUCTION

The excitation of guided waves has become a popular tool for the nondestructive inspection of pipes and other physical infrastructures due to their potential to travel great distances [1,2]. Current pipeline inspection technologies often use rings of transducers pneumatically fastened to a pipe and operate in a pulse-echo mode [2,3]. Unfortunately, the inspection of buried pipelines is often expensive since it requires excavation and uses high transmission powers to achieve long distance guided wave propagation [3].

J. Harley, N. O'Donoghue, J.M.F. Moura, Dept. of Electrical & Computer Engineering, Carnegie Mellon University, Pittsburgh, PA 15213, U.S.A.

J. States, Y.Ying, J.Garrett, I.Oppenheim*, L.Soibelman, Dept. of Civil & Environmental Engineering, Carnegie Mellon University, Pittsburgh, PA 15213, U.S.A., *ijo@cmu.edu

Y. Jin, Dept. of Engineering and Aviation Sciences, Univ. of Maryland Eastern Shore, Princess Anne, MD 21853, U.S.A.

This paper provides motivation for the use of time reversal acoustic methods for increasing low-power propagation distances and for the detection of damage within pipes. We demonstrate time reversal's applications for focusing waves, compensating for mode and dispersive effects, and illuminating damage through change detection. Unlike other time reversal experiments for pulse-echo pipeline inspection conducted by Deng [4], our work focuses on the use of pitch-catch operations for implementing low-cost, low-power, permanently installed monitoring systems.

THEORY

Guided Waves in Pipes

Guided waves form as a result of the interaction between harmonic waves propagating in a medium and those medium's boundaries. Guided waves that form in thin cylindrical shells, or pipes, (which will be referred to as pipe waves) share several characteristics with Lamb waves, which form in thin plates. Lamb waves are commonly used and have been widely studied [5,6]. Pipe waves are characterized by an infinite number of dispersive longitudinal and torsional modes and a doubly infinite number of dispersive flexural modes [7]. The longitudinal and torsional modes are both axisymmetric while each flexural mode exhibits an infinite number of non-axisymmetric circumferential mode orders [8].

Many pulse-echo systems use reflections from defects to localize and characterize damage. However, due to the reflections of numerous dispersive modes and the mode conversions that occur at the defects, the received echoes may be difficult to interpret. Figures 1a and 1b show that a 400 kHz Gaussian pulse is significantly distorted after traveling a distance of 1.8 meters in a pipe. This unwanted clutter resulting from multi-modal and dispersive behavior is sometimes referred to as coherent (not random) noise [2].

To reduce coherent noise, users and developers often use narrowband, low frequency, single mode excitations to suppress unwanted modes and to reduce the influence of dispersion. Transducer geometries and designs can often be exploited for mode selectivity [2,8,9]. Unfortunately, these solutions can often limit the effectiveness of guided wave propagation.

Time Reversal Focusing

Time reversal focusing is a technique developed and used to achieve improved spatial and temporal acoustic focusing over conventional methods in inhomogeneous mediums [10, 11]. The process relies on the reciprocity and linearity of a medium and the principle that physical processes, when reversed in time, will result with the time-reversed initial conditions of the original process. Time reversal has been studied for applications in pulse-echo nondestructive testing and imaging [12,13,14], radar [15,16,17], and communications [18]. It has been shown that time reversal is particularly effective in mediums with high concentrations of scatterers [15,16,17,19].

Time Reversal Compensation of Multiple Modes and Dispersion

Consider a pipe with two transducers. Waves traveling between transducers exhibit multiple modes and dispersion. When a signal $s(t)$ is transmitted from one transducer, the signal received at the second transducer can be expressed in the frequency domain as [20]

$$R(\omega) = K_e(\omega)K_r(\omega)G(\omega)S(\omega), \quad (1)$$

where $G(\omega)$ is the pipe transfer function (or the Fourier transform of the Green's function), $K_e(\omega)$ and $K_r(\omega)$ are the exciting and receiving transducer transfer functions, $S(\omega)$ is the Fourier Transform of $s(t)$, and ω is the angular frequency.

The pipe transfer function can be expressed as a linear combination, for each angular frequency ω , of M arbitrary modes

$$G(\omega) = \sum_{m=0}^M b_m(\omega) e^{-j\omega(d/v_m(\omega))}, \quad (2)$$

where d is the distance between the two transducers and $v_m(\omega)$ is the dispersive velocity of the mode. The complex exponential represents the travel time between the two transducers and $b_m(\omega)$ accounts for any propagation effects on that mode.

In the frequency domain, time reversal is equivalent to the negation of angular frequency ω . If we assume that $v_m(\omega)$ has even symmetry in frequency such that $v_m(\omega) = v_m(-\omega)$ and that $b_m(\omega)$ is real, then negating the angular frequency in $G(\omega)$ is equivalent to taking its complex conjugate and so

$$G(-\omega) = G^*(\omega). \quad (3)$$

To demonstrate that the benefits of time reversal derive from focusing and not from an overall increase in the excitation energy, we transmit the time reversed signal with the same energy as the original excitation. The excitation is scaled by

$$k = \sqrt{\frac{\int_{-\infty}^{\infty} |S(\omega)|^2 d\omega}{\int_{-\infty}^{\infty} |R(\omega)|^2 d\omega}}. \quad (4)$$

Now when the time reversed signal is transmitted back through the pipe, the received signal is expressed as

$$\begin{aligned} Y(\omega) &= kK_e^*(\omega)K_e(\omega)K_r^*(\omega)K_r(\omega)G^*(\omega)G(\omega)S^*(\omega) \\ &= k|K_e(\omega)|^2|K_r(\omega)|^2|G(\omega)|^2S^*(\omega) \end{aligned} \quad (5)$$

Due to the absolute values, the complex exponentials that represent time delays between each path and mode in (3) disappear. As a result, the delayed signals, which are generated by the modes and dispersion, focus at the receiver and significantly enhance the received signal.

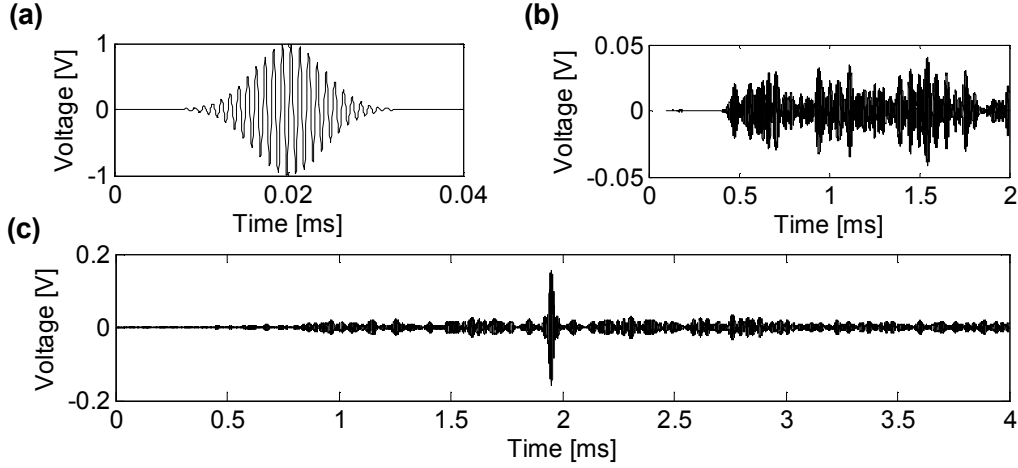


Figure 1. Experimental (a) 400 kHz Gaussian windowed excitation, (b) Received signal, (c) Time reversal focused signal

Time Reversal Focusing of Changes (Flaw-Induced Scattering)

A common method for detecting damage with pitch-catch experiments is change detection, where the change is caused by scattering from a flaw. Unfortunately, damage typically causes only small changes in the received signal. However, if those changes are time reversed and retransmitted through the medium, they are also focused. This provides a metric for detection of damage in the pipe.

Consider again a pipe with two transducers. For simplicity, assume that $K_e(\omega) = I$ and $K_r(\omega) = I$ so that the signal can be expressed as [17]

$$R(\omega) = G_{C+T}(\omega)S(\omega) = (G_C(\omega) + G_T(\omega))S(\omega). \quad (6)$$

Here $G_C(\omega)$ represents the “clutter” response found when no damage is present on the pipe. The term $G_T(\omega)$ represents the “target” response generated by damage. Assuming the clutter response can be measured before any damage occurred and is therefore known, it can be subtracted from the received signal,

$$X(\omega) = R(\omega) - G_C(\omega)S(\omega) = G_T(\omega)S(\omega). \quad (7)$$

If the difference signal $X(\omega)$ is then normalized, time-reversed, and sent back through the pipe, the signal received can be expressed as

$$Y(\omega) = G_{C+T}(\omega)kX^*(\omega) = k(G_C(\omega) + G_T(\omega))G_T^*(\omega)S^*(\omega). \quad (8)$$

Since $G_C(\omega)$ has been assumed to be known and $X^*(\omega)$ calculated, then $kX^*(\omega)G_C(\omega)$ can be subtracted from (8), resulting in the equation

$$Y_T(\omega) = kG_T(\omega)G_T^*(\omega)S^*(\omega) = k|G_T(\omega)|^2 S^*(\omega). \quad (9)$$

The final result is similar to (5), except the focused signal is now composed exclusively from signals scattered by damage. It should be noted that while (5) and (9) can be obtained experimentally, they can also be computed mathematically from the measurements of (1), (6), and (7).

RESULTS

Experimental Results

The experiments were conducted using two PZT wafers bonded to the surface of a pipe with inner radius 30.15mm, outer radius 36.75mm, and length 3050mm. Each wafer was 5mm wide, 10mm long, and 1mm thick, and the two wafers were positioned 1.8m apart. One transducer operated as a transmitter and one as a receiver. Due to the principle of reciprocity, the response between the two transducers should be equivalent regardless of direction. Figure 1b shows the signal received from the 400 kHz Gaussian pulse excitation shown in figure 1a to contain a large amount of coherent noise and few distinguishable features. By contrast, after performing the time reversal focusing process, figure 1c shows a distinguishable peak in the center of the plot. This peak is formed as a consequence of the focusing and compensation of modes and dispersion as explained by (5).

In this demonstration of time reversal focusing, a narrowband excitation with a 400 kHz center frequency and 37 kHz bandwidth was chosen for two reasons. First, that center frequency excited a large number of modes and dispersive effects, as evident from the coherent noise in figure 1b. The frequency also provided a significant gain in signal-to-noise ratio over many lower frequencies with fewer modes and less dispersion. By significantly reducing the coherent noise associated with high frequency excitations, time reversal techniques allow for a greater degree of freedom when choosing excitations. This freedom also allows us to benefit from the use of wideband signals to extract and utilize more frequency information as in the following experiment results.

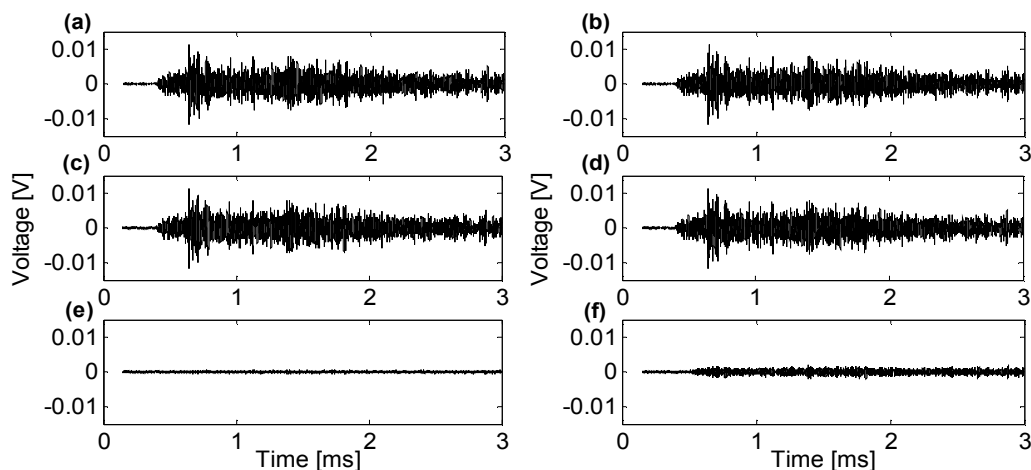


Figure 2. Experimental (a) Known clutter, (b) Known clutter, (c) Received signal with no damage present, (d) Received signal with damage present, (e) Difference of (a) and (c), (f) Difference of (b) and (d)

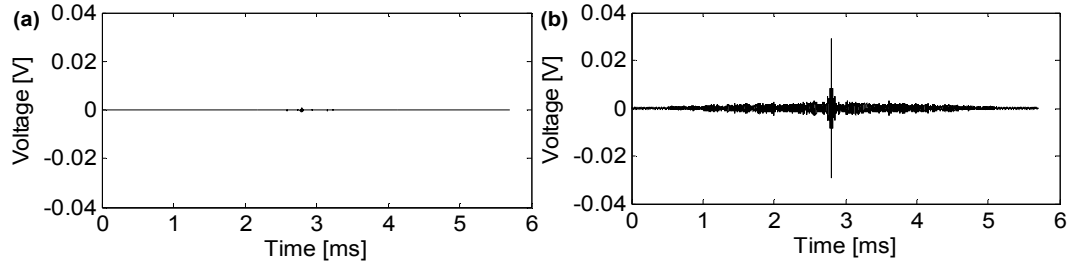


Figure 3. Experimental (a) Time reversal focusing of changes with no damage present, (b) Time reversal focusing of changes with damage present

To illustrate damage detection using time reversal, we used a wideband excitation. Figure 2 shows changes in a received signal from damage. The transmitter was excited by a wideband sinc pulse with a 300 kHz center frequency and 600 kHz bandwidth. To simulate damage physically, we created a small, partial-thickness sawcut. The cut is 1.5 mm deep, or only one-quarter of the pipe wall thickness, 1 mm wide, and 20 mm in arc dimension, less than one-tenth of the pipe's circumference; it is located 1095mm from the transmitting wafer. Figure 3 shows the signals which result by performing time reversal change focusing on figures 2e and 2f. In this instance, the plots in figure 3 were generated mathematically from the measured records using (9). The large peak in figure 3b is seen as an indication of change in the pipe due to the saw cut. The peak value with no damage is 1.05 mV whereas the peak value with damage measures 29.3 mV, a difference of almost 30 times or 29.5 dB.

Simulation Results

The experimental results were compared to simulation results obtained using the commercial PZFlex software suite. We matched the pipe and damage model to the specimen used in the laboratory. The excitation signal was modeled as a voltage across the two terminals of a PZT5a patch and the received signal modeled as the voltage induced at a second PZT5a patch, located 1.8m down the pipe. The received signal was recorded for 1.2ms during the forward transmission and 2.4ms while retransmitting.

Figure 4 illustrates the changes in the received signal for the undamaged and damaged cases. Figures 4a and 4b display the known background clutter with no noise. Figure 4c shows the received signal with no damage present and injected with white Gaussian noise to simulate additive measurement noise. Figure 4d displays the received signal with the simulated damage and injected white Gaussian noise. In both cases, the noise provided a signal-to-noise ratio of 40dB. Figures 4e and 4f show the two difference signals.

We performed time reversal change focusing on the two difference signals by transmitting them back through the channel and subtracting the extraneous information as in (8) and (9). We can see in figure 5 that the peak is 2.8mV when no damage is present and 35.3mV after damage has been added. This provides an increase of almost 13 times or 22dB. The reduced focusing gain, compared with the experimental results, can be explained by the shorter record length used.

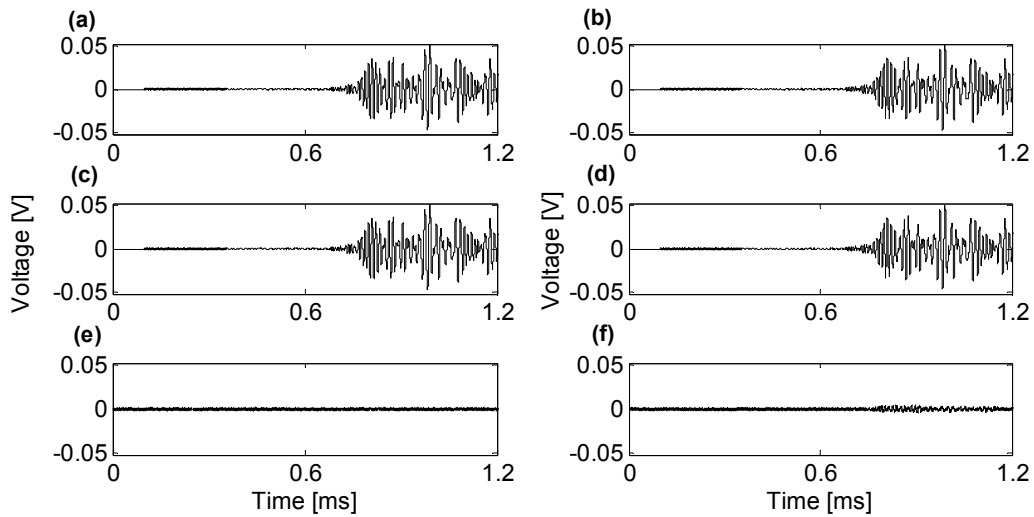


Figure 4. Simulation (a) Known clutter, (b) Known clutter, (c) Received signal with no damage present, (d) Received signal with damage present, (e) Difference of (a) and (c), (f) Difference of (b) and (d)

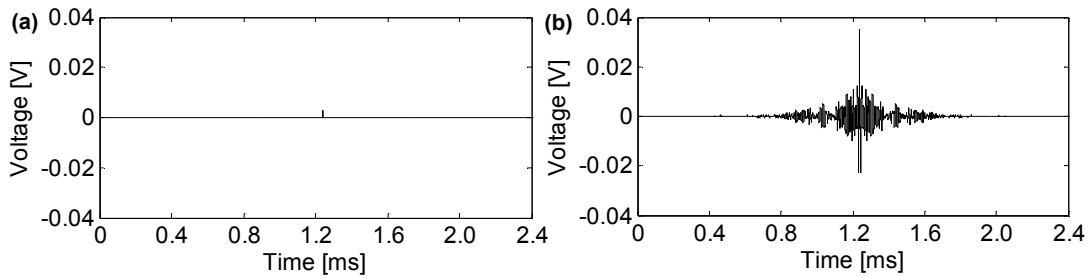


Figure 5. Simulation (a) Time reversal focusing of changes with no damage present, (b) Time reversal focusing of changes with damage present

CONCLUSIONS

The potential uses for time reversal focusing in pipes are numerous. Time reversal's ability to compensate for multiple modes and dispersion allow for the coherent transmission of waves between transducers. This allows investigators greater discretion when choosing a signal of excitation to achieve the greatest propagation distance and largest signal-to-noise ratios. Focused signals also present a distinguishable peak that can be used to better characterize a medium. For example, that peak is used as a metric for the presence of damage when performing a time reversal change focusing experiment. Due to its ability to compensate for modes and dispersion, time reversal also has much potential for nondestructive testing and structural health monitoring applications in other physical infrastructures as well as pipes.

ACKNOWLEDGMENTS

National Energy Technology Laboratory (NETL) is the funding source for this effort with Cost Share being provided by Carnegie Mellon University (CMU). Concurrent Technologies Corporation (CTC) is funded under a cooperative agreement with NETL. CMU is funded under a Subcontract Agreement with CTC. Nicholas O'Donoghue is supported by a National Defense Science and Engineering Graduate Fellowship, sponsored by the Army Research Office.

REFERENCES

1. Ditrai, John J. 1994. "Utilization of guided elastic waves for the characterization of circumferential cracks in hollow cylinders," *J. Acoust. Soc. Am.*, 96(6):3769-3775.
2. Cawley, P. 2003. "Practical Long Range Guided Wave Inspection - Managing Complexity," in *Rev. Prog. Quant. NDE*, 657:22-40.
3. Cawley, P. and M. J. S. Lowe. 2006. "Long Range Guided Wave Inspection Usage – Current Commercial Capabilities and Research Directions," Department of Mechanical Engineering, Imperial College London, London.
4. Deng, F., C. He, B. Wu. 2008. "Time Reversal Method for Pipe Inspection with Guided Wave," in *Rev. Prog. Quant. NDE*, 975:131-138.
5. Viktorov, I. A. 1967. *Rayleigh and Lamb waves: physical theory and applications*. Plenum Press.
6. Lowe, M. J. S., D. N. Alleyne, and P. Cawley. 1998. "The Mode Conversion of a Guided Wave by a Part-Circumferential Notch in a Pipe," *J. Appl. Mech.*, 65(3):649-656.
7. Li, J. and J. L. Rose. 2001. "Excitation and propagation of non-axisymmetric guided waves in a hollow cylinder," *J. Acoust. Soc. Am.*, 109(2):457-464.
8. Demma, A., et al. 2003. "The reflection of the fundamental torsional mode from cracks and notches in pipes," *J. Acoust. Soc. Am.*, 114(2):611-625.
9. Wilcox, P. D., M. J. S. Lowe, and P. Cawley. 2001. "Mode and Transducer Selection for Long Range Lamb Wave Inspection," *J. Intell. Matls. Sys. & Struct.*, 12(8):553-565.
10. Fink, M. 1992. "Time reversal of ultrasonic fields. I. Basic principles," *IEEE Trans. Ultrason. Ferroelec. Freq. Contr.*, 39(5):555-566.
11. Fink, M., C. Prada, F. Wu, and D. Cassereau. 1989. "Self focusing in inhomogeneous media with time reversal acoustic mirrors," in *IEEE Ultrasonics Symposium Proceedings*, 2:681-686.
12. Chakroun, N., M. Fink, and F. Wu. 1995. "Time reversal processing in ultrasonic nondestructive testing," *IEEE Trans. Ultrason. Ferroelec. Freq. Contr.*, 42(6):1087-1098.
13. Prada, Claire, et al. 2002. "Time reversal techniques in ultrasonic nondestructive testing of scattering media," *Inverse Problems*, 18(6):1761-1773.
14. Scalerandi, M., et al. 2008. "Selective source reduction to identify masked sources using time reversal acoustics," *J. Phys. D: Appl. Phys.*, 41(15):155504(12pp).
15. Moura, J. M. F. and Y. Jin. 2007. "Detection by Time Reversal: Single Antenna," *IEEE Trans. on Signal Processing*, 55(1):187-201.
16. Moura, J. M. F. and Y. Jin. 2008. "Time Reversal Imaging by Adaptive Interference Canceling," *IEEE Trans. on Signal Processing*, 56(1):233-247.
17. Jin, Y. and J. M. F. Moura. 2009. "Time-Reversal Detection using antenna arrays," *IEEE Trans. on Signal Processing*, 57(4):1396-1414.
18. Blomgren, P., et al. 2008. "Spatial Focusing and Intersymbol Interference in Multiple-Input-Single-Output Time Reversal Communication Systems." *IEEE Journal of Oceanic Engineering*, 33(3):341-355.
19. Prada, C., F. Wu, and M. Fink. 1991. "The iterative time reversal mirror: A solution to self-focusing in the pulse echo mode," *J. Acoust. Soc. Am.*, 90(2):1119-1129.
20. Prada, Claire, et al. 1996. "Decomposition of the time reversal operator: Detection and selective focusing on two scatterers," *J. Acoust. Soc. Am.*, 99(4):2067-2076.

Proceedings of Meetings on Acoustics

Volume 8, 2009

<http://asa.aip.org>

158th Meeting
Acoustical Society of America
San Antonio, Texas
26 - 30 October 2009
Session 2aEA: Engineering Acoustics

2aEA8. Time Reversal Focusing for Pipeline Structural Health Monitoring

Joel Harley*, Nicholas O'Donoghue, Yuanwei Jin and Jose M. Moura

***Corresponding author's address: Department of Electrical and Computer Engineering, Carnegie Mellon University, Pittsburgh, PA 15213, jharley@andrew.cmu.edu**

This paper investigates the use of time reversal processing techniques to compensate for multimodal and dispersive effects in a low-power structural health monitoring system for pipelines. We demonstrate the use of time reversal as a pitch-catch operation between two transducer arrays to illuminate changes caused by damage on a pipe. We then show and discuss how differences in the severity of damage affect the signals recorded at the receiving transducer array and demonstrate how these results can be interpreted to measure those changes. Our results are demonstrated through experimental observation.

Published by the Acoustical Society of America through the American Institute of Physics

INTRODUCTION

Over the last decade, the deterioration of the United States' infrastructure has become a subject of increasing concern. Pipeline networks are particularly difficult to maintain. The United States has approximately 305,000 miles of interstate and intrastate pipelines dedicated to the transmission of natural gas to local distribution plants [1].

Ultrasonic guided wave technology has become an important tool for evaluating the integrity of many civil structures. Guided waves can travel long distances in many materials and propagate through the entire thickness of the object under test [2]. These properties make them appealing for nondestructive inspection. Many ultrasonic pipeline inspection systems use large rings of transducers to excite guided waves and listen for echoes produced by cracks, corrosion, or other damage [9].

In a structural health monitoring environment, transducers are permanently attached to the structure. These systems can be used to monitoring large networks of pipelines in real-time. Processing techniques can also take advantage of the transducers' spatial diversity to improve detection performance while reducing power requirements.

In this paper, we demonstrate a monitoring technique using a method called Time Reversal Change Focusing (TRCF). In time reversal focusing, the response between a source and an array receiver is obtained. A time-reversed version of the response is then propagated backwards through the medium from the same array. These waves propagate as if traveling backward in time and focus spatially and temporally back at the original source. Time reversal focusing has been extensively investigated for pulse-echo ultrasonic inspection by Fink and others [3, 14, 5]. In TRCF, changes in medium caused by damage can be illuminated using time reversal's focusing properties. Through experimentation, we demonstrate how this method provides a metric for classifying the magnitude of damage in a pipe while relaxing the restrictions on excitation frequency and bandwidth that are imposed on many other nondestructive techniques.

PIPE WAVES AND WAVE MODES

When a guided wave is excited into a thin, solid pipe, the waves decompose into several orthogonal wave modes. Each of these wave modes propagate through the medium at different velocities. Pipe wave modes can be grouped into three distinct categories: longitudinal waves, flexural waves, and torsional waves [8]. Each mode group respectively oscillates in the direction of propagation, in the direction orthogonal to the surface of the pipe, and in the direction tangential to the surface of the pipe. Both longitudinal and torsional modes are axisymmetric, while flexural modes vary across both the length and circumference of the pipe. As the frequency of excitation increases, new modes are excited at various discrete frequencies. There are a countably infinite number of possible longitudinal and torsional modes and a doubly countably infinite number of possible flexural modes. These wave modes are also dispersive, such that their velocity changes as a function of frequency [10, 13].

At the receiving array, modes (without dispersion) appear as replicas of the original excitation waveform that arrive at different times. This closely resembles the effects seen from multipath wave propagation, which is common in many fields. Since no real life signal contains a single frequency, dispersion further distorts the waveforms as they propagate through the medium. As an example, the response of a wideband, 200 kHz signal after traveling across a 3 meter long pipe is shown in fig. 1. Due to the multimodal and dispersive effects, the responses from existing ultrasonic inspection and structural health monitoring systems are often difficult to interpret. To reduce these distorting effects, many systems are designed to operate at low frequencies and with small bandwidths [2]. Unfortunately, a monitoring system's frequency response depends on the properties of the structure under test and is not optimal at low frequencies. Transducer geometries can also be manipulated in order to excite specific modes, but this can reduce signal strength and the guided wave's sensitivity to particular defects [15].

While multimodal, dispersive, and multipath effects are seen as detrimental to conventional ultrasonic methods, these effects are actually beneficial for time reversal systems. Time reversal has been tested extensively in radar [11, 6], underwater acoustics [7], and non-destructive testing [3] applications to coherently focus signals across a channel. It has been shown that in the presence of multipath behavior, caused by boundaries or scatterers, the focusing achieved through time reversal improves detection and imaging significantly with respect to other conventional methods [4]. Further, it has also been shown that time reversal's focusing is further improved by more pronounced multimodal and dispersive effects [12].

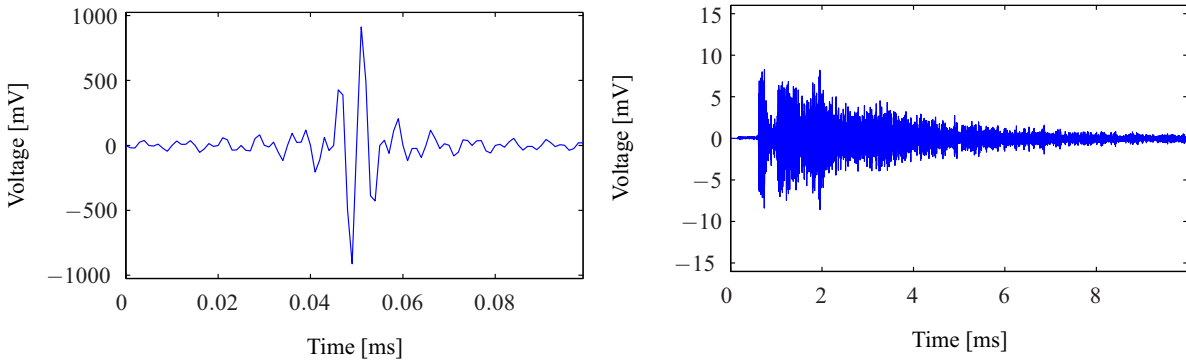


FIGURE 1. (left) A 200 kHz bandwidth sinc pulse modulated by a 200 kHz carrier excitation used in experiments. (right) The response of the above excitation after traveling across a 3 meter long pipe.

PHYSICAL TIME REVERSAL CHANGE FOCUSING

Time reversal focusing is a technique used to improve, over other conventional methods, the spatial and temporal focusing of waves through inhomogeneous media. In time reversal focusing, an array of transducers records a finite length response from a single source over a time interval $0 < t < T$. T must be large enough so that the entire time response exists within the interval. The measured response at each transducer is then normalized, reversed in time, and propagated backwards through the channel at time T . The waves return across the channel as if traveling backward through time and, at time $2T$, coherently focus at the original source. Throughout this process, we assume the channel is reciprocal [3]. This assumption, which is generally valid, ensures that the channel does not change when the direction of the propagating waves change. This section mathematically describes how background subtraction and time reversal are used in order to focus changes caused by damage in the pipe.

Consider a pipe or section of a pipe with, at one end, a single transducer A and, at the other end, a circular array B of N transducers around the pipe's circumference. When a signal $s(t)$ is transmitted from transducer A to array B , the Fourier transform of the received signal at transducer n for $1 \leq n \leq N$ is

$$Y_n(\omega) = H_n(\omega)S(\omega) + V_n(\omega) \quad (1)$$

where $H_n(\omega)$ denotes the transfer function, or the Fourier transform of the Green's function, from the transmitter A to the location of transducer n in array B . The term $V_n(\omega)$ denotes additive noise. We model $V_n(\omega)$ as a zero mean circularly symmetric complex Gaussian random variable.

We assume that we are able to observe and accurately measure the response of the pipe before any damage occurs and that this response is stationary over time. Therefore,

$$Y_{C,n}(\omega) = H_{C,n}(\omega)S(\omega), \quad (2)$$

which we refer to as the background clutter response, is known. Further, since $S(\omega)$ is also known, then $H_{C,n}(\omega)$, the transfer function of the clutter, can be determined. When damage is present within the pipe, we can express the response at each of the N receivers as

$$\begin{aligned} Y_{C+T,n}(\omega) &= H_{C+T,n}(\omega)S(\omega) + V_n(\omega) \\ &= [H_{C,n}(\omega) + H_{T,n}(\omega)]S(\omega) + V_n(\omega), \end{aligned} \quad (3)$$

where $H_{T,n}(\omega)$ denotes the target transfer function. Here target refers to damage in the environment. In (3), the background $H_{C,n}(\omega)S(\omega)$ is known and so can be subtracted to yield

$$Y_n(\omega) = H_{T,n}(\omega)S(\omega) + V_n(\omega). \quad (4)$$

In (4), the response is a function of changes due to damage. The response $Y_n(\omega)$ is then time reversed. In the frequency domain, time reversal, or time negation, is equivalent to frequency conjugation for real time signals. The

signal is also scaled by the constant

$$k = \sqrt{\frac{\int_{-\infty}^{\infty} |S(\omega)|^2 d\omega}{\sum_{n=1}^N \int_{-\infty}^{\infty} |Y_n(\omega)|^2 d\omega}} \quad (5)$$

so that the total energy of the responses from all N transducers is equal to the energy in the original excitation signal.

The time reversed, scaled signal is sent backwards. Since the medium is reciprocal, the transfer function between transducer n in array B and transducer A will remain $H_{C+T,n}(\omega)$. The signal received at transducer A is then expressed as a superposition of each of the responses from the N transducers in array B

$$X_{C+T}(\omega) = \sum_{n=1}^N (H_{C,n}(\omega) + H_{T,n}(\omega)) Y_n^*(\omega) + W_n(\omega), \quad (6)$$

where $W_n(\omega)$ is another additive noise term represented by a zero mean, circularly symmetric normal random variable, and where $(\cdot)^*$ denotes the complex conjugate operation. As stated previously, $H_{C,n}(\omega)$ and $Y_n^*(\omega)$ are known, and therefore the clutter component can be subtracted from (6). After the background subtraction, the resulting expression is only a function of the changes in the medium

$$X(\omega) = \sum_{n=1}^N H_{T,n}(\omega) Y_n^*(\omega) + W_n(\omega). \quad (7)$$

When the expression for $Y_n^*(\omega)$ is inserted into (6), the equation becomes

$$\begin{aligned} X(\omega) &= \sum_{n=1}^N H_{T,n}(\omega) (H_{T,n}^*(\omega) S^*(\omega) + V_n^*(\omega)) + W_n(\omega) \\ &= \sum_{n=1}^N |H_{T,n}(\omega)|^2 S^*(\omega) + H_{T,n}(\omega) V_n^*(\omega) + W_n(\omega). \end{aligned} \quad (8)$$

Since the noise components are zero mean and we assume the two measurements are independent observations, than the expected value of $X(\omega)$ is

$$E[X(\omega)] = \sum_{n=1}^N |H_n(\omega)|^2 S^*(\omega). \quad (9)$$

Equation (9) shows that, by back-propagating the time reversed signal, the response due to changes in the medium can be expressed as the magnitude-squared of the target transfer function times the time reversed excitation signal. This indicates that any phase information, which represents time delay information in the time domain, only derives from the excitation signal. This causes the time domain signal to be symmetric and to have a large peak in the center of that symmetry.

MATHEMATICAL TIME REVERSAL CHANGE FOCUSING

The previous section described time reversal processing when physically performed through experimentation. Often, we do not perform physical time reversal. To accomplish physical time reversal, the single transducer A and the transducer array B require the ability to transmit and receive signals, which may not be appropriate for all situations. In this section, we derive the mathematical time reversal solution in which A only acts as a transmitter and the transducers in B only need to act as receivers. Instead of receiving a signal at B , time reversing it, and retransmitting it, we transmit and receive two independent sets of signals from A to B . Those two sets of signals will be expressed as

$$\begin{aligned} Y_{1,n}(\omega) &= H_{T,n}(\omega) S(\omega) + V_{1,n}(\omega) \\ Y_{2,n}(\omega) &= H_{T,n}(\omega) S(\omega) + V_{2,n}(\omega). \end{aligned} \quad (10)$$

The equations in (10) assume that background subtraction, shown previously, has already been performed.

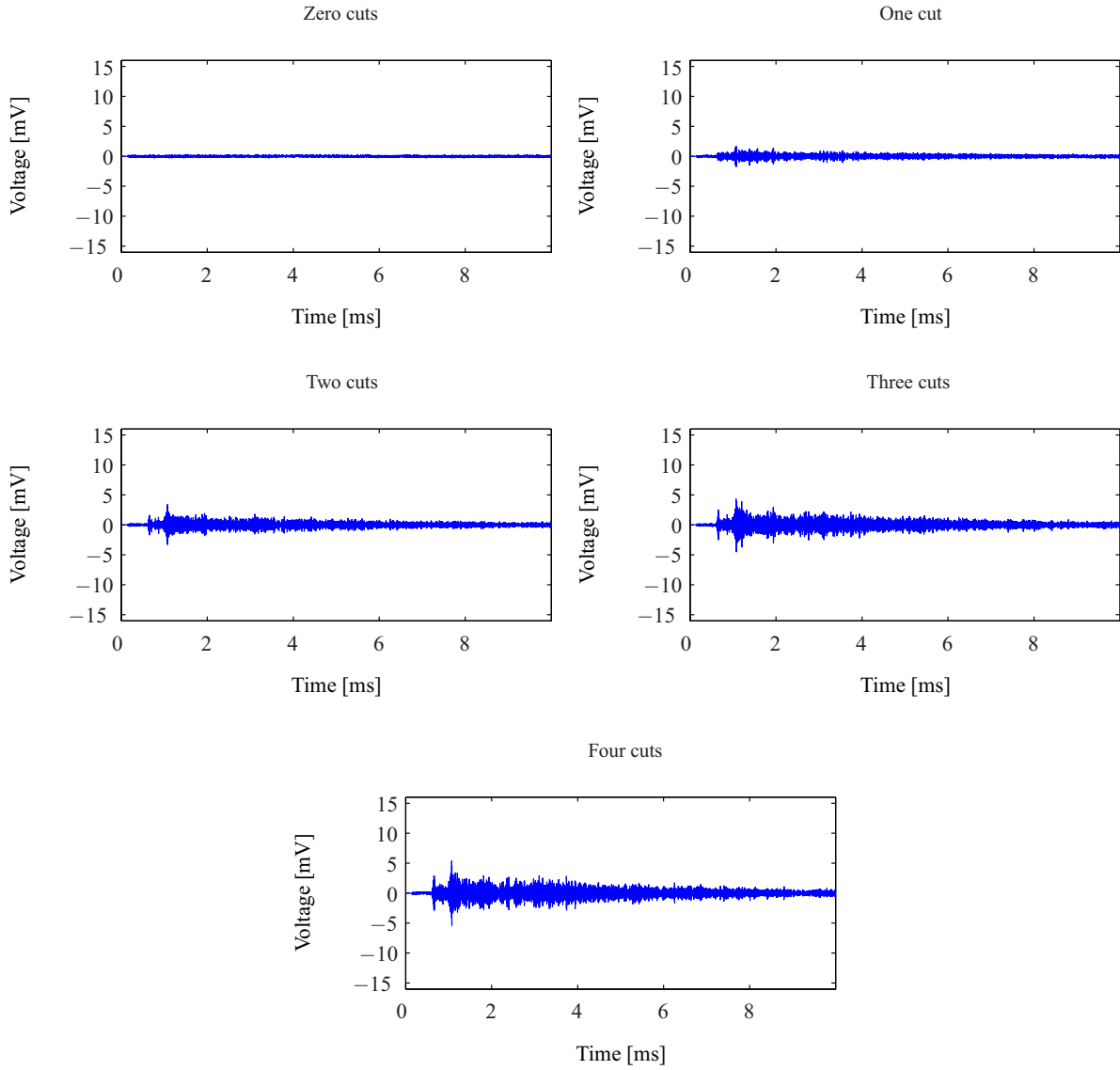


FIGURE 2. The differences between the background response in fig. 1 and the responses corresponding to the presence of zero, one, two, three, and four saw cuts on the pipe.

Physical time reversal can then be approximated as

$$\begin{aligned}
 X(\omega) &= \frac{1}{S(\omega)} \sum_{n=1}^N (Y_{1,n}(\omega)) (Y_{2,n}(\omega))^* \\
 &= \sum_{n=1}^N |H_{T,n}(\omega)|^2 S(\omega) + H_{T,n}^*(\omega) V_{w,1,n}(\omega) + H_{T,n}(\omega) V_{w,2,n}^*(\omega) + V_{w,1,n}(\omega) V_{w,2,n}^*(\omega). \quad (11)
 \end{aligned}$$

When the expected value of (11) is taken, we see that it is equivalent to the expected value of the physical time reversal derivation,

$$E[X(\omega)] = \sum_{n=1}^N |H_{T,n}(\omega)|^2 S(\omega). \quad (12)$$

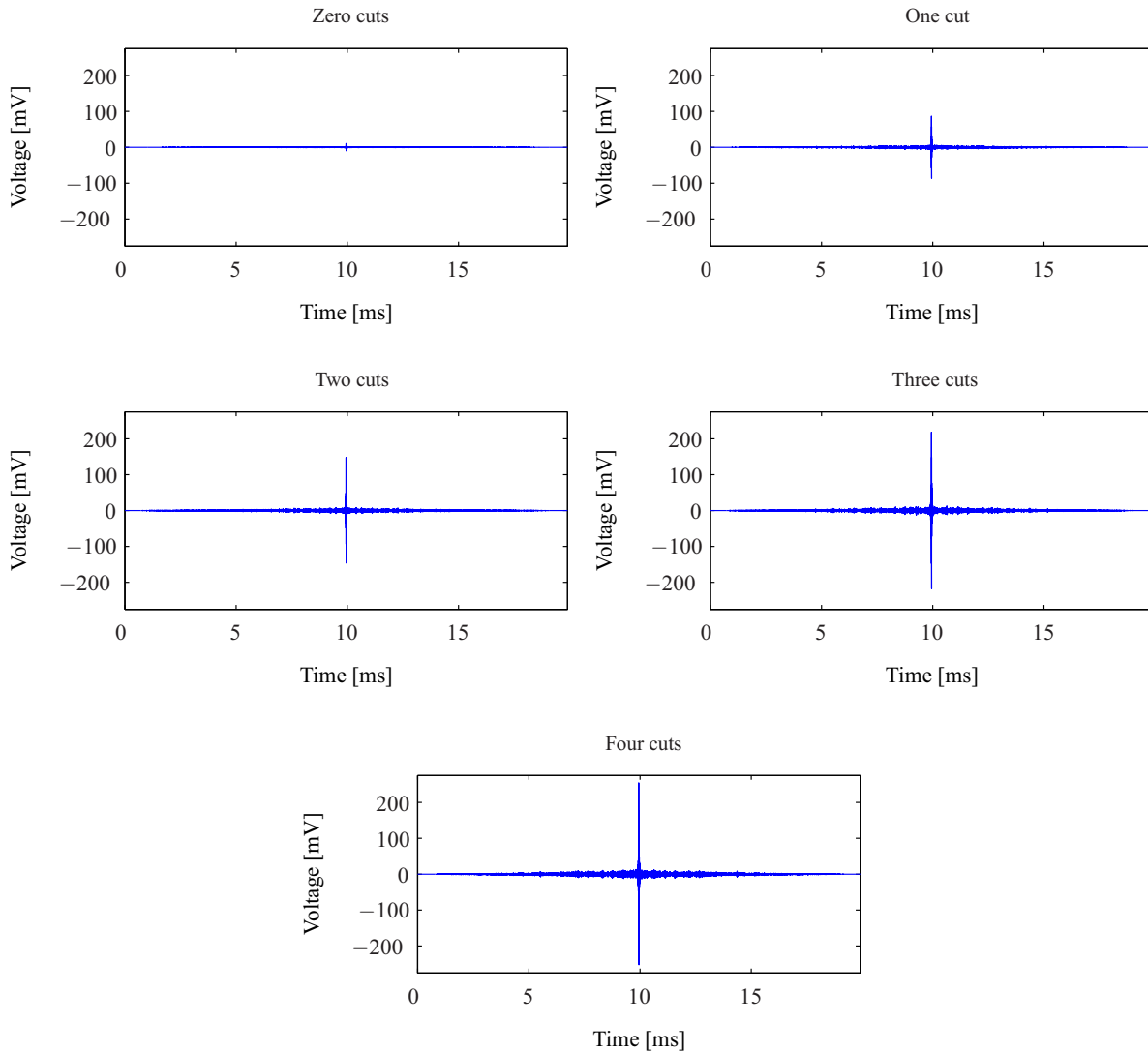


FIGURE 3. The result of performing time reversal change focusing on the difference responses found in fig. 2. The plots correspond to the presence of zero, one, two, three, and four saw cuts on the pipe.

Therefore, both physical and mathematical time reversal depict a focused signal resulting from change due to damage. In our experimental results, we will use mathematical time reversal to compute the time reversal change focusing results.

EXPERIMENTAL RESULTS

Our experiments use a single PZT wafer as our A transducer and an array of eight individual transducers that comprise array B . Each of the PZTs are directly bonded to the surface of a pipe and are 5mm wide, 10mm long, and 1mm thick. The pipe is 3050mm in length, has an inner radius of 30.15mm, and has outer radius of 36.75mm. The A transducer is positioned at one end of the pipe and each of the transducers in array B circle around the pipe at the opposite end. Transducer A operates as a transmitter, while each transducer in B acts as a receiver.

Fig. 1 shows the sinc excitation signal transmitted from A to B and the signal received from one of the eight transducers in the array. Similar responses were then obtained after creating several saw cuts in the pipe. Each saw cut

is approximately 1 mm deep (about one-quarter of the pipe wall thickness), 1 mm wide, and 25 mm in arc dimension (less than one-tenth of the pipe's circumference). To simulate damage, we added a line of four saw cuts positioned 590 mm, 1170 mm, 1760 mm, and 2510 mm away from the receiving array. Measurements were taken after adding each cut.

Fig. 2 shows the collection of responses after background subtraction, characterized by $Y_{1,n}$ in (10). This results from subtracting the background signal in fig. 1 with the responses from each damage scenario. These signals exhibit a weak structure and are complex and difficult to interpret. When we perform mathematical time reversal focusing using these signals and the counterparts from the other transducers in the array, the results focus with peaks that monotonically increase with the amount of damage in the pipe. These focusing results are shown in fig. 3.

The maxima of the signals in fig. 3 are (fewest to most cuts) 10.5 mV, 86.4 mV, 147.0 mV, 218.1 mV, and 254 mV. These focusing results show a clear monotonic correlation between the amount of damage present and the peak of the received signal. These results indicate that the peak can act as a useful metric or statistic to detect the presence and estimate the magnitude of damage on the pipe.

CONCLUSION

The ability of time reversal to focus improves as the number of modes and propagation paths as well as waveform dispersion increase. This stands in contradiction with traditional ultrasonic structural health monitoring systems that use low frequency and small bandwidth excitations. The peaks of the Time Reversal Change Focusing show a clear indication of the presence of damage in the pipe. Further, as the amount of damage in the pipe increases, so does the time reversal peak. This explains the efficacy of time reversal based detection algorithms [11, 6]. Further work will investigate how Time Reversal Change Focusing is sensitive to the stationarity of the clutter response.

ACKNOWLEDGMENTS

National Energy Technology Laboratory (NETL) is the funding source for this effort with Cost Share being provided by Carnegie Mellon University (CMU). Concurrent Technologies Corporation (CTC) is funded under a cooperative agreement with NETL. CMU is funded under a Subcontract Agreement with CTC. Joel Harley and Nicholas O'Donoghue are supported by a National Defense Science and Engineering Graduate Fellowship, sponsored by the Office of Naval Research and Army Research Office, respectively.

REFERENCES

1. "America's Infrastructure Report Card 2009." Technical report, American Society of Civil Engineers (2009).
2. Cawley, P. "Practical Long Range Guided Wave Inspection – Managing Complexity." *29th Annual Review of Progress in Quantitative Nondestructive Evaluation*, 22(657):22–40 (2003).
3. Fink, M. "Time reversal of ultrasonic fields. I. Basic principles." *IEEE Transactions on Ultrasonics, Ferroelectrics, and Frequency Control*, 39(5):555–566 (1992).
4. Fink, M., Cassereau, D., Derode, A., Prada, C., Roux, P., Tanter, M., Thomas, J., and Wu, F. "Time-reversed acoustics." *Reports on Progress in Physics*, 63(12):1933–1995 (2000).
5. Gruber, F. K., Marengo, E. A., and Devaney, A. J. "Time-reversal imaging with multiple signal classification considering multiple scattering between the targets." *The Journal of the Acoustical Society of America*, 115(6):3042–3047 (2004).
6. Jin, Y. and Moura, J. "Time-Reversal Detection Using Antenna Arrays." *Signal Processing, IEEE Transactions on*, 57(4):1396–1414 (2009).
7. Kuperman, W. A., Hodgkiss, W. S., Song, H. C., Akal, T., Ferla, C., and Jackson, D. R. "Phase conjugation in the ocean: Experimental demonstration of an acoustic time-reversal mirror." *The Journal of the Acoustical Society of America*, 103(1):25–40 (1998).
8. Li, J. and Rose, J. L. "Excitation and propagation of non-axisymmetric guided waves in a hollow cylinder." *The Journal of the Acoustical Society of America*, 109(2):457–464 (2001).
9. Lowe, M. and Cawley, P. "Long Range Guided Wave Inspection Usage – Current Commercial Capabilities and Research Directions." Technical report, Imperial College London, Department of Mechanical Engineering (2006).
10. Lowe, M. J. S., Alleyne, D. N., and Cawley, P. "The Mode Conversion of a Guided Wave by a Part-Circumferential Notch in a Pipe." *Journal of Applied Mechanics*, 65(3):649–656 (1998).
11. Moura, J. M. F. and Jin, Y. "Time Reversal Imaging by Adaptive Interference Canceling." *IEEE Transactions on Signal Processing*, 56(1):233–247 (2008).

12. Nunez, I. and Negreira, C. "Efficiency parameters in time reversal acoustics: Applications to dispersive media and multimode wave propagation." *The Journal of the Acoustical Society of America*, 117(3):1202–1209 (2005).
13. P., W., M., L., and P., C. "The effect of dispersion on long-range inspection using ultrasonic guided waves." *NDT and E International*, 34(1):1–9 (2001).
14. Prada, C. and Fink, M. "Separation of interfering acoustic scattered signals using the invariants of the time-reversal operator. Application to Lamb waves characterization." *Journal of the Acoustical Society of America*, 104(2):801–807 (1998).
15. Wilcox, P., Lowe, M., and Cawley, P. "Mode and Transducer Selection for Long Range Lamb Wave Inspection." *Journal of Intelligent Material Systems and Structures*, 12(8):553–565 (2001).

Detection of Structural Defects in Pipes using Time Reversal of Guided Waves

Nicholas O'Donoghue, Joel Harley, José M.F. Moura
Electrical and Computer Engineering
Carnegie Mellon University
Pittsburgh, PA 15213

Yuanwei Jin
Engineering and Aviation Sciences
Univ. of Maryland, Eastern Shore
Princess Anne, MD 21853

Abstract—Structural health monitoring of buried pipelines is of vital importance as infrastructures age. Ultrasonic guided waves are a popular method for inspecting buried pipes, due to their potential for long propagation. Unfortunately, the large number of wave modes present, and the effects of dispersion, in a pipeline make analysis of the received signals difficult. We plan to use Time Reversal Acoustics to compensate for these complex signals, and improve performance for the detection of faults in a pipeline. We will present theoretical performance results for conventional and Time Reversal detectors, verified with simulations conducted in PZFlex. Time Reversal shows a potential for a reduction in the power requirements of a fault detection system.

Index Terms—Time Reversal, structural health monitoring, dispersion, buried pipelines, PZFlex

I. INTRODUCTION

Buried pipelines are an integral part of any country's infrastructure, as they are commonly used to transport liquids and gases, such as crude oil and natural gas, from their excavation sites to processing facilities, and to the consumers. In the United States alone, there were 180 natural gas pipeline accidents in 2008. These accidents accounted for 7 fatalities, 66 injuries, and \$302,268,941 in property damage [1]. Consequently, it is of vital importance that these buried pipelines be inspected and certified to be free of damage. Many current solutions utilize guided waves [2], [3] due to their long propagation distances. However, dispersion and mode-dependent group speeds make interpretation of wideband signals difficult [4]. In order to alleviate these problems, large rings of transducers are used to selectively excite a single wave mode, and a narrow bandwidth is used to limit dispersive effects. This results in large power requirements, and a relatively short probing distance from the transducer array. We will alleviate these restrictions by exploiting the benefits of Time Reversal, a signal processing technique first pioneered in acoustics by M. Fink [5].

The use of guided waves for non-destructive testing in pipes is complicated by the propagation environment. When a thin plate is excited by acoustic pressure waves, it responds with a countably-infinite number of discrete guided waves. These

National Energy Technology Laboratory (NETL) is the funding source for this effort with Cost Share being provided by Carnegie Mellon University (CMU). Concurrent Technologies Corporation (CTC) is funded under a cooperative agreement with NETL. CMU is funded under a Subcontract Agreement with CTC. N.O'Donoghue is supported by National Defense Science and Engineering Graduate Fellowship, sponsored by the Army Research Office.

waves all travel with independent velocities, and experience an effect termed frequency dispersion. We consider here a hollow pipe, which has the added complexity of multiple independent paths that can be taken by each wave around the pipe as they progress. All of these factors complicate the system's response to input, and make conventional processing more difficult. Many of the wave modes can be suppressed by utilizing relatively small frequency bands, and by intelligently designing the excitation transducer array, and the effects of frequency dispersion can be similarly limited. But these approaches unnecessarily restrict the design of inspection systems.

Time Reversal has been shown to compensate for both dispersiveness and the multi-modal environments found in thin plates, where lamb waves exist [6], [7], and in hollow pipes, where guided waves exist [8], resulting in a compression of the wave in both time and space and an increase in the peak signal level. From [9], [10], we know that Time Reversal's focusing effects are most visibly seen in extremely dense channels, with discrete echoes generated from scattering objects. In this paper, we apply detection algorithms derived for Time Reversal arrays [10] to the hollow pipe scenario under consideration. We show that in both the ideal case (with the channel response known fully) and the realistic case (where it must be estimated), time reversal processing achieves a notable increase in detection performance. We note that, while many systems operate in a pulse-echo mode, we are devising this system for a pitch-catch scenario, and make the comparison in this paper between only pitch-catch scenarios.

The remainder of the paper is organized as follows. Section II describes our physical model. Section III lays out the transmission scheme and detectors used, while the reader is referred to [10] for a detailed derivation. We describe the numerical simulations performed in Section IV, and provide our conclusions in Section V.

II. PHYSICAL MODEL

In this paper, we consider a hollow pipe, with thin walls relative to its length and diameter. The thin walled assumption allows us to consider guided wave propagation. Guided waves in hollow cylinders fall into three general categories: torsional, longitudinal, and flexural [4]. The torsional modes induce particle motion in the circumferential direction, a "twisting" of the pipe as they propagate, while longitudinal and flexural modes induce particle motion both along the main axis of

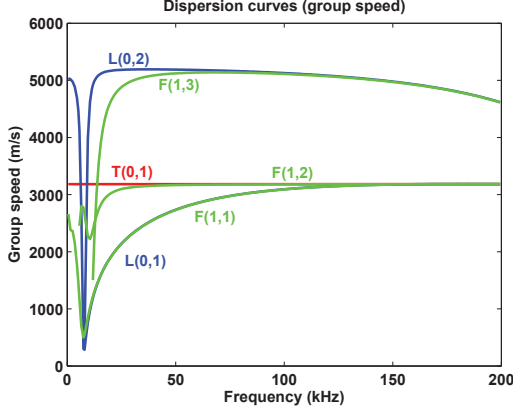


Fig. 1. Dispersion curve for the pipe modeled in our simulations, showing wavenumber vs. frequency for Longitudinal, Torsional, and first-order Flexural modes for $f=0$ -50kHz.

the pipe and orthogonal to the surface of the pipe, and arise as an extension of the symmetric and anti-symmetric modes present in thin plates. Torsional and longitudinal modes are both axisymmetric, while flexural modes are not.

An important component of guided wave propagation is frequency dispersion [4], [8]. Each wave mode has its own dispersion curve, a representation of both the group velocity and phase velocity of that wave mode for various frequencies. See figure 1 for a plot of wavenumber ($k = 2\pi f/\nu(f)$), with propagation speed $\nu(f)$ vs. frequency. Some wave modes, like the second longitudinal mode (see L(0,2) in figure 1), have a region of relatively low dispersion (40-100kHz here). This encourages many system designers to limit the frequencies that they utilize. Other wave modes, like most of the flexural modes (see F(*,*) in figure 1), exhibit dispersion over most of their frequency range, although its effects are also most clear near the lower frequencies of support for each mode. The first torsional wave mode (see T(0,1) in figure 1), however, is unique in that it, alone among guided waves, does not experience dispersion. This is why many system designers choose to employ large arrays of transducers (on the order of 64 or 128), to selectively excite the first Torsional wave mode. Unfortunately, this mode is not always the most favorable in terms of propagation distance, thus we hope to excite all of the pipe's supported wave modes.

In lieu of a detailed analysis of each wave mode, for which the reader is referred to [8], we will simply consider the overall response of the system. This response is expressed as a function of the input frequency, and the transmitter and receiver locations: $H(\omega, \mathbf{x}_t, \mathbf{x}_r)$. In this paper, we make the assumption that the response is reciprocal. We consider a system with a single transmitter A, and an array of receivers B, placed around the pipe, some distance away. We assume that array B has N elements. The response of the system from transmitter A to the i^{th} element of B is written

$$h_i(\omega) = H(\omega, \mathbf{x}_A, \mathbf{x}_{B_i}), \quad i = 0, \dots, N-1. \quad (1)$$

From this, we construct the frequency-dependent response matrix of dimension $N \times 1$:

$$\mathbf{H}(\omega) = [h_0(\omega), h_1(\omega), \dots, h_{N-1}(\omega)]^T. \quad (2)$$

Furthermore, we assume that the background, or clutter, response of the system when there is no damage present is a stationary signal of the form $H_c(\omega)$, while the response of the system following damage is the superposition of $H_c(\omega)$ with a new set of waves induced by the damage:

$$H_{d+c}(\omega) = H_c(\omega) + H_d(\omega) \quad (3)$$

Finally, we make the assumption that, through repeated measurements, the clutter response $H_c(\omega)$ is known perfectly. For simplicity, we will refer to $H_d(\omega)$ as simply $H(\omega)$ for the remainder of this paper. It has been shown in [9], [10] that utilization of this damage response matrix in Time Reversal will result in coherent focused waves, under the presence of damage, and will result in white noise when the damage is absent. It is this principle that allows for Time Reversal detection of defects and damage.

A. Data Model

Many of the following array definitions are taken directly from [10], and are repeated here merely to aid in the interpretation of our results. From (2), we can write the received signal for a snapshot at array B as

$$\mathbf{Y}_m(\omega) = \mathbf{H}(\omega)S(\omega) + \mathbf{V}_m(\omega) \quad (4)$$

Where the subscript m refers to the snapshot number, and we have the complex white noise term $\mathbf{V}_m(\omega) \sim \mathcal{CN}(0, \sigma_v^2 \mathbf{I}_N)$. Next, we consider a band of frequencies $\{\omega_q\}_{q=0 \dots Q-1}$ and define the column-stacked representation:

$$\begin{aligned} \mathbf{Y}_m &= [\mathbf{Y}_m(\omega_0)^T, \dots, \mathbf{Y}_m(\omega_{Q-1})^T]^T \\ &= \mathbf{H}\mathbf{s}_A + \mathbf{v}_m \end{aligned} \quad (5)$$

$$\mathbf{H} = \text{diag}[\mathbf{H}(\omega_0), \dots, \mathbf{H}(\omega_{Q-1})]_{N \times Q} \quad (6)$$

$$\mathbf{s}_A = [S(\omega_0), \dots, S(\omega_{Q-1})]^T \quad (7)$$

$$\mathbf{v}_m = [\mathbf{V}_m(\omega_0)^T, \dots, \mathbf{V}_m(\omega_{Q-1})^T]^T \quad (8)$$

III. FAULT DETECTION

In this section, we will briefly lay out the detectors derived in [10]. We begin with the ideal (channel matched filter) detectors for both conventional and Time Reversal processing, for which the damage response $\mathbf{H}_d(\omega)$ is assumed to be known, and then describe the Generalized Likelihood Ratio Test detectors, for which a maximum likelihood estimate $\hat{\mathbf{H}}_d(\omega)$ must be computed. First, however, we will describe the transmission schemes used to generate the data for detection.

A. Time Reversal Transmission

We begin by transmitting \mathbf{s}_A from antenna A into the damaged pipe, and remove the known clutter response.

$$\mathbf{Y}_m = \mathbf{H}\mathbf{s}_A + \mathbf{v}_m \quad (9)$$

This signal is then energy normalized, using the parameter:

$$k_m = \sqrt{\|\mathbf{s}_A\|^2 / \|\mathbf{Y}_m\|^2}. \quad (10)$$

The time-reversal probing signal to be sent from array B back to antenna A is given by:

$$\mathbf{s}_{TR} = k_m \mathbf{Y}_m^*. \quad (11)$$

Note that reversal of the time axis (for real-valued signals) is analogous to phase conjugation of the frequency content. The response after removal of the known clutter, at antenna A, to this input is given by:

$$\mathbf{X}_m = k_m \mathbf{H}^T \mathbf{Y}_m^* + \mathbf{w}_m \quad (12)$$

$$= k_m \mathbf{H}^T \mathbf{H} \mathbf{s}_A^* + k_m \mathbf{H}^T \mathbf{v}_m^* + \mathbf{w}_m \quad (13)$$

where we have the white Gaussian noise term $\mathbf{w}_m \sim \mathcal{CN}(0, \sigma_w^2 \mathbf{I}_Q)$. Note the second term in the summation, which represents a retransmission of noise (\mathbf{v}_m^*) from the forward transmission.

B. Conventional Transmission

For conventional detection, we will begin with the signal $S(\omega_q)$ transmitted from array B. Each element will transmit the same probing signal:

$$\mathbf{s}_B(\omega_q) = S(\omega_q) \mathbf{1}_{N \times 1} \quad (14)$$

$$\mathbf{s}_B = [\mathbf{s}_B(\omega_0)^T, \dots, \mathbf{s}_B(\omega_{Q-1})^T]^T \quad (15)$$

We define the energy normalization factor

$$\beta = \sqrt{1/N} \quad (16)$$

and transmit the scaled signal $\beta \mathbf{s}_B$. The received signal at A, following removal of the known clutter response, is:

$$\mathbf{r}_m = \beta \mathbf{H}^T \mathbf{s}_B + \mathbf{w}_m \quad (17)$$

C. Channel Matched Filter

For the conventional case, the binary hypothesis test is:

$$\begin{aligned} \mathbb{H}_1 : \mathbf{r}_m &= \beta \mathbf{H}^T \mathbf{s}_B + \mathbf{w}_m \\ \mathbb{H}_0 : \mathbf{r}_m &= \mathbf{w}_m. \end{aligned} \quad (18)$$

Let $\mathbf{R} \triangleq [\mathbf{r}_0^T, \dots, \mathbf{r}_{M-1}^T]^T$ be the stacked snapshots of \mathbf{r}_m . From [10], it can be shown that this results in the CDCMF test statistic:

$$\ell_{CDCMF}(\mathbf{R}) = \Re \left\{ \frac{(\beta \mathbf{H}^T \mathbf{s}_B)^H \sum_{m=1}^M \mathbf{r}_m}{\sigma_w \|\beta \mathbf{H}^T \mathbf{s}_B\|} \right\}. \quad (19)$$

While, for Time Reversal, we have the binary hypothesis test:

$$\begin{aligned} \mathbb{H}_1 : \mathbf{x}_m &= k_m \mathbf{H}^T \mathbf{H} \mathbf{s}_A + \mathbf{w}_m \\ \mathbb{H}_0 : \mathbf{x}_m &= \mathbf{w}_m \end{aligned} \quad (20)$$

with \mathbf{X} similarly defined. The TRCMF test statistic is given:

$$\ell_{TRCMF}(\mathbf{X}) = \Re \left\{ \frac{(\mathbf{H}^T \mathbf{H}^* \mathbf{s}_A^*)^H \sum_{m=1}^M \mathbf{x}_m}{\sigma_w \|\mathbf{H}^T \mathbf{H}^* \mathbf{s}_A^*\|} \right\}. \quad (21)$$

Note that, because the channel response is known fully, for the TRCMF, there is no retransmission of the noise term \mathbf{v}_m , as in (12).

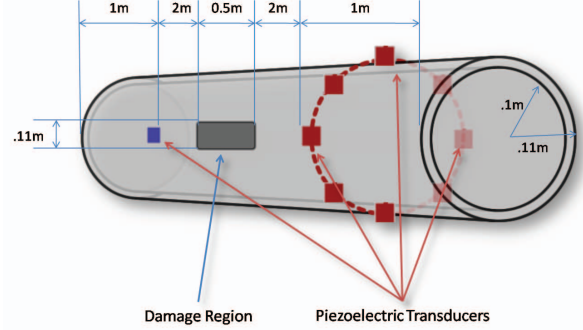


Fig. 2. Geometry of the pipe modeled.

D. Generalized Likelihood Ratio Test

For the GLRT, it is assumed that both \mathbf{Y} and \mathbf{R} are available for conventional detection, and that both \mathbf{Y} and \mathbf{X} are available for Time Reversal detection. We refer the reader to [10] for a detailed derivation of the ML estimates $\hat{\mathbf{H}}$ under both Time Reversal and conventional processing, as well as for the derivation of the GLRT detectors.

In the conventional case, we have the binary hypothesis test:

$$\begin{aligned} \mathbb{H}_1 : \begin{bmatrix} \mathbf{y}_m \\ \mathbf{r}_m \end{bmatrix} &= \begin{bmatrix} \mathbf{H} \mathbf{s}_A \\ \beta \mathbf{H}^T \mathbf{s}_B \end{bmatrix} + \begin{bmatrix} \mathbf{v}_m \\ \mathbf{w}_m \end{bmatrix} \\ \mathbb{H}_0 : \begin{bmatrix} \mathbf{y}_m \\ \mathbf{r}_m \end{bmatrix} &= \begin{bmatrix} \mathbf{v}_m \\ \mathbf{w}_m \end{bmatrix} \end{aligned} \quad (22)$$

which results in the CDGLRT test statistic:

$$\ell_{CDGLRT}(\mathbf{R}, \mathbf{Y}) = \frac{1}{\sigma_v^2 \sigma_w^2} \sum_{m=1}^M \left\{ 2\Re \left\{ \beta \sigma_v^2 \mathbf{s}_B^H \hat{\mathbf{H}}^* \mathbf{r}_m + \sigma_w^2 \mathbf{y}_m^T \hat{\mathbf{H}}^* \mathbf{s}_A^* \right\} - \sigma_w^2 \left\| \hat{\mathbf{H}} \mathbf{s}_A \right\|^2 - \beta^2 \sigma_v^2 \left\| \hat{\mathbf{H}}^T \mathbf{s}_B \right\|^2 \right\}. \quad (23)$$

For TR detection, we have the binary hypothesis test:

$$\begin{aligned} \mathbb{H}_1 : \begin{bmatrix} \mathbf{y}_m^* \\ \mathbf{x}_m \end{bmatrix} &= \begin{bmatrix} \mathbf{H}^* \mathbf{s}_A^* \\ k_m \mathbf{H}^T \mathbf{H}^* \mathbf{s}_A^* \end{bmatrix} + \begin{bmatrix} \mathbf{v}_m^* \\ k_m \mathbf{H}^T \mathbf{v}_m^* + \mathbf{w}_m \end{bmatrix} \\ \mathbb{H}_0 : \begin{bmatrix} \mathbf{y}_m^* \\ \mathbf{x}_m \end{bmatrix} &= \begin{bmatrix} \mathbf{v}_m^* \\ \mathbf{w}_m \end{bmatrix} \end{aligned} \quad (24)$$

and the TRGLRT test statistic:

$$\ell_{TRGLRT}(\mathbf{X}, \mathbf{Y}) = \frac{1}{\sigma_v^2 \sigma_w^2} \sum_{m=1}^M \left\{ 2\Re \left\{ k_m \sigma_v^2 \mathbf{y}_m^T \hat{\mathbf{H}}^* \mathbf{x}_m + \sigma_w^2 \mathbf{y}_m^T \hat{\mathbf{H}}^* \mathbf{s}_A^* \right\} - \sigma_w^2 \left\| \hat{\mathbf{H}} \mathbf{s}_A \right\|^2 - k_m^2 \sigma_v^2 \left\| \hat{\mathbf{H}}^T \mathbf{y}_m^* \right\|^2 \right\}. \quad (25)$$

IV. NUMERICAL SIMULATION

For numerical simulations, we use the commercial modeling software PZFlex. A sample pipe was generated, see figure 2 for the pipe dimensions and transducer layout. In this simulation, we consider corrosion on the interior surface of the pipe, modeled as a loss of wall thickness, while the transducers

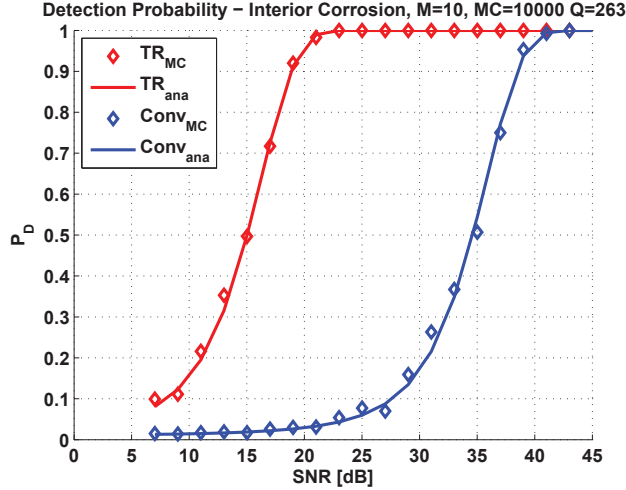


Fig. 3. Channel Matched Filter results show P_D vs. SNR [dB] for both CDCMF(right) and TRCMF(left)

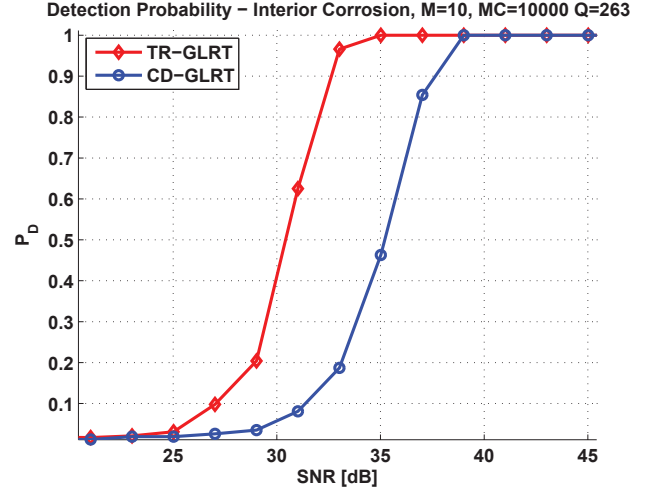


Fig. 4. Generalized Likelihood Ratio Test results show P_D vs. SNR [dB] for both CDGLRT(right) and TRGLRT(left)

are attached to the outside of the pipe. The input pulse was a sinc with cutoff frequency $f_c = 200kHz$.

For detection, we generate random noise at various SNR levels, and run Monte Carlo simulations with 10,000 trials. For each trial, we take $M = 10$ snapshots, set $P_{FA} = 0.01$ and compute the analytical threshold according to (45) in [10]. The array B has $N = 8$ elements evenly spaced around the pipe. We used $Q = 263$ frequency samples, this number was computed from the coherence bandwidth with (74) in [10].

The results for the ideal channel matched filter are provided in figure 3. As can be seen from that image, Time Reversal can achieve comparable performance to conventional detection in the presence of an additional 20dB of noise. Although the 20dB improvement may seem extreme, it is corroborated by analytical predictions from (71) in [10] (reproduced below), which predicts 27.8dB for the data we provided.

$$SNRG_{max} = \frac{\|\mathbf{s}_A\|^2 \|\mathbf{H}^T \mathbf{H}^* \mathbf{s}_A^*\|^2}{\beta^2 \|\mathbf{H}^T \mathbf{s}_B\|^2 \|\mathbf{H} \mathbf{s}_A\|^2} \quad (26)$$

Moving to the GLRT case, we computed the threshold numerically using the data under \mathbb{H}_0 and $P_{FA} = 0.01$, and compared to the output of (23) and (25). The detection results are shown in figure 4. From these results, we can see a performance increase of 5dB. The difference between performance increase in the CMF and GLRT can be explained by 1) uncertainty and errors in the estimate of the channel response \mathbf{H} and 2) the retransmission of noise terms, which causes some of the energy budget in the TR retransmission to be wasted on signal components that do not coherently focus.

V. CONCLUSION

In this paper, we have shown the application of Time Reversal change detectors to acoustic guided waves propagating in a hollow pipe. We have demonstrated that the performance of such a system shows significant improvement, roughly 5dB

with the GLRT, and shows the potential for as much as 30dB in the scenario described. Furthermore, we have shown that such results are possible by utilizing effects of dispersion, which allows broadband operation. This opens the possibility of improved resolution and efficiency, when compared to narrowband implementations. It remains to be shown what additional range this will impart on a Time Reversal based system, as well as what performance increase is seen over a pulse-echo design.

REFERENCES

- [1] "PHMSA stakeholder communications: Pipeline incidents and mileage reports," U.S. Department of Transportation Pipeline and Hazardous Materials Safety Administration, Tech. Rep.
- [2] J. J. Ditrai, "Utilization of guided elastic waves for the characterization," *J. Acoustic. Soc. Am.*, vol. 96, pp. 3769–3775, 1994.
- [3] P. Cawley, "Practical long range guided wave inspection - managing complexity," in *29th Annual Review of Progress in Quantitative Nondestructive Evaluation*. American Institute of Physics, 2003, vol. 22, pp. 22–40.
- [4] J. Li and J. L. Rose, "Excitation and propagation of non-axisymmetric guided waves in a hollow cylinder," *J. Acoust. Soc. Am.*, vol. 109, no. 2, pp. 457–464, February 2000.
- [5] M. Fink, "Time Reversal of ultrasonic fields, I: Basic principles," *IEEE Trans. on Ultrasonics, Ferroelectrics, and Frequency Control*, vol. 39, pp. 555–566, 1992.
- [6] R. K. Ing and M. Fink, "Time-reversed Lamb Waves," *IEEE Trans. on Ultrasonics, Ferroelectrics, and Frequency Control*, vol. 45, no. 4, pp. 1032–1043, 1998.
- [7] C. Prada and M. Fink, "Separation of interfering acoustic scattered signals using the invariants of the time-reversal operator. application to lamb waves characterization." *J. Acoustic. Soc. Am.*, vol. 104, no. 1, pp. 801–807, 1998.
- [8] N. O'Donoghue, J. Harley, J. M. F. Moura, Y. Jin, I. Oppenheim, Y. Ying, J. States, J. Garrett, and L. Soibelman, "Single-antenna time reversal of guided waves in pipes," *Proceedings of 158th Meetings on Acoustics*, April 2009.
- [9] J. M. F. Moura and Y. Jin, "Detection by Time Reversal: Single antenna," *IEEE Trans. on Signal Processing*, vol. 55, no. 1, pp. 187–201, January 2007.
- [10] Y. Jin and J. M. F. Moura, "Time-Reversal detection using antenna arrays," *IEEE Trans. on Signal Processing*, vol. 57, no. 4, pp. 1396–1414, April 2009.

Proceedings of Meetings on Acoustics

Volume 6, 2009

<http://asa.aip.org>

**157th Meeting
Acoustical Society of America
Portland, Oregon
18 - 22 May 2009
Session 3aSA: Structural Acoustics and Vibration**

3aSA7. Single Antenna Time Reversal of Guided Waves in Pipelines

Nicholas O'Donoghue*, Joel Harley, Jose M. Moura, Yuanwei Jin, Irving Oppenheim, Yujie Ying, Joseph States, James Garrett and Lucio Soibelman

***Corresponding author's address: Electrical & Computer Engineering, Carnegie Mellon University, PH B9 - ECE Dept, Pittsburgh, PA 15213, nodonoug@andrew.cmu.edu**

The volatile nature of natural gas makes it extremely important to ensure that distribution pipelines remain free from defects, as leakage can result in explosions. Many current methods for testing buried pipelines rely on periodic excavation of a section of pipe and attachment of large acoustic or magneto-restrictive sensors. These systems, while reliable, suffer from a high cost-per-test ratio. Our group hopes to reduce the power constraints of such a detection system, in order to allow for permanent installations that monitor the pipelines continuously. We propose to use Time Reversal, a signal processing technique, in order to achieve this improvement. This paper will focus on the modes generated by various acoustic probing signals, and the echoes received with and without Time Reversal. We argue that TR will be most beneficial when there are several dispersive modes present, a scenario avoided in conventional techniques. We will present simulation results for the analysis of wave modes in a cylindrical pipe before and after Time Reversal using PZFlex.

Published by the Acoustical Society of America through the American Institute of Physics

1. INTRODUCTION

The previous title of this paper was 'Detection of Structural Defects in Time Reversal', and the title was changed due to a decision to continue our study of detection methods before presenting results. Instead, this paper focuses on the actual time reversal stage, and analyzed the effects on wave modes generated and signals received. The author list has been expanded to include additional members of the research team.

Ultrasonic guided waves are used in many commercial nondestructive testing applications due to their long propagation distances, but often suffer from the need to excavate sections of buried pipelines in order to attach the sensory equipment. What we hope to achieve is a reduction in the power constraints, and the number of transducers required at each testing position. This will make a permanent solution, one which remains in a monitoring mode, as opposed to periodic tests, more feasible. We will accomplish this task by exploiting the benefits of Time Reversal, a signal processing technique first pioneered by M. Fink (Fink 1992).

The use of guided waves for non-destructive testing in pipes is complicated by the propagation environment, which contains wave modes with frequency-dependent speed. In order to alleviate effects, many conventional systems use large rings of transducers to selectively excite a single wave mode, and a narrow bandwidth to limit dispersive effects. We hope to use Time Reversal to compensate for the effects without the need for expensive and power-hungry hardware.

Time Reversal has been shown to compensate for both dispersiveness and the multi-modal environments found in thin plates, where lamb waves exist (Ing & Fink 1998; Prada & Fink 1998), resulting in a compression of the wave in both time and space, as well as an increase in the peak signal level. From (Ing & Fink 1998; Prada & Fink 1998; Moura & Jin 2007; Moura & Jin 2008; Jin & Moura 2009), we know that Time Reversal's focusing effects are most visibly seen in extremely dense channels, with discrete echoes generated from scattering objects. We theorize that the same effect will be experienced from the superposition of a large number of wave modes. Although we do not test that theory within this paper, we rely on the results of (Ing & Fink 1998) and their conclusion that dispersion is beneficial to Time Reversal. Thus, we plan to excite as many modes as possible, with as much dispersion as possible, in order to maximize the potential for TR processing gain. We should note that, while many systems operate in a pulse-echo mode, we are devising this system for a pitch-catch scenario.

The scope of this paper is to analyze what modes are present in a thin-walled pipe before and after Time Reversal processing, and to demonstrate the time compression and focusing effects of TR for pipes. These properties will be exploited in future work, to devise a detection scheme for structural defects within a pipe. We present here results from PZFlex numerical simulations, analyzed using the methodology laid out in (Alleyne & Cawley 1991). We will first introduce guided wave modes (Sec. 2), outline the time reversal stage (Sec. 3), then discuss what modes are present before and after Time Reversal has been applied for two different input waveforms (Sec. 4).

2. GUIDED WAVE MODES

Guided waves present in thin-walled cylinders, or thin shells, are very similar to Lamb waves seen in thin plates and rods. The thin shell allows for the generation of the symmetric and asymmetric wave modes, which result in Longitudinal and Flexural guided waves. In addition, there are Torsional guided waves, a propagation along the pipe of displacement in the circumferential direction, that has no analog in thin plates. In order to study these briefly, we begin with the general equation for displacement due to a guided wave mode in a thin-plate excited by a sinusoid of frequency ω is (Brekhovskikh 1960):

$$\mathbf{u}_m(\mathbf{x}, t) = \mathbf{a}_m(\omega) e^{j(\omega t - k_M(\omega)R(\mathbf{x}) - \phi)} \quad (1)$$

where $\mathbf{u}_m(\mathbf{x}, t)$ is the 3-dimensional displacement from the m^{th} wave mode at position \mathbf{x} , a distance $R(\mathbf{x})$ from the wave source, and at time t . $\mathbf{a}_m(\omega)$ is that wave mode's frequency-dependent amplitude, $\omega = 2\pi f$

is the angular frequency, $k_M = \omega/\nu_m(\omega)$ is the wave number, $\nu_m(\omega)$ is the wave mode's frequency-dependent phase velocity, and ϕ is the phase term. We will ignore ϕ for the remainder of this article. Although (Brekhovskikh 1960) defines eq. 1 for (x, y, z) coordinates, we will consider cylindrical coordinates (r, θ, z) .

$$\mathbf{u}_m(\mathbf{x}, t) = \begin{bmatrix} u_{m,r}(\mathbf{x}, t) \\ u_{m,\theta}(\mathbf{x}, t) \\ u_{m,z}(\mathbf{x}, t) \end{bmatrix} \quad (2)$$

Since it is difficult to measure and excite 3-axis displacement values, we will assume that the excitation and response are both restricted to one dimension, the radial axis (r). Thus, for the remainder of this paper, we will consider only the out-of-plane displacement ($u_m(\mathbf{x}, t) = u_{m,r}(\mathbf{x}, t)$). This simplification means that Torsional modes, which exhibit no displacement in the z or r dimensions, can be ignored. Their presence, however, does not change any of the results, this simplification is made in the interest of brevity.

2.1 Propagation Distance

In order to continue, we need to determine the effective propagation distance R for each guided wave mode. Longitudinal and Flexural waves are formed by the superposition of many symmetric and asymmetric modes traversing the pipe. The Longitudinal waves are axisymmetric, thus the wavefront is perpendicular to the pipe's central axis. This means that the propagation distance between a source and point of interest depends only on their separation along the central axis. Given a source at point $\mathbf{x}_0 = (0, 0, r)$, the displacement at point $\mathbf{x} = (r, \theta, z)$ in cylindrical coordinates is

$$R_L(\mathbf{x}) = z \quad (3)$$

Flexural waves, however, are non axisymmetric, so their propagation distance is more difficult to compute analytically, so we simply write: $R_F(\mathbf{x})$.

2.2 Amplitude Function

From (Li & Rose 2000), we know that the amplitude function for Longitudinal wave modes, if we ignore attenuation, is independent of distance z . Furthermore, a property of axisymmetry is that their displacement (in cylindrical coordinates) is also independent of angle θ (Gazis 1959). Thus, for these modes we can simply write $a_L(r, \omega)$. Flexural wave modes, however, have an amplitude function that is wholly dependent on position \mathbf{x} . Thus, we write $a_F(\mathbf{x}, \omega)$.

2.3 Displacement Equation

There are an infinite number of wave modes (for Longitudinal, Torsional and Flexural), but each Flexural mode also has an infinite number of circumferential orders, making them doubly infinite, each mode-order pair resulting in its own amplitude function $a_F^M(\mathbf{x}, \omega)$, wavenumber $k_F^M(\omega)$, and propagation distance $R_F^M(\omega)$. If we consider the aggregate superposition of every mode excited, we have the channel response:

$$u(\mathbf{x}, t) = \underbrace{\sum_{L=0}^{\infty} a_L(r, \omega) e^{j(\omega t - k_L(\omega)z)}}_{\text{Longitudinal}} + \underbrace{\sum_{F=0}^{\infty} \sum_{M=0}^{\infty} a_F^M(\mathbf{x}, \omega) e^{j(\omega t - k_F^M(\omega)R_F^M(\mathbf{x}))}}_{\text{Flexural}} \quad (4)$$

In order to continue, we now take the Fourier transform along the time domain for angular frequency at some sample point ω_q .

$$U(\mathbf{x}, \omega_q) = \int_{-\infty}^{\infty} \left\{ \sum_{L=0}^{\infty} a_L(r, \omega) e^{j(\omega t - k_L(\omega)z)} + \sum_{F=0}^{\infty} \sum_{M=0}^{\infty} a_F^M(\mathbf{x}, \omega) e^{j(\omega t - k_F^M(\omega)R_F^M(\mathbf{x}))} \right\} e^{-j\omega_q t} dt \quad (5)$$

$$= \left\{ \sum_{L=0}^{\infty} a_L(r, \omega) e^{-jk_L(\omega)z} + \sum_{F=0}^{\infty} \sum_{M=0}^{\infty} a_F^M(\mathbf{x}, \omega) e^{-jk_F^M(\omega)R_F^M(\mathbf{x})} \right\} \delta(\omega - \omega_q) \quad (6)$$

$$= \left\{ \sum_{L=0}^{\infty} a_L(r, \omega_q) e^{-jk_L(\omega_q)z} + \sum_{F=0}^{\infty} \sum_{M=0}^{\infty} a_F^M(\mathbf{x}, \omega_q) e^{-jk_F^M(\omega_q)R_F^M(\mathbf{x})} \right\} \delta(\omega - \omega_q) \quad (7)$$

where $\delta(x)$ is the indicator (or dirac) function. We call this expression the **Channel Transfer Function** at that frequency. Thus, if we consider a broadband input signal $S(\omega)$, as a strain at some point, we can expect the output at any position \mathbf{x} down the pipe to be:

$$Y(\mathbf{x}, \omega_q) = S(\omega_q)U(\mathbf{x}, \omega_q) \quad (8)$$

2.4 2-D FFT Analysis

We will use the 2-D FFT of the incident wave at a series of transducers in order to analyze the dispersion curve for our pipe. In order to take the FFT of (7) along the z axis, we must first make two fundamental assumptions. 1) That the z -extent of the region in question is small enough to ignore attenuation and variation of the Flexural mode amplitude function. This leads to the approximations $a_L(r, \omega) \approx a_L(r, z_0, \omega)$ and $a_F^M(\mathbf{x}, \omega) \approx a_F^M(r, \theta, z_0, \omega)$ for some z_0 inside the region. 2) That the flexural propagation distance $R_F^M(\mathbf{x})$ is linear in z ($R_F^M(\mathbf{x}) = b_F^M(r, \theta)z + c_F^M(r, \theta)$). Under these assumptions:

$$U(k, \omega_q) = \left[\sum_{L=0}^{\infty} a_L(r, z_0, \omega) \delta(k - k_L(\omega_q)) + \sum_{F=0}^{\infty} \sum_{M=0}^{\infty} a_F^M(r, \theta, z_0, \omega) e^{-jk_F^M(\omega_q)c_F^M(r, \theta)} \delta(k - k_F^M(\omega_q)b_F^M(r, \theta)) \right] \delta(\omega - \omega_q) \quad (9)$$

If we plot this 2-D image, using a grayscale for intensity, then we will see each wave mode trace out a single line along the coordinates $(\omega_q, k_L(\omega_q))$ or $(\omega_q, k_F^M(\omega_q)b_F^M(r, \theta)) \forall \omega_q$. This series of mode-curves is seen in the theoretical dispersion curve (Figure 1) and the computed dispersion curves (Figures 4 and 7).

3. TIME REVERSAL PROCESSING

Time Reversal is based on the assumptions of channel reciprocity and stationarity. In other words, ignoring noise, if we have transducers A and B, then if we transmit some pulse from A to B, we will receive the same result as if we transmit that pulse from B to A (reciprocity), and if we repeat that transmission at any later time, the results will be the same. In time reversal, we perform a three-stage process.

- *Conventional Probing* A pulse is transmitted from A, through the channel, to B
- *Time Reversal Processing* The received signal is time-reversed and energy-normalized
- *Time Reversal Probing* The new TR signal is transmitted from B, back through the channel, to A

So, if we define \mathbf{x}_B as the position of antenna B and $\mathbf{x}_0 = (0, 0, r)$ as the position of antenna A, then the received signal due to a real input $S(\omega)$ at A is:

$$Y(\omega_q) = S(\omega_q)U(\mathbf{x}_B, \omega_q) \quad (10)$$

And, if this is time reversed (negation of the angular frequency term in the frequency domain), then the probing signal becomes

$$S_{TR}(\omega_q) = kY(-\omega_q) = kS(-\omega_q)U(\mathbf{x}_B, -\omega_q) \quad (11)$$

where k is the energy normalization term, given by:

$$k = \sqrt{\frac{\sum_{q=0}^{Q-1} |S(\omega_q)|^2}{\sum_{q=0}^{Q-1} |S(\omega_q)U(\mathbf{x}_B, \omega_q)|^2}} \quad (12)$$

We note that the signal $S(\omega)$ has a real-valued Fourier Transform, thus $S(-\omega) = S^*(\omega)$. The received signal, back at antenna A is

$$Y_{TR}(\omega_q) = S_{TR}(\omega_q)U(\mathbf{x}_B, \omega_q) \quad (13)$$

$$= kY(-\omega_q)U(\mathbf{x}_B, \omega_q) \quad (14)$$

$$= kS^*(\omega_q)U(\mathbf{x}_B, -\omega_q)U(\mathbf{x}_B, \omega_q) \quad (15)$$

We make the assumption that phase speed is even symmetric with respect to ω , thus $\nu_m(\omega_q) = \nu_m(-\omega_q)$. This leads to the relationship

$$k_M(-\omega_q) = -k_M(\omega_q), \quad k_F^M(-\omega_q) = -k_F^M(\omega_q) \quad (16)$$

The same even symmetry assumption is made for the real gain terms $a_L(r, \omega)$ and $a_F^M(\mathbf{x}, \omega)$. Thus, we have the product

$$U(\mathbf{x}_B, -\omega_q)U(\mathbf{x}_B, \omega_q) = \left[\sum_{L=0}^{\infty} a_L(r, \omega) e^{jk_L(\omega_q)z} + \sum_{F=0}^{\infty} \sum_{M=0}^{\infty} a_F^M(\mathbf{x}, \omega_q) e^{jk_F^M(\omega_q)R_F^M(\mathbf{x})} \right] \\ * \left[\sum_{L=0}^{\infty} a_L(r, \omega) e^{-jk_L(\omega_q)z} + \sum_{F=0}^{\infty} \sum_{M=0}^{\infty} a_F^M(\mathbf{x}, \omega_q) e^{-jk_F^M(\omega_q)R_F^M(\mathbf{x})} \right] \quad (17)$$

$$= \left| \sum_{L=0}^{\infty} a_L(r, \omega) e^{-jk_L(\omega_q)z} + \sum_{F=0}^{\infty} \sum_{M=0}^{\infty} a_F^M(\mathbf{x}, \omega_q) e^{-jk_F^M(\omega_q)R_F^M(\mathbf{x})} \right|^2 \quad (18)$$

Thus, (15) becomes:

$$Y_{TR}(\omega_q) = kS^*(\omega_q) |U(\mathbf{x}_B, \omega_q)|^2 \quad (19)$$

We can see from (19) that the received signal has the same phase-profile as the transmitted signal. Thus, the channel now behaves like a linear phase filter, with no dispersion effects. This is the cause of Time Reversal's time compression (Ing & Fink 1998). Furthermore, the $|U(\mathbf{x}_B, \omega_q)|^2$ term acts like an adaptive power allocation scheme, concentrating power in those frequency bands that are passed through the channel more efficiently, and attenuating those bands which do not effectively transmit energy.

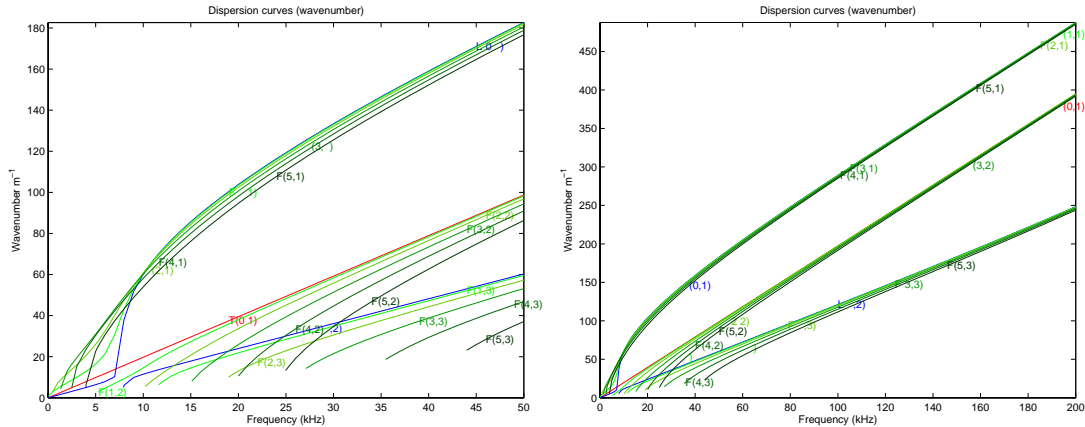


Figure 1: Dispersion curve for the pipe modeled, showing wavenumber vs. frequency for Longitudinal, Torsional, and first-order Flexural modes for $f=0-50\text{kHz}$ (left) and $f=0-200\text{kHz}$ (right).

4. NUMERICAL SIMULATIONS

We used the commercial PZFlex software package on a Dell Inspiron running 64-bit Fedora 9 to run the numerical simulations. The pipe modeled has outside diameter .22m, inside diameter .204m, and length 6m. We placed the transmitter at $x=.5\text{m}$ from the end of the pipe, and measured the incident wave down the pipe at 400 sample points from $x=3\text{m}$ to $x=5\text{m}$, with a spacing of 5mm between the sample points. We model the input as a voltage across the terminals of a PZT5a patch, with dimensions 2.8mm x 0.7mm. The pipe has a hole, 1mm wide, extending 50mm from $x=2.5\text{m}$ to $x=3\text{m}$. In order to verify that Time Reversal will indeed be beneficial for detection of structural defects, it was necessary to test performance on a defected pipe, as the boundary conditions and mode conversions made analysis unclear. We consider this single set of tests as verification that TR focusing is a valid procedure in both structurally clean and damaged pipes.

Inputs are modeled as a compressive strain in the z direction, and the received signal is the z -axis displacement of a particle at the receiver position.

Using the freely available PCDISP (Seco, Martín, Jiménez, Pons, Calderón & Ceres 2002) package for MATLAB, we computed the expected dispersion curves for guided waves within this pipe. We computed the Longitudinal, Torsional, and first 5 circumferential orders of Flexural modes, and show the plot of wavenumber vs. frequency in figure 1 for two different cutoff frequencies. In the absence of dispersion, each mode's propagation velocity ν is independent of frequency, resulting in a wavenumber that is linear in frequency (recall that $k = \omega/\nu$). Thus, any non-linearity of the traces in the dispersion curves is an artifact of dispersion.

4.1 Narrowband Gaussian Pulse Excitation

We first use a relatively narrowband Gaussian pulse, centered at $f_c = 100\text{kHz}$, with a two-sided -6dB bandwidth of $BW = 50\text{kHz}$. Figure 2 shows the probing signal (left) and received response at $x=5\text{m}$ (right). It is evidently clear that, even for this relatively narrow-band system, there is a large contribution from delayed arrivals of the signal.

We then time-reverse and energy-normalize the received signal before using it as the TR excitation signal. Figure 3 shows the TR probing signal (left) and received response at $x=5\text{m}$ (right). Even in this narrowband system, we can see the significant amount of time compression achieved by Time Reversal. Furthermore the maximum amplitude of the received signal has increased from roughly $.2\mu\text{m}$ to $.6\mu\text{m}$.

In order to analyze the wave modes present, we take the received signal, sampled at 400 points with

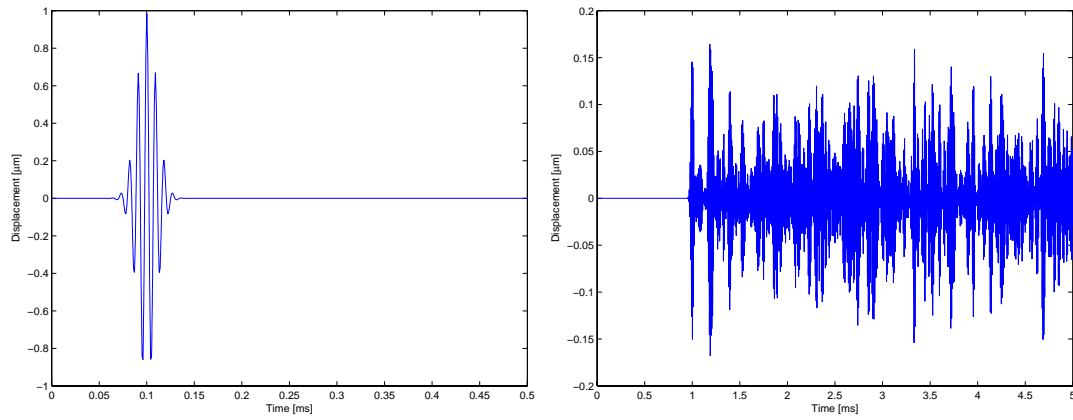


Figure 2: Probing signal (left) and response (right) for the narrowband Gaussian excitation, centered at 100kHz.

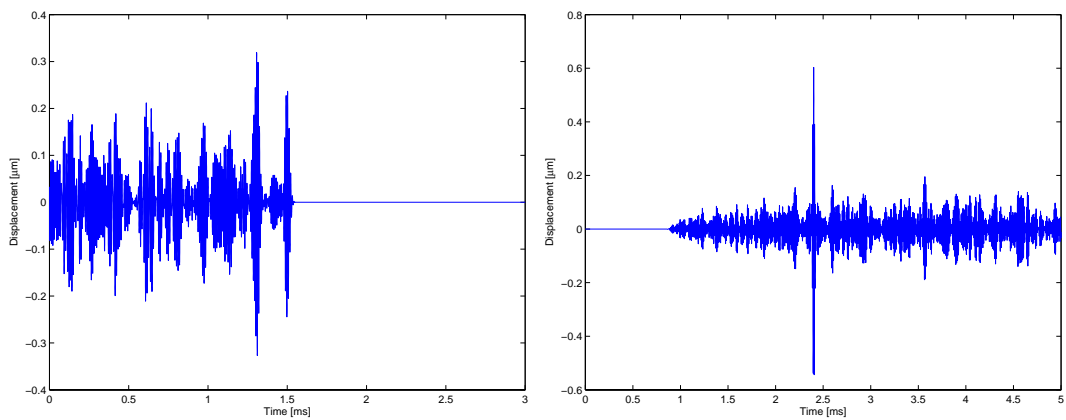


Figure 3: TR probing signal (left) and response (right) for the narrowband Gaussian excitation, centered at 100kHz.

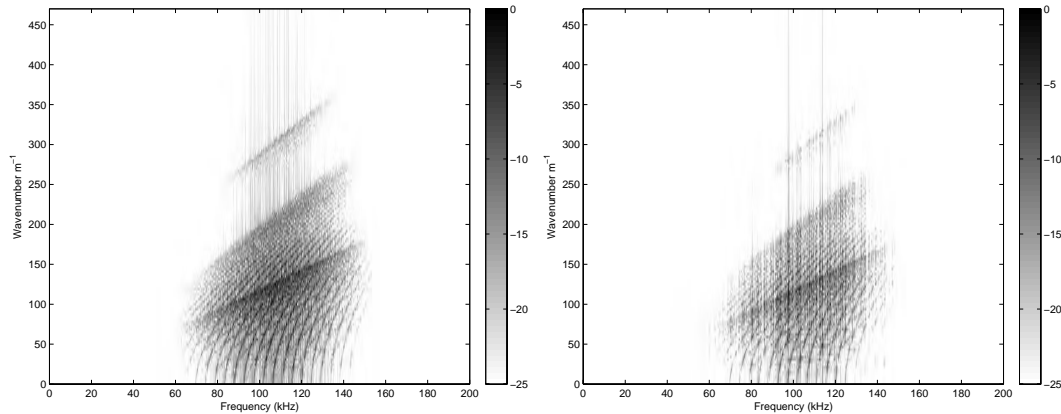


Figure 4: Calculated dispersion curves (plotted in log scale) for the conventional (left) and TR (right) cases.

a spacing of $\delta_x = 5mm$, for a period of .5ms with a sampling frequency of roughly $f_s = 6MHz$. In figure 4, we show the 2-D FFT of this received signal both for the standard (left) and the Time Reversal (right) probing signals. Compare the results to figure 1. The results in figure 4 show many more modes converging to similar wavenumber paths as those shown in figure 1. This is because the theoretical curves were only plotted for the first 5 circumferential orders of the Flexural waves, while an infinite number of circumferential orders exist in the pipe.

Between the two dispersion curves, it is evident that there are some wave-modes present in the forward transmission that are not replicated in the TR transmission, or are present with a lower amplitude. This is due to the channel matching property of Time Reversal. In utilizing the time-reversed received signal from the forward case, the TR probing signal adaptively allocates power to those wave-modes which exhibit more efficient transmission of power. Most significantly, we can see that the 1st-order modes (see Figure 1, L(0,1) and F(M,1)) are suppressed in the TR case. Whether these variations in mode amplitude are due to well known dependence on the characteristics of the source loading (Li & Rose 2000), or as a result of the defect modeled in our simulation is unclear.

4.2 Wideband Sinc Pulse Excitation

Next, we show the results for a wideband sinc pulse with cutoff frequency of $f_{cutoff} = 200kHz$. Figure 5 shows the probing signal (left) and received response at $x=5m$ (right). It is clear from the result that the effects of dispersion and mode superposition are amplified in this case, over the narrowband scenario. That is to be expected, as the sinc is exciting a much larger bandwidth, resulting in higher modes and more dispersion.

We then time-reverse and energy-normalize the received signal before using it as the TR excitation signal. Figure 6 shows the TR probing signal (left) and received response at $x=5m$ (right). As before, we again see a significant time compression, with the maximum received amplitude increasing from roughly $.1\mu m$ to $.55\mu m$, a 7.4dB increase.

Taking the 2-D FFT, we have the dispersion curves shown in figure 7. After Time Reversal, we can see a reduction in the higher order flexural modes (seen in the bottom-right and center-right portions of the plot). Figure 8 shows the spectrum of the originally transmitted sinc waveform (solid line), as well as the TR waveform used in step 3 (dotted line). In this scenario, the band from 150kHz-200kHz is not as efficient as the lower frequency bands, so less power is transmitted there, resulting in a lower amplitude for those high-order wave modes.

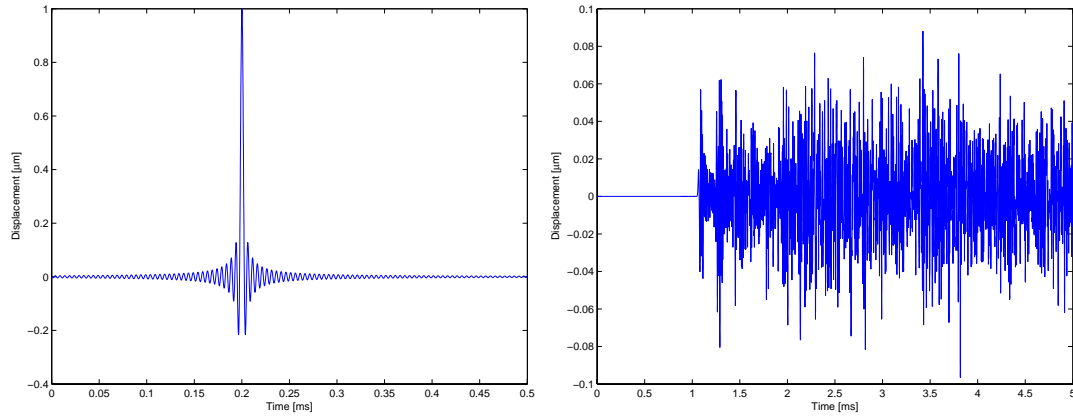


Figure 5: Probing signal (left) and response (right) for the wideband Sinc excitation, with cutoff of 200kHz.

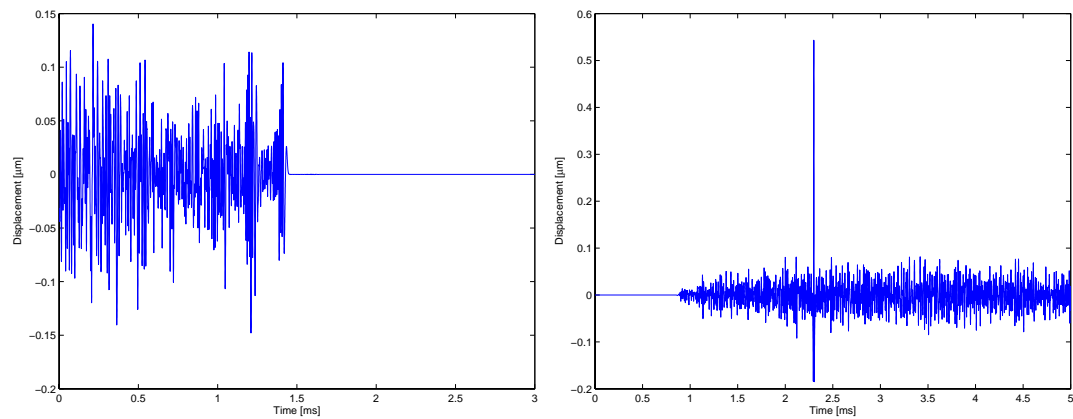


Figure 6: TR probing signal (left) and response (right) for the wideband Sinc excitation, with cutoff at 200kHz.

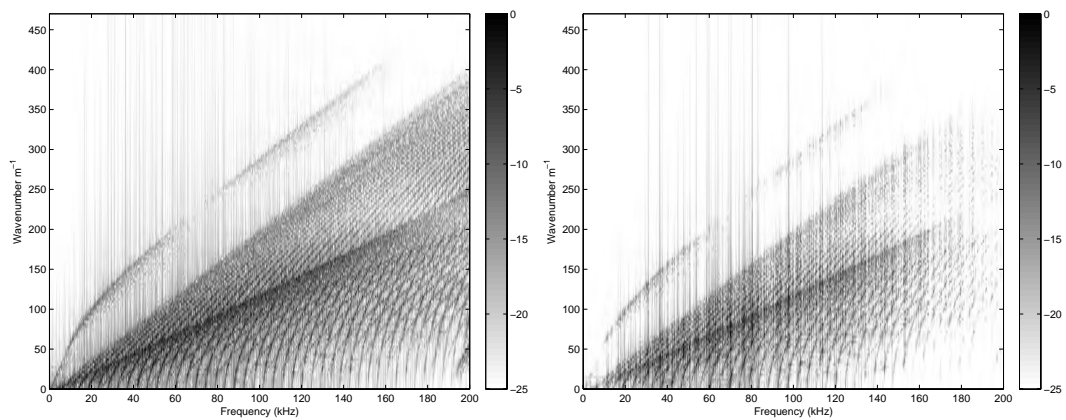


Figure 7: Calculated dispersion curves (plotted in log scale) for the conventional (left) and TR (right) cases.

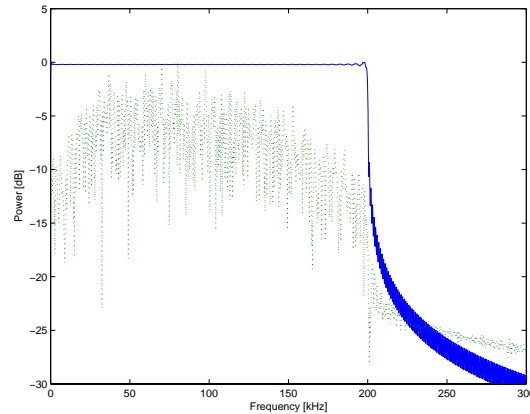


Figure 8: Spectrum of Sinc (solid) and TR (dotted) probing signals.

5. CONCLUSION

We have shown here a derivation for the effect of Time Reversal on the received signal when exciting guided wave modes within a cylindrical pipe. Through numerical simulations, we have confirmed the time compression effect of Time Reversal with guided waves, as well as the selective excitation of those wave modes which most effectively transmit energy through the pipe. This matches the results reported by Ing and Fink (Ing & Fink 1998) for thin plates. This is a promising preliminary study, and will guide our future work in devising a Time Reversal based detector for structural faults within pipes. Specifically, it is necessary to analyze the differences in TR focusing for clean pipes and pipes with various amounts of damage, in order to determine how best to enhance the effects of damage.

6. ACKNOWLEDGMENTS

National Energy Technology Laboratory (NETL) is the funding source for this effort with Cost Share being provided by Carnegie Mellon University (CMU). Concurrent Technologies Corporation (CTC) is funded under a cooperative agreement with NETL. CMU is funded under a Subcontract Agreement with CTC. Nicholas O'Donoghue is supported by National Defense Science and Engineering Graduate Fellowship, sponsored by the Army Research Office.

REFERENCES

- Alleyne, D. N., & Cawley, P. A. (1991), "A two-dimensional Fourier transform method for the measurement of propagating multi-mode signals," *J. Acoust. Soc. Amer.*, 89, 1159–1168.
- Brekhovskikh, L. M. (1960), *Waves in Layered Media* Academic.
- Fink, M. (1992), "Time Reversal of Ultrasonic Fields, I: Basic Principles," *IEEE Trans. on Ultrasonics, Ferroelectrics, and Frequency Control*, 39, 555–566.
- Gazis, D. C. (1959), "Three-Dimensional Investigation of the Propagation of Waves in Hollow Circular Cylinders. I. Analytical Foundation," *J. Acoust. Soc. Am.*, 31(5), 568–573.
- Ing, R. K., & Fink, M. (1998), "Time-Reversed Lamb Waves," *IEEE Trans. on Ultrasonics, Ferroelectrics, and Frequency Control*, 45(4), 1032–1043.

- Jin, Y., & Moura, J. M. F. (2009), "Time-Reversal Detection Using Antenna Arrays," *IEEE Trans. on Signal Processing*, 57(4), 1396–1414.
- Li, J., & Rose, J. L. (2000), "Excitation and propagation of non-axisymmetric guided waves in a hollow cylinder," *J. Acoust. Soc. Am.*, 109(2), 457–464.
- Moura, J. M. F., & Jin, Y. (2007), "Detection by Time Reversal: Single Antenna," *IEEE Trans. on Signal Processing*, 55(1), 187–201.
- Moura, J. M. F., & Jin, Y. (2008), "Time Reversal Imaging by Adaptive Interference Canceling," *IEEE Trans. on Signal Processing*, 56(1), 233–247.
- Prada, C., & Fink, M. (1998), "Separation of interfering acoustic scattered signals using the invariants of the time-reversal operator. Application to Lamb waves characterization," *J. Acoustic. Soc. Am.*, 104(1), 801–807.
- Seco, F., Martín, J. M., Jiménez, A., Pons, J. L., Calderón, L., & Ceres, R. (2002), PCDISP: A Tool for the simulation of wave propagation in cylindrical waveguides., in *Proc. 9th Int'l Congress on Sound and Vibration*, pp. 23–29.

Adaptive Time Reversal for Pipeline Defect Detection

Joel Harley, Nicholas O'Donoghue, and José M.F. Moura

Department of Electrical and Computer Engineering
Carnegie Mellon University
Pittsburgh, PA 15213
Email: jharley@andrew.cmu.edu

Abstract—Time reversal signal processing is a technique for temporally and spatially focusing signals. This technique has been shown to take advantage of multi-path as well as multi-mode and dispersive effects to improve the signal-to-noise ratio at the original source. Reference [1] developed a time reversal change detection framework for sensor arrays with known additive Gaussian noise that demonstrates the gain provided by time reversal over conventional techniques.

We expand on this work by deriving a time reversal detector for unknown additive (possibly colored) Gaussian noise. This allows time reversal detection to be utilized in more practical problems. We demonstrate the performance of these detection algorithms using a channel model extracted from experimental data of ultrasonic guided waves in a pipe. These results show that time reversal provides better performance and greater robustness when compared with conventional detection algorithms.

Index Terms—Time Reversal, Adaptive Signal Detection, Non-destructive Testing

I. INTRODUCTION

Ultrasonic guided wave technology has become an important tool for the nondestructive testing and structural health monitoring of many infrastructures such as pipelines, bridges, and rails. Guided waves can propagate large distances with little attenuation and are sensitive to defects throughout the entire depth of the structure. However, the propagation of the ultrasonic waves is very complex. When an ultrasonic wave is launched into the pipe, it is affected by multi-modal and dispersive effects [2].

Multi-modal effects separate a wave into a potentially infinite number of discrete waves, each with unique group velocities. Dispersion then varies each group velocity as a function of frequency. This tends to stretch the ultrasonic signals in the time domain. In many ways, these multi-modal effects' impact on signals are similar to that of multi-path effects found in many other fields. As a result, received signals are often difficult to predict and interpret. Fig. 1a shows an

ultrasonic sinc pulse after it has propagated through a steel pipe and experienced multi-modal and dispersive effects. We describe the experimental setup used to measure this waveform in greater detail in section IV. It is easy to see that the resulting signal in Fig. 1a no longer resembles the original sinc pulse. These distorting effects can be reduced, but this often requires systems to operate at low frequencies and with small bandwidths [3]. These restrictions may be sub-optimal for many applications.

Time reversal is a signal processing technique that has been shown to spatially and temporally focus signals [4], [5]. The process is straightforward. A group of sensors record a signal emitted from an active source. Each of these recorded signals is then time-reversed, as if passed through a last-in, first-out register, and normalized. These time-reversed signals are then transmitted back through the medium and received at the original active source. The time-reversed waves transmit backward through the medium as if traveling backward in time.

As a result, the time reversal process temporally compresses and spatially focuses the time-reversed waveforms to reduce multi-path-like effects and provide a high signal-to-noise ratio. While performing the time reversal process, we assume the channel to be linear, time-invariant, and reciprocal [4]. This reciprocity condition, which is generally valid, ensures that the channel does not change when the direction of the propagating wave changes. Fig. 1b demonstrates the response after time reversing and transmitting the signal from Fig. 1a backward through the environment. This demonstrates how time reversal compresses the signal in time.

Time reversal processing has already been applied to radar [6], underwater communication [7], and non-destructive testing [8] applications to coherently focus signals across a channel. References [1] and [9] develop a time reversal framework for change detection within an unknown channel by using the generalized likelihood ratio test. This is useful for many practical applications, such as nondestructive testing, where the channel characteristics are often unknown or not well defined. However, measurement systems and noise statistics are often also sensitive to environmental factors, such as temperature or electrical interference. For example, Fig. 2

National Energy Technology Laboratory (NETL) is the funding source for this effort with Cost Share being provided by Carnegie Mellon University (CMU). Concurrent Technologies Corporation (CTC) is funded under a cooperative agreement with NETL. CMU is funded under a Subcontract Agreement with CTC. Joel Harley and Nicholas O'Donoghue are supported by National Defense Science and Engineering Graduate Fellowships, sponsored by the Office of Naval Research and Army Research Office, respectively.

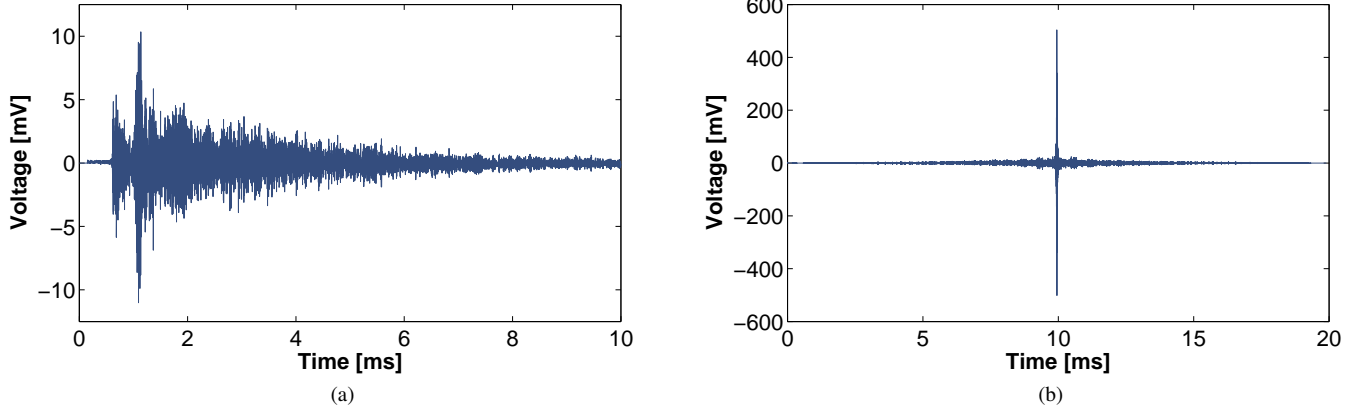


Fig. 1. (a) The response of an ultrasonic sinc pulse after propagating through a steel pipe. The multi-modal and dispersive effects cause the received signal to be very complex. (b) The focused time reversal signal received after transmitting the time-reversed signal from (a) backward through the channel.

demonstrates how the noise variance varies in our experimental setup during a 10.5 hour period. Therefore, it is necessary that we adapt to these changing statistics in order to have meaningful detectors.

In this paper, we extend the multi-antenna (or multi-sensor) time reversal detection framework presented in [1] to assume the presence of a zero mean Gaussian noise source with an *unknown* variance. In this paper, we present algorithms for both white and colored noise environments. We test these detection algorithms using a channel response taken from nondestructive testing experiments on a pipe.

II. THE BACK-PROPAGATION MODEL

This section presents the back-propagation data model for detection. This model is a generalized version of the time reversal data model presented in [1]. A system with two pairs of stationary sensor arrays A and B is considered. Array A consists of P sensors A_1, \dots, A_P , and array B consists of N sensors B_1, \dots, B_N .

The forward response is measured at each sensor in B at Q discrete frequencies. This response is represented as

$$Y_n(\omega_q) = H_{n,p}(\omega_q)S_p(\omega_q) \quad , q \in \{1, \dots, Q\} \quad (1)$$

where $Y_n(\omega_q)$ denotes a single snapshot of the forward response received at B_n , $H_{n,p}(\omega_q)$ denotes the transfer function from sensor A_p to sensor B_n , and $S_p(\omega_q)$ denotes the signal transmitted from A_p .

The forward response of each sensor at frequency ω_q is stacked to form a vector

$$\begin{aligned} \mathbf{y}_q &= [Y_1(\omega_q), \dots, Y_N(\omega_q)]^T \\ &= \mathbf{H}_q \mathbf{s}_q + \mathbf{v}_q \end{aligned} \quad (2)$$

In order to simplify and condense notation, subscripts are used to indicate frequency. At each frequency ω_q , \mathbf{s}_q denotes the $P \times 1$ transmitted signal, \mathbf{H}_q the $N \times P$ target response matrix for each transducer sensor, and \mathbf{v}_q represents an additive noise term. In previous experiments, as in this one, the

target response matrix is determined through the background subtraction of known clutter as described in [9] and [1]. The collection of vectors \mathbf{y}_q , \mathbf{v}_q , and \mathbf{s}_q at each frequency ω_q are then stacked to form another vector

$$\begin{aligned} \mathbf{y} &= [\mathbf{y}_1^T, \dots, \mathbf{y}_Q^T]^T \\ &= \mathbf{H} \mathbf{s} + \mathbf{v} \end{aligned} \quad (3)$$

where vectors \mathbf{s} , \mathbf{v} , and \mathbf{y} contain PQ , NQ , and NQ elements, respectively. The target channel matrix \mathbf{H} is an $NQ \times PQ$ block diagonal matrix

$$\mathbf{H} = \text{diag}[\mathbf{H}_1, \dots, \mathbf{H}_Q] \quad (4)$$

Another signal \mathbf{f} , which may be a function of \mathbf{y} , is then transmitted backward through the medium. The medium is assumed to be reciprocal, which implies that, if the transfer matrix from $A \rightarrow B$ is \mathbf{H} , then the transfer matrix from $B \rightarrow A$ is \mathbf{H}^T . Therefore, the backward response may be expressed as

$$\begin{aligned} \mathbf{x} &= [\mathbf{x}_1^T, \dots, \mathbf{x}_Q^T]^T \\ &= \mathbf{H}^T \mathbf{f} + \mathbf{w} \end{aligned} \quad (5)$$

where vectors \mathbf{f} , \mathbf{w} , and \mathbf{x} contain NQ , PQ , and PQ elements respectively. The noise terms \mathbf{v} and \mathbf{w} are assumed to be multivariate circularly symmetric normal random variables with diagonal covariance matrices Σ_w and Σ_v

$$\begin{aligned} \Sigma_v &= \text{diag}[\sigma_{v,1}^2 \mathbf{I}_N, \dots, \sigma_{v,Q}^2 \mathbf{I}_N] \\ \Sigma_w &= \text{diag}[\sigma_{w,1}^2 \mathbf{I}_P, \dots, \sigma_{w,Q}^2 \mathbf{I}_P] \end{aligned} \quad (6)$$

In this paper, we consider two possible choices for \mathbf{f} . We refer to the first case as the conventional scenario in which $F_n(\omega_q) = \beta S_p(\omega_q)$ for all n, p , and q . Here $F_n(\omega_q)$, which denotes the ω_q frequency component transmitted from sensor n in A , is an element of \mathbf{f} . For simplicity, we assume that $S_p(\omega_q)$ is the same for all possible p . Therefore, each element of B transmits the same signal (neglecting the normalization factor β) as each element of A . In this scenario, the signals

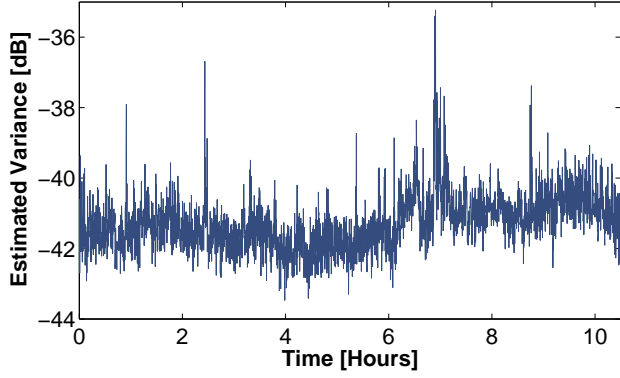


Fig. 2. The measured noise variance of an ultrasonic inspection system over a period of 10.5 hours. This plot demonstrates how noise statistics are often not consistent for all time.

received and sent by B are independent of each other. The term β normalizes the excitations

$$\beta = \sqrt{\frac{P}{N}} \quad (7)$$

so that $\|\mathbf{f}\| = \|\mathbf{s}\|$. The second case we consider is the time reversal scenario, where $\mathbf{f} = k\mathbf{y}^*$. Here, each element of B transmits the time reversed version of what was previously received. In the frequency domain, time reversal is equivalent to phase conjugation. The term k is also a normalization term

$$k = \frac{\|\mathbf{s}\|}{\|\mathbf{y}\|} \quad (8)$$

to ensure that $\|\mathbf{f}\| = \|\mathbf{s}\|$.

III. DETECTION WITH AN UNKNOWN CHANNEL

A. The Generalized Likelihood Ratio Test

This section derives the multiple sensor generalized likelihood ratio test for an unknown channel \mathbf{H} . This was previously derived in reference [1]. We show that these results can be written in a much more compact form than in [1]. We consider the binary hypothesis test with null hypothesis \mathcal{H}_0 and alternative hypothesis \mathcal{H}_1 such that

$$\begin{aligned} \mathcal{H}_1 : \begin{bmatrix} \mathbf{y} \\ \mathbf{x} \end{bmatrix} &= \begin{bmatrix} \mathbf{H}\mathbf{s} + \mathbf{v} \\ \mathbf{H}^T\mathbf{f} + \mathbf{w} \end{bmatrix} \\ \mathcal{H}_0 : \begin{bmatrix} \mathbf{y} \\ \mathbf{x} \end{bmatrix} &= \begin{bmatrix} \mathbf{v} \\ \mathbf{w} \end{bmatrix}. \end{aligned} \quad (9)$$

The resulting multivariate probability distribution function for \mathbf{x} and \mathbf{y} under each hypothesis is expressed as

$$f(\mathbf{x}, \mathbf{y} | \mathcal{H}_1) = \prod_{q=0}^{Q-1} \left(\frac{1}{(2\pi)^{N+P} \sigma_{v,q}^{2N} \sigma_{w,q}^{2P}} \right)^{1/2} e^{-\frac{\|\mathbf{x}_q - \mathbf{H}_q^T \mathbf{f}_q\|^2}{2\sigma_{w,q}^2} - \frac{\|\mathbf{y}_q - \mathbf{H}_q \mathbf{s}_q\|^2}{2\sigma_{v,q}^2}} \quad (10)$$

$$f(\mathbf{x}, \mathbf{y} | \mathcal{H}_0) = \prod_{q=0}^{Q-1} \left(\frac{1}{(2\pi)^{N+P} \sigma_{v,q}^{2N} \sigma_{w,q}^{2P}} \right)^{1/2} e^{-\frac{\|\mathbf{x}_q\|^2}{2\sigma_{w,q}^2} - \frac{\|\mathbf{y}_q\|^2}{2\sigma_{v,q}^2}}. \quad (11)$$

The generalized likelihood ratio test for an unknown channel \mathbf{H} is defined as

$$\ell = \max_{\mathbf{H}} \frac{f(\mathbf{x}, \mathbf{y}; \mathbf{H} | \mathcal{H}_1)}{f(\mathbf{x}, \mathbf{y} | \mathcal{H}_0)}. \quad (12)$$

Since \mathbf{H} is a block diagonal matrix, the log-likelihood ratio can be written as the sum of log-likelihood ratios at each individual frequency.

$$\ln[\ell] = \sum_{q=0}^{Q-1} \mathcal{L}_q. \quad (13)$$

Reference [1] shows that these log-likelihood ratios are defined by

$$\begin{aligned} \mathcal{L}_q &= \frac{\|\mathbf{x}_q\|^2 - \|\mathbf{x}_q - \mathbf{H}_q^T \mathbf{f}_q\|^2}{\sigma_{w,q}^2} + \frac{\|\mathbf{y}_q\|^2 - \|\mathbf{y}_q - \mathbf{H}_q \mathbf{s}_q\|^2}{\sigma_{v,q}^2} \quad (14) \\ &= \text{Re} \left\{ 2\text{Tr} [\mathbf{H}_q^* \mathbf{A}_q] - \text{Tr} [\mathbf{H}_q^T \mathbf{H}_q^* \mathbf{C}_q] - \text{Tr} [\mathbf{H}_q^* \mathbf{H}_q^T \mathbf{D}_q] \right\}, \end{aligned}$$

where

$$\mathbf{A}_q = \frac{\mathbf{s}_q^* \mathbf{y}_q^T}{\sigma_{v,q}^2} + \frac{\mathbf{x}_q \mathbf{f}_q^H}{\sigma_{w,q}^2}, \quad \mathbf{C}_q = \frac{\mathbf{s}_q^* \mathbf{s}_q^T}{\sigma_{v,q}^2}, \quad \mathbf{D}_q = \frac{\mathbf{f}_q \mathbf{f}_q^H}{\sigma_{w,q}^2}. \quad (15)$$

Reference [1] also demonstrates that the maximum likelihood estimate of the channel response at each frequency $\hat{\mathbf{H}}_q$ can be determined by solving the Lyapunov-Sylvester equation

$$\begin{aligned} \hat{\mathbf{H}}_q \mathbf{C}_q^T + \mathbf{D}_q^T \hat{\mathbf{H}}_q &= \mathbf{A}_q^T \\ ((\mathbf{C}_q \otimes \mathbf{I}_N) + (\mathbf{I}_P \otimes \mathbf{D}_q^T)) \text{vec}[\hat{\mathbf{H}}_q] &= \text{vec}[\mathbf{A}_q^T] \\ \text{vec}[\hat{\mathbf{H}}_q] &= \mathbf{G}_q^{-1} \text{vec}[\mathbf{A}_q^T]. \end{aligned} \quad (16)$$

Although we will not show it here, by plugging $\hat{\mathbf{H}}_q$ into the log-likelihood ratio in (14), this expression can be reduced to

$$\mathcal{L}_q = \text{Re} \left\{ \text{Tr} [\hat{\mathbf{H}}_q^* \mathbf{A}_q] \right\}. \quad (17)$$

Since \mathbf{G} is a positive-definite matrix

$$\text{Tr} [\hat{\mathbf{H}}_q^* \mathbf{A}_q] = \text{vec}[\mathbf{A}_q^T]^T (\mathbf{G}_q^{-1})^* \text{vec}[\mathbf{A}_q^T]^* \geq 0, \quad (18)$$

the real function can be dropped from the log-likelihood ratio expression.

By placing the expressions from (17) into (13), we can express the generalized log-likelihood ratio in the compact form

$$\ln[\ell] = \text{Tr} [\hat{\mathbf{H}}^* \mathbf{A}] \quad (19)$$

where \mathbf{A} is a $PQ \times NQ$ block diagonal matrix

$$\mathbf{A} = \text{diag}[\mathbf{A}_1, \dots, \mathbf{A}_Q] \quad (20)$$

It should be noted that, with our choice of $\hat{\mathbf{H}}$, the log-likelihood ratio resembles the sum of two channel matched filters,

$$\begin{aligned} \ln[\ell] &= \sum_{q=0}^{Q-1} \text{Tr} \left[\hat{\mathbf{H}}_q^* \left(\frac{\mathbf{s}_q^* \mathbf{y}_q^T}{\sigma_{v,q}^2} + \frac{\mathbf{x}_q \mathbf{f}_q^H}{\sigma_{w,q}^2} \right) \right] \\ &= \sum_{q=0}^{Q-1} \frac{(\hat{\mathbf{H}}_q \mathbf{s}_q)^H \mathbf{y}_q}{\sigma_{v,q}^2} + \frac{(\hat{\mathbf{H}}_q^T \mathbf{f}_q)^H \mathbf{x}_q}{\sigma_{w,q}^2}. \end{aligned} \quad (21)$$

B. Generalized Likelihood Ratio Test with White Gaussian Noise of Unknown Variance

This section considers the same hypotheses as in (9), but the channel characteristics as well as the noise variances are both considered to be unknown. We first consider the situation where the noise is known to be white. We also assume that the noise at both arrays have equal statistics,

$$\sigma_{v,q}^2 = \sigma_{w,q}^2 = \sigma^2. \quad (22)$$

This is a reasonable assumption when the measurement systems for arrays A and B are the same or comparable. For this scenario, the generalized likelihood ratio test is defined as

$$\ell = \frac{\max_{\mathbf{H}, \sigma^2} f(\mathbf{x}, \mathbf{y}; \mathbf{H}, \sigma^2 | \mathcal{H}_1)}{\max_{\sigma^2} f(\mathbf{x}, \mathbf{y}; \sigma^2 | \mathcal{H}_0)}. \quad (23)$$

To determine the maximum likelihood estimate of the unknown variance, the derivative of the log-likelihood function is taken and set to zero. For the alternative hypothesis,

$$\frac{\partial \ln [f(\mathbf{z}; \mathbf{H} | \mathcal{H}_1)]}{\partial \sigma^2} = \frac{\|\mathbf{x} - \mathbf{H}^T \mathbf{f}\|^2 + \|\mathbf{y}^* - \mathbf{H}^* \mathbf{s}^*\|^2}{2\sigma^4} - \frac{Q(N+P)}{2\sigma^2}. \quad (24)$$

By solving for the variance, the maximum likelihood estimate for the alternative hypothesis is shown to be

$$\widehat{\sigma^2}_{\mathcal{H}_1} = \frac{\|\mathbf{x} - \mathbf{H}^T \mathbf{f}\|^2 + \|\mathbf{y}^* - \mathbf{H}^* \mathbf{s}^*\|^2}{Q(N+P)}. \quad (25)$$

Through the same steps, the maximum likelihood estimate for the null hypothesis can be shown to be

$$\widehat{\sigma^2}_{\mathcal{H}_0} = \frac{\|\mathbf{x}\|^2 + \|\mathbf{y}\|^2}{Q(N+P)}. \quad (26)$$

After substituting the maximum likelihood estimates (25) and (26) into (23), the generalized likelihood ratio can be expressed by the equivalent statistic ℓ_0 where

$$\ell = \prod_{q=0}^{Q-1} (\ell_0)^{(N+P)} \quad (27)$$

$$\ell_0 = \frac{\widehat{\sigma^2}_{\mathcal{H}_0}}{\min_{\mathbf{H}} \widehat{\sigma^2}_{\mathcal{H}_1}} = \frac{\|\mathbf{x}\|^2 + \|\mathbf{y}\|^2}{\min_{\mathbf{H}} \|\mathbf{x} - \mathbf{H}^T \mathbf{f}\|^2 + \|\mathbf{y}^* - \mathbf{H}^* \mathbf{s}^*\|^2}. \quad (28)$$

The denominator in (28) is similar to the negation of the log-likelihood ratio function in (14). Since $\widehat{\mathbf{H}}$ in (16) was shown to maximize (14), it will also minimize the denominator in (28). Therefore, (16) remains the maximum likelihood estimate for the channel response. Notice that, when $\sigma_{v,q}^2 = \sigma_{w,q}^2$, the channel estimate $\widehat{\mathbf{H}}$ becomes invariant to the noise statistics. After $\widehat{\mathbf{H}}$ is substituted into (28), the likelihood ratio becomes

$$\ell_0 = \frac{\|\mathbf{x}\|^2 + \|\mathbf{y}\|^2}{\|\mathbf{x}\|^2 + \|\mathbf{y}\|^2 - \text{Tr}[\widehat{\mathbf{H}}^* \widetilde{\mathbf{A}}]}. \quad (29)$$

where

$$\widetilde{\mathbf{A}}_q = \mathbf{s}_q^* \mathbf{y}_q^T + \mathbf{x}_q \mathbf{f}_q^H \quad (30)$$

$$\widetilde{\mathbf{A}} = \text{diag}[\widetilde{\mathbf{A}}_1, \dots, \widetilde{\mathbf{A}}_Q]. \quad (31)$$

The expression in (29) can be rewritten in the form

$$\ell_0 = \frac{1}{(1-\eta)} \quad (32)$$

where

$$\eta = \frac{\text{Tr}[\widehat{\mathbf{H}}^* \widetilde{\mathbf{A}}]}{\|\mathbf{y}\|^2 + \|\mathbf{x}\|^2} \quad (33)$$

is an equivalent likelihood ratio in which $0 \leq \eta \leq 1$. As η approaches 1, ℓ_0 approaches ∞ , and, as η approaches 0, ℓ_0 approaches 1.

C. Generalized Likelihood Ratio Test with Colored Gaussian Noise of Unknown Variance

This section now considers the unknown noise variance to be potentially colored. We assume a large time-bandwidth product so that in the frequency domain, the covariance matrix is diagonal with the noise power spectral density on that diagonal. We also still assume both arrays have equal noise statistics,

$$\sigma_{v,q}^2 = \sigma_{w,q}^2 = \sigma_q^2. \quad (34)$$

The generalized likelihood ratio test for the colored noise case is defined as

$$\forall q : \ell = \frac{\max_{\mathbf{H}, \sigma_q^2} f(\mathbf{x}, \mathbf{y}; \mathbf{H}, \sigma_q^2 | \mathcal{H}_1)}{\max_{\sigma_q^2} f(\mathbf{x}, \mathbf{y}; \sigma_q^2 | \mathcal{H}_0)}. \quad (35)$$

Using the same approach as in the white noise case, the partial derivative of the log-likelihood function is taken with respect to the variance at frequency ω_q and set to zero. After following those steps, the maximum likelihood estimate of the variance for the alternative hypothesis becomes

$$\widehat{\sigma^2}_{q, \mathcal{H}_1} = \frac{\|\mathbf{x}_q - \mathbf{H}_q^T \mathbf{f}_q\|^2 + \|\mathbf{y}_q^* - \mathbf{H}_q^* \mathbf{s}_q^*\|^2}{(N+P)} \quad (36)$$

and the maximum likelihood estimate for the null hypothesis becomes

$$\widehat{\sigma^2}_{q, \mathcal{H}_0} = \frac{\|\mathbf{x}_q\|^2 + \|\mathbf{y}_q\|^2}{(N+P)}. \quad (37)$$

Therefore, the equivalent generalized likelihood ratio is defined, similar to the white noise case, to be

$$\ell_0 = \prod_{q=0}^{Q-1} \frac{\|\mathbf{y}_q\|^2 + \|\mathbf{x}_q\|^2}{\|\mathbf{y}_q\|^2 + \|\mathbf{x}_q\|^2 - \text{Tr}[\widehat{\mathbf{H}}_q^* \widetilde{\mathbf{A}}_q]}. \quad (38)$$

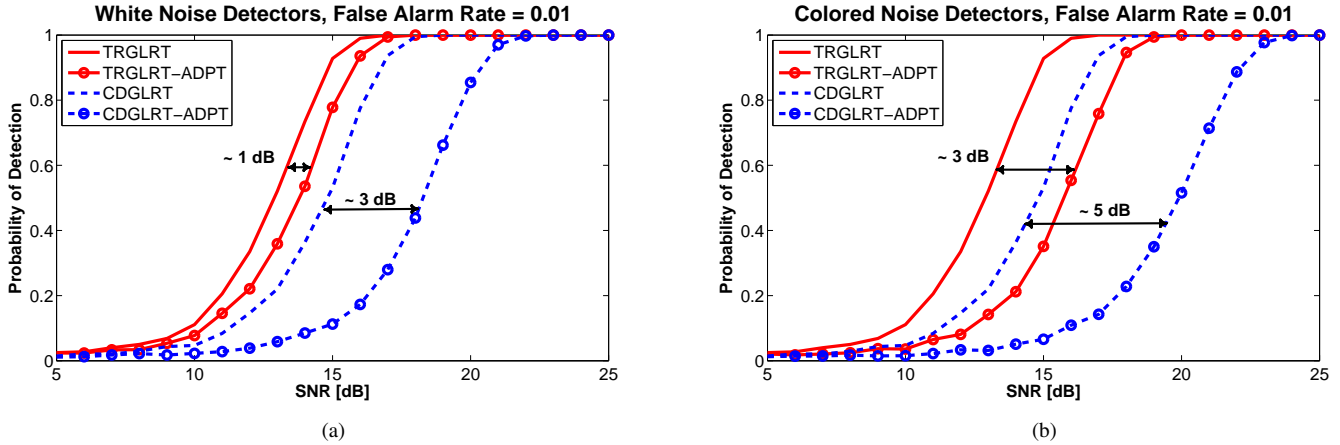


Fig. 3. The plot show the TRGLRT (solid lines) and CDGLRT (dotted lines) detectors under known (no markers) and unknown (circular markers) conditions. (a) The noise is modeled as a *white*, complex Gaussian random variable. (b) The noise is modeled as a *colored*, complex Gaussian random variable.

IV. EXPERIMENTS AND SIMULATIONS

Using two arrays, A and B , of PZT (lead zirconate titanate) transducers bonded to the surface of a steel pipe, we measured the channel response between each of the sensors. Array A consisted of one transducer while B consisted of four. The pipe had dimensions with inner radius 30.15 mm, outer radius 36.75 mm, and length 3050 mm. Each wafer was 5 mm wide, 10 mm long, and 1 mm thick. The arrays were positioned 1.8m apart and the sensors in B equally spaced around half of the circumference of the pipe.

Using a National Instrument PXI data acquisition device, the background response between A and B was measured, with a 300kHz sinc pulse, for a sufficiently long time to accurately estimate the channel. After adding four equally spaced 5 mm wide, 10 mm long, and 1 mm thick saw cuts into the pipe between the two arrays, the response was again measured for a long time to estimate the channel. The difference in these two channel estimates forms the target channel matrix in (4).

Using MATLAB, white noise was added to the measured responses, and the probability of detection was calculated at various levels of signal-to-noise ratio (SNR) by Monte Carlo simulation. The SNR is calculated to be consistent with [1],

$$SNR = \frac{\|\mathbf{H}\mathbf{s}\|^2}{N\sigma_v^2}. \quad (39)$$

Fig. 3a and 3b show the SNR versus probability of detection for the white noise and colored noise Time Reversal Generalized Likelihood Ratio Test (TRGLRT) ($\mathbf{f} = k\mathbf{y}^*$) and Conventional Detection Generalized Likelihood Ratio Test (CDGLRT) ($F_n(\omega_q) = \beta S_p(\omega_q) \forall n, p, q$). The threshold for a false alarm rate $P_{FA} = 0.01$ was determined from 10,000 Monte Carlo trials. The probability of detection at each SNR level was determined using 2000 Monte Carlo trials.

The TRGLRT shows approximately a 2 dB gain over the CDGLRT. When the noise is estimated and known to be white, the TRGLRT performance drops by 1 dB and the CDGLRT performance drops by 3 dB. When the noise is estimated and

not known to be white, the TRGLRT performance drops by 3 dB and the CDGLRT drops by 5 dB.

V. CONCLUSION

We derived a generalized likelihood ratio detector for a back-propagation data model with an unknown channel and unknown Gaussian noise variance. The detector performance was then demonstrated using a time reversal and conventional method of back-propagation. The detector was tested using a complex, multi-modal, and dispersive channel model extracted from nondestructive testing experiments. The simulation results demonstrate that, compared to a more conventional approach, time reversal achieves an overall superior detection performance and smaller drop in performance under unknown noise conditions.

REFERENCES

- [1] Y. Jin and J. M. F. Moura, "Time-Reversal detection using antenna arrays," *IEEE Transactions on Signal Processing*, vol. 57, no. 4, pp. 1396–1414, 2009.
- [2] P. D. Wilcox, M. J. S. Lowe, and P. Cawley, "The effect of dispersion on long-range inspection using ultrasonic guided waves," *NDT and E International*, vol. 34, no. 1, pp. 1–9, 2001.
- [3] P. Cawley, "Practical long range guided wave inspection – managing complexity," *29th Annual Review of Progress in Quantitative Nondestructive Evaluation*, vol. 22, no. 657, pp. 22–40, 2003.
- [4] M. Fink, "Time reversal of ultrasonic fields – part I. basic principles," *IEEE Transactions on Ultrasonics, Ferroelectrics, and Frequency Control*, vol. 39, no. 5, pp. 555–566, 1992.
- [5] A. Derode, P. Roux, and M. Fink, "Acoustic time-reversal through high-order multiple scattering," in *Proceedings of the 1995 IEEE Ultrasonics Symposium*, vol. 2, Seattle, WA, USA, Nov. 1995, pp. 1091–1094.
- [6] J. M. F. Moura and Y. Jin, "Time reversal imaging by adaptive interference canceling," *IEEE Transactions on Signal Processing*, vol. 56, no. 1, pp. 233–247, 2008.
- [7] G. Edelmann, T. Akal, W. Hodgkiss, S. Kim, W. Kuperman, and H. C. Song, "An initial demonstration of underwater acoustic communication using time reversal," *Oceanic Engineering, IEEE Journal of*, vol. 27, no. 3, pp. 602–609, 2002.
- [8] C. Prada, E. Kerbrat, D. Cassereau, and M. Fink, "Time reversal techniques in ultrasonic nondestructive testing of scattering media," *Inverse Problems*, vol. 18, no. 6, pp. 1761–1773, 2002.
- [9] J. M. F. Moura and Y. Jin, "Detection by time reversal: Single antenna," *IEEE Transactions on Signal Processing*, vol. 55, no. 1, pp. 187–201, 2006.

SINGLE ANTENNA TIME REVERSAL DETECTION OF MOVING TARGET

Yuanwei Jin

Engineering and Aviation Sciences
University of Maryland Eastern Shore
Princess Anne, MD 21853
yjjin@umes.edu

José M.F. Moura, Nicholas O'Donoghue, Joel Harley*

Electrical and Computer Engineering
Carnegie Mellon University
Pittsburgh, PA 15213
{moura, nodonoug, jharley}@ece.cmu.edu

ABSTRACT

This paper is concerned with a moving target detection using time reversal in dense multipath environments. We show that the Doppler shift in the time reversal re-transmission simplifies the detector design, yet still achieves the focusing effect. Thus, the Doppler diversity is utilized to achieve high target detectability by time reversal.

Index Terms— Time Reversal, Doppler, Detection

1. INTRODUCTION

Multipath is a common physical phenomenon in radar, sonar and wireless communication applications. For example, the development of underwater sonar and communication systems must cope with challenging environmental conditions, such as severe multipath due to sound reflection on the surface and bottom. For radar systems, the urban scenario is rich in multipath propagation generated by multiple reflections, refractions, and scattering of the radar signal from buildings and other structures. Time reversal has been explored as a complement to conventional multipath compensation [1]. We have developed time-reversal based data processing algorithms for target detection and localization [2]. In addition to the theoretical analysis of time reversal, experiments have been conducted in underwater acoustics and electromagnetic to demonstrate the focusing effect of time reversal [3, 4]. In a typical time reversal experiment, the signal received by an antenna would be digitized, energy normalized, time-reversed, and re-transmitted from the same antenna element. The underlying condition for time reversal is that the propagation media is reciprocal. Under this condition, time reversal achieves spatial and temporal focusing of energy. In reality, the source, the antennas, and the medium may not be strictly stationary. Questions rise if the time reversal focusing is still achievable when either the medium or the source is non-stationary. Underwater acoustic experiments and theoretical analysis have demonstrated that the focusing can still be achieved [1, 3, 5]. In this paper, we address the problem of time reversal detection of moving target using a bi-static radar. For simplicity, we assume that the target moves, while the channel and the antennas are stationary. In this paper, we analyze the impact of Doppler shift due to target motion in a dense multipath

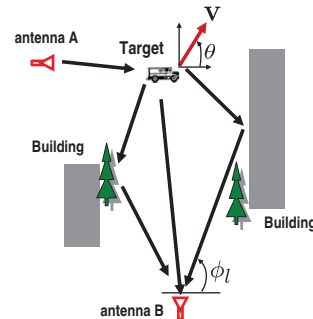


Fig. 1. Moving target detection in dense multipath environment using a bi-static radar. Antenna A sends a probe signal; Antenna B acts like a mirror by re-sending the time-reversed received signal; Detection is implemented by Antenna A.

environment on time reversal focusing, and subsequently the detector design and performance.

2. PROBLEM DESCRIPTION AND SIGNAL MODEL

2.1. Multipath Environments

We assume that the background environment is stationary and can be probed before the target appears. This assumption implies that the dominant multipath due to the background can be identified by successive probing and then subtracted from the test data that may contain the reflections from a moving target. This assumption simplifies the problem and our analysis. In a multipath rich environment, for example, urban environments, building walls produce specular reflections of the radar signal, which impinge on the target from different incident angles. Thus, multipath propagation increases the spatial diversity of the radar system. Furthermore, each multipath component is affected by a different Doppler shift corresponding to the projection of the target velocity on the direction-of-arrival (DOA) of each path. The Doppler frequency shift is widely used to separate moving targets from stationary clutter [6]. Exploitation of multiple Doppler shifts should increase the ability of the radar to detect targets. In this paper, we discuss the impact of target motion on time reversal based detectors.

*This joint work is supported in part by the Department of Energy under award no. DE-NT-0004654, the National Science Foundation under award no. CNS-093-868, and the Defence Advanced Research Projects Agency through the Army Research Office under grant no. W911NF-04-1-0031. N. O'Donoghue and J. Harley are supported by a National Defense Science and Engineering Graduate Fellowship, sponsored by the Army Research Office and the Office of Naval Research, respectively.

2.2. Signal Model

We consider, for example, a ground moving target in a urban canyon environment rich in multipath reflections as illustrated in Fig. 1. Let $s(t)$ represent the transmit signal from the radar antenna with total energy $E_s = \int_0^T s(t)^2 dt$, where T is the signal duration. This signal impinges on the target; the reflected signal from the target, as well as from the surrounding reflectors, reaches the receive antenna. Let $h_l(t)$ denote the l -th propagation path channel impulse response between the transmitter, the target, and the receiver. The target is assumed to be in the far-field and is moving with a constant velocity $\mathbf{v} = (|\mathbf{v}|\cos\theta, |\mathbf{v}|\sin\theta)$ relative to the radar, where θ is the relative angle. Since L multipath signals impinge on the target from different incident angles, they produce L different relative Doppler shifts. We let $\mathbf{u}_l = (\cos\phi_l, \sin\phi_l)$ denote the unit vector of the direction of arrival (DOA) along the l -th propagation path, where

$$\phi_l \in [0, 2\pi], \quad l = 0, \dots, L-1. \quad (1)$$

Therefore, the scaling factor of the differential Doppler shift for the l -th path can be written as

$$\beta_l = \frac{\langle \mathbf{v}, \mathbf{u}_l \rangle}{c} = \frac{|\mathbf{v}|(\cos\theta\cos\phi_l + \sin\theta\sin\phi_l)}{c}, \quad (2)$$

where c is the speed of propagation; $\langle \cdot, \cdot \rangle$ denotes the inner-product operator over the real vector space. Thus, the multipath propagation provides enhanced spatial diversity to a radar system. Next, we describe the signal model of forward transmission and time reversal backward retransmission.

2.2.1. Initial Probing - Forward Transmission

Antenna A transmits a probe waveform $s(t)$, the received l -th path signal reflected from the target is (ignore noise for the moment) is recorded at the antenna B.

$$x_l(t) = \int h_l(\tau) s(t - \tau) e^{j\omega_c \beta_l (t - \tau)} d\tau \quad (3)$$

$$= s(t) e^{j\omega_c \beta_l t} * h_l(t), \quad (4)$$

where the symbol $*$ represents the convolution. Eqn. (4) shows that the pulse shape $s(t)$ is distorted by the l -th Doppler shift. Next, let

$$h(t) = \sum_{l=0}^{L-1} h_l(t), \quad 0 \leq t \leq T_s \quad (5)$$

denote the time dispersive channel response; $h(t)$ is a time spreading function of effective length T_s . To be more specific, $h_l(t)$ is defined as

$$h_l(t) = \alpha_l \delta(t - \tau_l). \quad (6)$$

Hence, the total received signal from the forward transmission is given by

$$x(t) = \sum_{l=0}^{L-1} x_l(t) + v(t) \quad (7)$$

$$= \sum_{l=0}^{L-1} \alpha_l s(t - \tau_l) e^{j\omega_c \beta_l (t - \tau_l)} + v(t) \quad (8)$$

where $v(t)$ is the additive Gaussian noise and is independent of the signal; L is the number of dominant paths.

2.2.2. Time Reversal - Backward Retransmission

In the backward transmission, the antenna B acts as a time reversal mirror. Because this is a single antenna that acts like a mirror, this scenario represents the limiting case for time reversal. Based on the assumption we made in 2.1, the signals due to background can be subtracted. The residue received signal $x(t)$ is time-reversed, energy normalized, and re-sent. We assume that the delay between the forward and time-reversed transmissions is sufficiently small so that the target displacement during that interval will be negligible, and the multipath structure of the channel can be regarded as constant. The purpose of time reversal re-transmission is to utilize the spatial and temporal focusing of time reversal to compensate for the multipath. The target detection will be implemented at the original antenna location, i.e., at the antenna A. The received signal at Antenna A becomes

$$y(t) = \sum_{l=0}^{L-1} h_l(t) * k x^*(-t) e^{j\omega_c \beta_l t} \quad (9)$$

$$= k \sum_{l=0}^{L-1} h_l(t) * \left(\sum_{l'=0}^{L-1} s^*(-t) e^{j\omega_c \beta_{l'} t} * h_{l'}^*(-t) \right) e^{j\omega_c \beta_l t}$$

$$= k \sum_{l=0}^{L-1} \sum_{l'=0}^{L-1} \alpha_l \alpha_{l'}^* s^*(-t + \tau_l - \tau_{l'}) e^{j\omega_c \beta_{l'} (-t + \tau_l - \tau_{l'})} e^{j\omega_c \beta_l (t - \tau_l)}$$

$$= k \sum_{l=0}^L |\alpha_l|^2 s^*(-t) e^{-j\omega_c \beta_l \tau_l} + \quad (10)$$

$$k \sum_{l \neq l'}^{L-1} \alpha_l \alpha_{l'}^* s^*(-t + \tau_l - \tau_{l'}) e^{j\omega_c \beta_{l'} (-t + \tau_l - \tau_{l'})}$$

$$\approx k \sum_{l=0}^L |\alpha_l|^2 s^*(-t) e^{-j\omega_c \beta_l \tau_l} \quad (11)$$

$$= k G_L s^*(-t) \quad (12)$$

where

$$G_L \triangleq \sum_{l=0}^L |\alpha_l|^2 e^{-j\omega_c \beta_l \tau_l} \quad (13)$$

$$k \triangleq \sqrt{\frac{E_s}{\int_0^{T_s} |x(t)|^2 dt}} \quad (14)$$

In the above derivation, we use Eqn. (6) to represent a multipath channel. The approximation in (11) is valid because of the focusing effect in time reversal re-transmission. The scaling factor k is to ensure the same amount of transmission energy. Eqn. (13) is the total gain of the L paths, each path has its own Doppler shift. It implies that multipath compensation is achieved by time reversal even in the presence of differential Doppler shifts, however, the focus gain is modulated by phase rotation. To further quantify the focusing gain in the presence of the Doppler shift, we analyze the term G_L by statistical approaches. Note that the phase term

$$\theta_l \triangleq \omega_c \beta_l \tau_l = 2\pi f_c \beta_l \tau_l \quad (15)$$

will change by 2π rad whenever $\beta_l \tau_l$ changes by $\frac{1}{f_c}$, where f_c is the radar carrier frequency. But $\frac{1}{f_c}$ is a small number and, hence, θ_l can change by 2π rad with relatively small motions of the target or a propagation path. Because the number of multipaths L is assumed to be large, the impinging angle of the path to the antenna is assumed to be $[-\pi, \pi]$ in an unpredictable (random) manner. This implies that G_L can be modeled as a random process. When there are a large number of paths, the central limit theorem applies. This means G_L is a complex valued Gaussian random process,

$$G_L \simeq \mathcal{CN} \left(\sum_{l=1}^L \mu_l, \sum_{l=1}^L \Phi_l \right), \quad (16)$$

where

$$\mu_l = E\{|\alpha_l|^2 e^{j\omega_c \beta_l \tau_l}\} = 0, \quad (17)$$

$$\Phi_l = \text{Var}\{|\alpha_l|^2 e^{j\omega_c \beta_l \tau_l}\} = \text{Var}\{|\alpha_l|^2\} \quad (18)$$

Here we assume that the l -th path gain α_l is a complex Gaussian random variable with zero mean and variance σ_α^2 . Hence, $|\alpha_l|^2$ is distributed as a $\sigma_\alpha^2 \chi_2^2$, where χ_2^2 denotes the central chi-squared distribution with 2 degrees of freedom. Therefore, $\Phi_l = 4\sigma_\alpha^4$, i.e., (16) can be re-written as

$$G_L \simeq \mathcal{CN}(0, 4L\sigma_\alpha^4), \quad (19)$$

3. DETECTORS

In this section, we formulate the time reversal detection problem for moving target where the Doppler shift is present. To emphasize that we have a multipath rich environment in which time reversal achieves full advantage, we make the following assumptions: (A1) The number of paths L is sufficiently large; (A2) The multipath direction of arrival $0 \leq \phi_l \leq 2\pi$ is uniformly random; and (A3) The multipath complex gain is Gaussian distributed with zero mean and variance σ_α^2 , i.e., $\alpha_l \sim \mathcal{CN}(0, \sigma_\alpha^2)$.

3.1. Time reversal detector

From Eqn. (12), we know that the received signal after time-reversal re-transmission can be written as follow:

$$y(t) = z(t) + w(t), \quad 0 \leq t \leq T \quad (20)$$

where $w(t)$ is the additive noise, T is the observation time of the signal, and

$$z(t) \triangleq k G_L s^*(-t). \quad (21)$$

Finally, we assume that the received signal is converted to baseband prior to sampling and then sampled at sampling rate $f_s = B$. The discrete version of (20) is

$$y(n) = z(n) + w(n), \quad n = 0, \dots, N-1 \quad (22)$$

where $N = f_s T$. Define

$$\mathbf{y} = [y(0), y(1), \dots, y(N-1)]^T \quad (23)$$

$$\mathbf{z} = [z(0), z(1), \dots, z(N-1)]^T \quad (24)$$

$$\mathbf{w} = [w(0), w(1), \dots, w(N-1)]^T \quad (25)$$

Using (19), we have

$$z(n) \sim \mathcal{CN}(0, k^2 4L\sigma_\alpha^4 |s(-n)|^2). \quad (26)$$

Here we assume that the scalar k is approximately a constant. This assumption is approved to be valid [2]. Hence, the time-reversal detection problem in the presence of target motion is

$$\begin{aligned} \mathbb{H}_1 : \mathbf{y} &= \mathbf{z} + \mathbf{w} \\ \mathbb{H}_0 : \mathbf{y} &= \mathbf{w} \end{aligned} \quad (27)$$

3.2. Conventional detector

The discrete form of the received signal from the forward transmission, (8), can be written as

$$x(n) = \sum_{l=0}^{L-1} \alpha_l s(n-l) e^{j\omega_c \beta_l (n-l)/f_s} + v(n), \quad (28)$$

$$= r(n) + v(n) \quad (29)$$

where $n = 0, \dots, N-1$, $L = f_s T_s$, and

$$r(n) \triangleq \sum_{l=0}^{L-1} \gamma_{n,l} s(n-l) \quad (30)$$

$$\gamma_{n,l} \triangleq \alpha_l e^{j\omega_c \beta_l (n-l)/f_s} \sim \mathcal{CN}(0, \sigma_\alpha^2). \quad (31)$$

We notice that, in the absence of Doppler shift (i.e., if $\beta_l = 0$), the likelihood ratio test detector would be the replica correlation integration detector given in [7]. In the presence of the Doppler shift, and given the assumptions (A1) and (A2), we will employ the central limit theorem to simplify the detector design. From (30) and (31), by the central limit theorem, we obtain

$$r(n) \simeq \mathcal{CN} \left(\sum_{l=1}^L \eta_l, \sum_{l=1}^L \Psi_l \right), \quad (32)$$

where

$$\eta_l = E\{\gamma_{n,l} s(n-l)\} = 0, \quad (33)$$

$$\Psi_l = \text{Var}\{\gamma_{n,l} s(n-l)\} = \sigma_\alpha^2 |s(n-l)|^2 \quad (34)$$

Therefore, the statistics for $r(n)$ can be written as

$$r(n) \simeq \mathcal{CN} \left(0, \sigma_\alpha^2 \sum_{l=0}^{L-1} |s(n-l)|^2 \right), \quad (35)$$

Define

$$\mathbf{x} = [x(0), x(1), \dots, x(N-1)]^T \quad (36)$$

$$\mathbf{r} = [r(0), r(1), \dots, r(N-1)]^T \quad (37)$$

$$\mathbf{v} = [v(0), v(1), \dots, v(N-1)]^T \quad (38)$$

which leads to the conventional detection problem formulated as

$$\begin{aligned} \mathbb{H}_1 : \mathbf{x} &= \mathbf{r} + \mathbf{v} \\ \mathbb{H}_0 : \mathbf{x} &= \mathbf{v} \end{aligned} \quad (39)$$

4. PERFORMANCE ANALYSIS AND SIMULATION

In this section, we will analyze the performance of the TR detector. The signal-to-noise ratio is defined as $\text{SNR} = 10 \cdot \log_{10} \frac{E_s \sigma_\alpha^2}{\sigma_n^2}$. To derive the data statistics, we first consider the noise-only case under \mathbb{H}_0 . For the detection problem (27), the data is distributed as $\mathbf{y} \sim \mathcal{CN}(0, \sigma_n^2 \mathbf{I})$; For the detection problem (39), the data is distributed as $\mathbf{x} \sim \mathcal{CN}(0, \sigma_n^2 \mathbf{I})$. Under the signal plus noise case (i.e., \mathbb{H}_1), for the detection problem (27), the data is distributed as

$$\mathbf{y} \sim \mathcal{CN}(0, k^2 L \sigma_\alpha^4 \mathbf{s}^* \mathbf{s}^T + \sigma_n^2 \mathbf{I}). \quad (40)$$

where $\mathbf{s} = [s(0), s(1), \dots, s(N-1)]^T$. For the detection problem (39), the data is distributed as

$$\mathbf{x} \sim \mathcal{CN}(0, \Psi + \sigma_n^2 \mathbf{I}) \quad (41)$$

where $\Psi = \text{diag}[\psi_0, \dots, \psi_{N-1}]$, and

$$\psi_i = \frac{1}{\sigma_n^2 + \sigma_\alpha^2 \sum_{l=0}^{L-1} |s(i-l)|^2}, \quad i = 0, \dots, N-1 \quad (42)$$

We notice that (27) or (39) can be formulated as the Gauss-Gauss problem where both the signal and the noise have Gaussian distributions [8]. Hence, the detector can be derived using the likelihood ratio test

$$\ell(\mathbf{x}) = \log \frac{f(\mathbf{x}; \mathbb{H}_1)}{f(\mathbf{x}; \mathbb{H}_0)}, \quad (43)$$

where $f(\cdot; \mathbb{H}_i)$ is the probability density function under \mathbb{H}_i , $i = 0, 1$, respectively. Due to space limitation, we present here the final test statistic and omit the detailed mathematical derivation. The time reversal detector is

$$\ell_{\text{TR}}(\mathbf{y}) = \left| \sum_{n=0}^{N-1} y(n) s(-n) \right|^2. \quad (44)$$

The conventional detector is

$$\ell_{\text{CON}}(\mathbf{x}) = \sum_{l=0}^{L-1} \sum_{n=0}^{N-1} \frac{|x(n) s^*(n-l)|^2}{\sigma_n^2 + \sigma_\alpha^2 \sum_{l=0}^{L-1} |s(n-l)|^2} \quad (45)$$

Next, we conduct numerical simulations. The transmitting signal is a linear frequency modulated (LFM) signal (in baseband)

$$s(t) = e^{j2\pi B/(2T)t^2}, \quad -T/2 \leq t \leq T/2 \quad (46)$$

where $B = f_s = 20$ MHz, $T = 5$ μ second. Assume that the channel dispersion is $T_s = 1$ μ second, $\sigma_\alpha^2 = 2$. Hence, $N = f_s T = 100$, and $L = f_s T_s = 20$. Fig. 2 shows the receiver operating characteristic (ROC) curve at the false alarm rate of $P_{\text{FA}} = 10^{-4}$ using 300,000 Monte Carlo runs. The result shows that the time reversal method has about 2.5-dB gain over the conventional detector at $P_d = 0.8$.

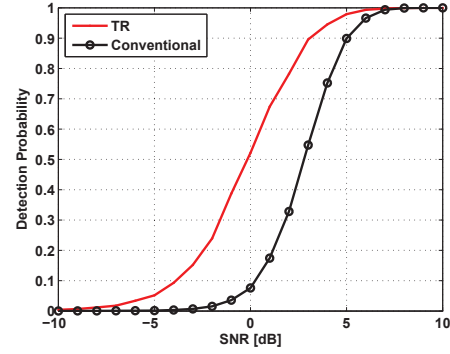


Fig. 2. Receiver operating characteristics. The number of dominant paths $L = 20$; The false alarm rate $P_{\text{FA}} = 10^{-4}$.

5. CONCLUSION

In this paper, we develop a time reversal detector for moving target. Our analysis shows that time reversal achieves spatial focusing in the presence of Doppler shifts. Due to target motion, the focusing gain is modulated with a phase rotation. In dense multipath, the time reversal detector shows a significant performance gain over the conventional detector.

6. REFERENCES

- [1] D. R. Jackson and D. R. Dowling, "Phase conjugation in underwater acoustics," *Journal of Acoustical Society of America*, vol. 89, no. 1, pp. 171–181, January 1990.
- [2] Y. Jin and J. M. F. Moura, "Time reversal detection using antenna arrays," *IEEE Transactions on Signal Processing*, vol. 57, no. 4, pp. 1396–1414, April 2009.
- [3] W. J. Higley, P. Roux, W. A. Kuperman, W. S. Hodgkiss, H. C. Song, T. Akal, and M. Stevenson, "Synthetic aperture time-reversal communications in shallow water: Experimental demonstration at sea," *Journal of Acoustical Society of America*, vol. 118, no. 4, pp. 2365–2372, October 2005.
- [4] Y. Jin, J. M. F. Moura, Y. Jiang, D. Stancil, and A. Cepni, "Time reversal detection in clutter: additional experimental results," *IEEE Transactions on Aerospace and Electronic Systems*, to appear.
- [5] J. Gomes and V. Barroso, "Doppler compensation in underwater channels using time-reversal arrays," in *ICASSP'03, IEEE International Conference on Acoustics, Speech, and Signal Processing*, vol. V. Hong Kong, China: IEEE, April 2003, pp. 81–84.
- [6] M. Skolnik, *Radar Handbook*, 3rd ed. New York, NY: McGraw Hill, 2008.
- [7] B. Friedlander and A. Zeira, "Detection of broadband signals in frequency and time dispersive channels," *IEEE Transactions on Signal Processing*, vol. 44, no. 7, pp. 1613–1622, July 1996.
- [8] L. L. Scharf, *Statistical Signal Processing: Detection, Estimation, and Time Series Analysis*. Reading, MA: Addison-Wesley Publishing Company, 1991.

Cognitive Sensor Networks for Structure Defect Monitoring and Classification Using Guided Wave Signals

Yuanwei Jin^{*}, Nicholas O'Donoghue[†], José M. F. Moura[†], Joel Harley[†], James H. Garrett[‡],
Irving J. Oppenheim[‡], Lucio Soibelman[‡], Yujie Ying[‡], and Lin He^{^b}

^{*}Engineering and Aviation Sciences, University of Maryland Eastern Shore, Princess Anne, MD
21853

[†]Electrical and Computer Engineering, Carnegie Mellon University, Pittsburgh, PA 15213

[‡]Civil and Environmental Engineering, Carnegie Mellon University, Pittsburgh, PA 15213

^bSchool of Civil Engineering, Harbin Institute of Technology, Harbin, China 150090

ABSTRACT

This paper develops a framework of a cognitive sensor networks system for structure defect monitoring and classification using guided wave signals. Guided ultrasonic waves that can propagate long distances along civil structures have been widely studied for inspection and detection of structure damage. Smart ultrasonic sensors arranged as a spatially distributed cognitive sensor networks system can transmit and receive ultrasonic guided waves to interrogate structure defects such as cracks and corrosion. A distinguishing characteristic of the cognitive sensor networks system is that it adaptively probes and learns about the environment, which enables constant optimization in response to its changing understanding of the defect response. In this paper, we develop a sequential multiple hypothesis testing scheme combined with adaptive waveform transmission for defect monitoring and classification. The performance is verified using numerical simulations of guided elastic wave propagation on a pipe model and by Monte Carlo simulations for computing the probability of correct classification.

Keywords: Sensor networks, guided waves, structure defects, monitoring, classification

1. INTRODUCTION

Sensor networks have been widely used in civil structure monitoring and defect detection.^{1,2,3} Active sensors, or actuators, are increasingly being deployed in structure health monitoring applications in complex environments. Smart structures and sensor systems within complex environments require adaption via constant monitoring of interference signals, cooperation with other sensors, and optimized transmission waveforms. Cognitive sensor networking is an emerging technology that aims to optimize the performance of active sensors within resource-constrained and interference limited environments. Cognition is a term that is interpreted as “knowing, perceiving, or conceiving as an act.” A cognitive system possesses three distinct capabilities, i.e., intelligent sensing and monitoring its environment through interaction between the sensor system and the environment; feedback from the receive sensor to the transmit sensor that enables adaptive transmission; and sophisticated signal processing and information fusion. A cognitive sensor networks system combines various recent technology advancement in information fusion, intelligent sensors, sensing grids, communication protocols, network routing, and complex event processing architectures. There are a growing number of cognitive systems being developed. For example, cognitive radio is a novel approach in wireless communications.^{4,5} In a cognitive radio network, radio devices can figure out which frequencies are quiet and pick one or more over which to transmit and receive data. By changing its transmission or reception parameters based on the active monitoring of radio environment, such as radio frequency spectrum, user behavior and network state, the system achieves improved communication efficiency. Cognitive radar is a remote sensing system that builds up its knowledge of the environment from received radar echoes.⁶ From a signal processing perspective, the radar system can achieve cognition by forming a hypothesis regarding targets in the radar scene, and then testing that hypothesis for the likelihood of its correctness. The cognition can be realized by adaptively transmitting illumination signals to learn about the environment and the target of interest using a Bayesian representation of the target channel.

Contact information: Y. Jin; phone: (410)621-3410, fax: (410)651-4436, e-mail: yjin@umes.edu.

In this paper, we develop the framework of a cognitive sensor networks system for structure defect monitoring and classification using guided wave signals. In the structure health monitoring application, the goal of cognitive sensor networking is to provide the overall sensing system with the capability to integrate information about the elastic wave propagation environment, and capabilities and cooperate with other sensors, as well as obtain inputs from external knowledge bases. This paper focuses on defect classification and monitoring by Lamb wave signals using a group of piezoelectric transducers. Guided elastic waves form as a result of the interaction between harmonic waves propagating in a medium, for example, pipes and plates, and those medium's boundaries. Guided waves that form in thin plates and cylindrical shells are commonly used for non-destructive inspection of structure defects^{7,8} and are extensively studied.^{9,10} Guided waves that propagate in cylindrical shells, i.e., pipes, are characterized by an infinite number of dispersive longitudinal and torsional modes and a doubly infinite number of flexural modes.^{8,11} The longitudinal and torsional modes are both axisymmetric while each flexural mode exhibits an infinite number of non-axisymmetric circumferential mode orders. Due to the complexity of the guided wave propagation in solid medium, various wave mode control and design schemes are developed. For example, transmission schemes with narrowband, low frequency, single mode excitations are used to suppress unwanted modes and to reduce the influence of dispersion. Transducer geometries and designs can often be exploited for mode selectivity.^{12,13,14} Furthermore, sensors designed and manufactured using smart materials have been introduced in health structure monitoring. For example, the conventional acoustic sensors made of piezo-ceramic materials are brittle and unsuitable for curved pipelines; smart materials such as Macro Fiber Composite (MFC) sensors are more rugged, flexible, and durable. Hence, MFC are appealing to the field operational conditions of pipelines. All these efforts improve the sensitivity and accuracy of the sensor network systems and provide a platform for developing a unified cognitive sensor system based on guided Lamb wave propagation and signaling.

Recently, a growing amount of research has been devoted to time reversal based waveform transmission for the applications of detection, localization, and classification.^{15,16,17,18} Time reversal is considered as an adaptive waveform transmission scheme that implements iterative probing and learning from the returned sensing signals based on the interaction of the sensor and the environment. For the problem of defect monitoring and classification, in this paper, the cognition of a sensor work system is characterized by the sequential hypothesis probability testing and adaptive waveform transmission. The rationale for combining sequential hypothesis test and adaptive waveform transmission is to enable the cognitive sensor system to update its understanding of the defect channel and the surrounding environment without necessarily making hard decisions after each transmission. The understanding of the defect channel and the environment by the cognitive system is formulated by the Bayesian representation of the defect channel in a statistical sense. By a sequential test of a statistical hypothesis, the statistical test procedure at any stage of the experiment will either (1) accept the hypothesis being tested, (2) reject the hypothesis, or (3) to continue the experiment by making an additional observation. Thus, such a test procedure is carried out sequentially.¹⁹ On average, a sequential test requires fewer observations than an equal-strength test with a fixed number of observation.¹⁹ Hence, a sequential test for defect classification is appealing to the sensor networks system because of the improved efficiency and reduced energy consumption for each sensor. In our case, we will discuss a multiple-hypothesis sequential test for structure defect classification in order to distinguish the received sensor data of a particular defect (a hypothesis) from other possible defects (other hypotheses).

The paper is organized as follows. Section 2 presents problem formulation and signal models. Section 3 develops the multiple hypothesis sequential test and discusses waveform design strategies and their connection with the time reversal scheme. Section 4 presents simulation based results for defect classification. Conclusion is drawn in section 5.

2. PROBLEM FORMULATION AND SIGNAL MODELS

We consider the defect classification problem in which there are M possible defects on a structure. In many real applications, typical structure defects such as corrosion and cracks can be pre-surveyed from historical field test data under given environment conditions. For example, pipelines are widely used engineering structures for the transportation of fluid from one place to another. In many instances pipelines are placed underground, under runways, railways or roadways. Usually pipelines suffer various degrees of deterioration due to aggressive environments such as temperature, soil conditions, ground activities, etc. The environmental conditions where the pipelines are positioned can be pre-surveyed and the typical defects such as corrosion (e.g., pitting or crevice corrosion) and cracks under this environment given the pipe material properties can be pre-determined. From the historical field test data and the given environmental condition, a data base can be established regarding the type of defects that are most likely to occur under this environment and their profile in response to guided elastic wave probing.

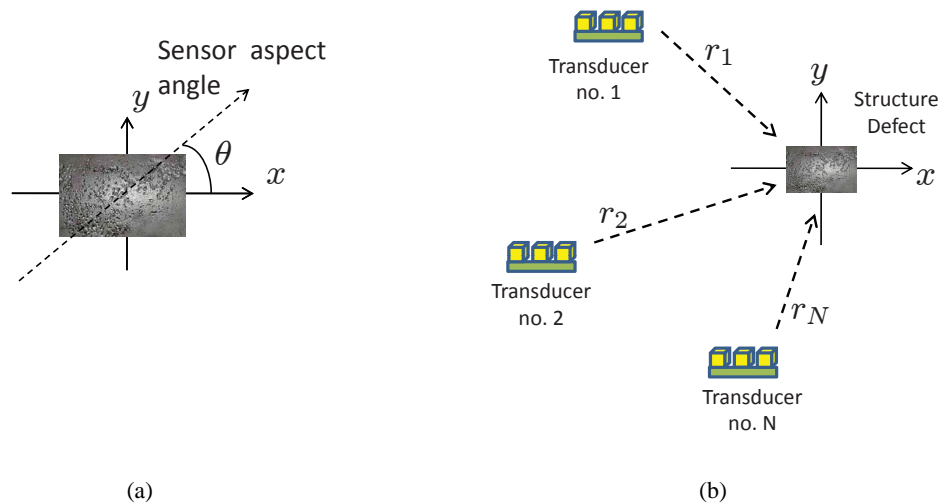


Figure 1. (a) Defect (e.g., corrosion pitting) aspect angle. (b) Geometry of cognitive transducer network for structure defect monitoring.

We use a group of networked active piezoelectric sensors to probe the region of interest on a structure and record the received signals. The objective of the sensor networks deployed is to identify which structure defect is present with high accuracy under the constraint of limited transmission energy. In this section, we first describe a general framework of cognitive sensor networks for monitoring and classifying structure defects. We then establish a signal model.

2.1 Monitoring configuration

We consider a network of piezoelectric sensors that are mounted on the surface of a thin civil structure. For simplicity, we assume that the defects and the sensors are located in the same plane. Fig. 1(a)-(b) depict the monitoring geometry using a transducer network. Each defect is characterized by a known impulse response $h(t; \theta, H_j)$, $j = 1, 2, \dots, M$. The impulse response can be measured offline from every aspect angle. This aspect angle θ is defined as the angle between the major axis of the defect and the sensor light-of-sight. From the linear elastic wave theory, the wave motion in elastic solids is governed by the wave propagation equations under various boundary conditions. The displacement function that describes the wave groups propagation along a solid medium over time should be handled with respect to position and time.⁹ In this paper, we consider the defect classification problem in which we try to recognize what defect is present given the received sensor data. Thus, we use the channel impulse response $h(t; \theta, H_j)$ to represent the defect response in which the position argument is omitted.

Fig. 1(b) shows a cognitive sensor network that monitors and classifies a structure defect. The network consists of N sensors, each sensor can generate transmission signal at a propagation angle θ respect to the defect. An example of the acoustical sensor that is capable of steering excitation angle is the ultrasonic transducer phased arrays.^{20,21} Ultrasonic phased arrays are made of multiple piezoelectric elements which are subsequently activated by time delay pulses. In general, phased arrays can be categorized as linear arrays, planar arrays, and annular arrays by their geometry. A linear array is composed of a number of individual elements arranged in a single line assembly. Beamforming techniques are the most significant advantage of phased arrays over conventional ultrasonic transducers, which is achievable by adjusting the time delays between array transducer elements. The beamforming includes beam steering and focusing. Beam steering of a linear phased array can be achieved by sequentially exciting individual elements with fixed time delays. The sound field of such configuration can be represented by the synthesis of pressure contributed by individual elements, according to the Huygens' principle. The steering angle (θ) or the propagation angle of the beam is a function of wave speed in the medium (v), time delay between adjacent elements ($\Delta\tau$), and the spacing between the elements (d), such that $\Delta\tau = \frac{d \sin \theta}{v}$. Beam focusing is accomplished by variably delaying a group of elements with respect to the center element. In this paper, we refer the steering angle of the transducer array as the aspect angle of the structure defect shown in Fig. 1(a). The cognitive sensor network system interrogates the structure defect from different aspect angles. The relative distance between the defect and each sensor is denoted as r_n , $n = 1, \dots, N$. If the wave propagation speed (phase velocity v_p or group velocity

v_g), the relationship between the distance r_n can be determined as $r_n = v_g \times \Delta t_n$, where Δt_n is the round trip time delay between the sensor, the defect, and back to the sensor. Here we assume that each sensor within the network is composed of a few elements and is capable of generating focused beams. In principle, this sensor network system is able to detect, locate and classify the defect. In this paper, we focus on defect classification and monitoring using a network of ultrasonic sensors.

2.2 Signal model

For simplicity, we consider the backscattered echo transmitted from each sensor in the network. This implies that each sensor probes the environment by transmitting a waveform and receives the returned signal for processing. We also assume that the interference between the sensors is negligible. This assumption is valid in general for spatially sparsely displaced sensors for large civil structure monitoring. Hence, the signal model for n -th sensor in the network can be written as

$$x_n(t) = a_n h(t; \theta_n, H_j) * s_n(t) + w_n(t) \quad (1)$$

where $h(t; \theta_n, H_j)$ is the defect impulse response for the j -th hypothesis H_j at aspect angle θ_n . Note that in the linear elastic wave theory, the displacement is in general a function of position and time. Because both the sensor and the defect are fixed and we are only interested in the signals received at each sensor, we hence omit the position argument in (1). The defect impulse response is defined as the response of the medium between the sensor and the defect. In general, it can be described as the Green's function.^{9,10} The symbol $*$ denotes the linear convolution. The symbol a_n denotes an unknown complex coefficient representing the amplitude uncertainty of the backscattered signal from the defect. $w_n(t)$ is the additive white complex Gaussian noise at the receiver. $s(t)$ is the transmitted signal. We assume that the waveform is energy-limited, i.e.,

$$E_s = \int_0^T |s(t)|^2 dt \quad (2)$$

where E_s is the energy allocated to a single transmission and T is the waveform duration in which the signal is non-zero. This assumption has both theoretical importance and practical significance. The energy constraint allows to construct an optimal transmission waveform that achieves maximal signal-to-noise ratio at the receiver output. In practice, each sensor in the network is usually powered by battery, thus, energy aware or constraint sensor network design is a practical issue.

Suppose that the continuous time signals in (1) are sampled with a sampling frequency of f_s , which yields the discrete-time signal $\{s_n(i), i = 0, \dots, L_s - 1\}$, $\{h(i; \theta_n, H_j), i = 0, \dots, L_h - 1\}$, $\{x_n(i), i = 0, \dots, L - 1\}$, and $\{w_n(i), i = 0, \dots, L - 1\}$, where $L = L_s + L_h - 1$, we can re-write equation (1) in a discrete-time form as follows:

$$\mathbf{x}_n = a_n \mathbf{H}_{\theta_n, H_j} \mathbf{s}_n + \mathbf{w}_n, \quad (3)$$

where

$$\mathbf{x}_n = [s_n(0), s_n(1), \dots, s_n(L - 1)]^T, \quad (4)$$

$$\mathbf{w}_n = [w_n(0), w_n(1), \dots, w_n(L - 1)]^T, \quad (5)$$

$$\mathbf{s}_n = [s_n(0), s_n(1), \dots, s_n(L_s - 1)]^T, \quad (6)$$

and $L \times L_s$ convolution matrix is

$$\mathbf{H}_{\theta_n, H_j} = \begin{pmatrix} h(0; \theta_n, H_j) & 0 & \dots & 0 \\ h(1; \theta_n, H_j) & h(0; \theta_n, H_j) & \dots & \vdots \\ \vdots & h(1; \theta_n, H_j) & \dots & \vdots \\ h(L_h - 1; \theta_n, H_j) & \vdots & \vdots & 0 \\ 0 & h(L_h - 1; \theta_n, H_j) & \dots & h(0; \theta_n, H_j) \\ \vdots & \vdots & \dots & h(1; \theta_n, H_j) \\ \vdots & \vdots & \dots & \vdots \\ 0 & 0 & 0 & h(L_h - 1; \theta_n, H_j) \end{pmatrix}. \quad (7)$$

Note that $L_s = T f_s$, we can re-write (2) as

$$E_s = \sum_{l=0}^{L_s-1} |s_n(l)|^2 = \mathbf{s}_n^H \mathbf{s}_n. \quad (8)$$

3. MULTI-HYPOTHESIS SEQUENTIAL PROBABILITY RATIO TEST

A cognitive sensor network system interrogates the defect channel in order to update its probabilistic understanding of the defect. This system contrasts to the conventional sensor network systems that concern mainly with making hard decisions, i.e., the presence of the defects. However, for the purpose of continuous monitoring of defects in civil structure, it would be the system operator that draws actionable conclusions based on the Bayesian representation of the defect channel in a statistical sense. Sequential hypothesis test has been applied to structure health monitoring in the past.^{22,23,24} Although the majority of research in sequential hypothesis testing has been restricted to two hypotheses, there are several situations, particularly in engineering applications, where it is natural to consider more than two hypotheses.^{25,26} For example, in the context of multiple-resolution-element radar, we have sequential decision problems with a single null hypothesis and multiple alternative hypotheses.^{27,28} In this work, we focus on defect recognition using adaptive waveforms and formulate a sequential probability ratio test for M possible hypotheses of structure defects.

3.1 Maximum likelihood estimate for unknown scalar a_n

The scalar a_n accounts for the unknown defect reflectivity in response to the probe signals. When the aspect angle θ_n is known, the maximum likelihood estimate (MLE)²⁹ of the scalar $\hat{a}_{n|H_j}$ under hypothesis H_j is given as

$$\hat{a}_{n|H_j} = \left[(\mathbf{H}_{\theta_n, H_j} \mathbf{s}_n)^H \mathbf{H}_{\theta_n, H_j} \mathbf{s}_n \right]^{-1} (\mathbf{H}_{\theta_n, H_j} \mathbf{s}_n)^H \mathbf{s}_n. \quad (9)$$

Hence, the generalized likelihood function under H_j is given by

$$f(\mathbf{s}_n; \hat{a}_{n|H_j}, \theta_n | H_j) = \frac{1}{(\pi \sigma_n^2)^{L_s}} e^{-\frac{1}{\sigma_n^2} (\mathbf{s}_n - \hat{a}_{n|H_j} \mathbf{H}_{\theta_n, H_j} \mathbf{s}_n)^H (\mathbf{s}_n - \hat{a}_{n|H_j} \mathbf{H}_{\theta_n, H_j} \mathbf{s}_n)}. \quad (10)$$

Furthermore, the aspect angle θ_n can be estimated from as the phaser representation of the distance vector \mathbf{r}_n :

$$\hat{\theta}_n = \angle \mathbf{r}_n, \quad (11)$$

which yields

$$f(\mathbf{s}_n; \hat{a}_{n|H_j}, \hat{\theta}_n | H_j) = \frac{1}{(\pi \sigma_n^2)^{L_s}} e^{-\frac{1}{\sigma_n^2} (\mathbf{s}_n - \hat{a}_{n|H_j} \mathbf{H}_{\hat{\theta}_n, H_j} \mathbf{s}_n)^H (\mathbf{s}_n - \hat{a}_{n|H_j} \mathbf{H}_{\hat{\theta}_n, H_j} \mathbf{s}_n)}. \quad (12)$$

3.2 Multi-hypothesis sequential test

A major characteristic of cognitive sensor systems is that the system can preserve the information content of backscattered signals from defect targets. This implies that the cognitive sensor system will continuously update its understanding of the environment and the defect target. The characterization of the defect target is formulated using the Bayesian method whereby different channel hypotheses are given a probabilistic rating.⁶ Every time when a probe signal is transmitted and the received data is recorded, the sensor networks system collects more information and updates the parameters of the defect channel hypotheses and their relative likelihoods. Hence, the uncertainty attributed to each defect channel hypothesis is reduced by this sequential defect probing and understanding process.

The multi-hypothesis sequential test can be summarized as follows.^{26,30} Let H_1, H_2, \dots, H_M denote the M defect target hypotheses. We let $\mathbf{s}_n^{(k)}$ denote the k -th observation of the backscattered signal from the defect target received at the n -th transducer in the network, where $n = 1, \dots, N$, and N is the total number of active sensors. After all the sensors receive, say k -th data, the likelihood functions are combined to update the probability of every defect target hypothesis

$H_j, j = 1, \dots, M$. Let $p^{(k)}(H_j)$ denote the *posteriori* probability for H_j after the k -th observation has been made by the network. Then according to the well known formula of Bayes we have

$$p^{(k)}(H_j) = \frac{f(\mathbf{s}_1^{(k)}, \mathbf{s}_2^{(k)}, \dots, \mathbf{s}_N^{(k)} | H_j) p^{(k-1)}(H_j)}{\sum_{j=1}^M f(\mathbf{s}_1^{(k)}, \mathbf{s}_2^{(k)}, \dots, \mathbf{s}_N^{(k)} | H_j) p^{(k-1)}(H_j)} \quad (13)$$

where $p^{(k-1)}(H_j)$ denotes the probability for H_j before the k -th data observation. Furthermore, note that since the mutual interference between sensors are assumed to be negligible, the joint likelihood function under H_j , $f(\mathbf{s}_1^{(k)}, \mathbf{s}_2^{(k)}, \dots, \mathbf{s}_N^{(k)} | H_j)$, can be written as

$$f(\mathbf{s}_1^{(k)}, \mathbf{s}_2^{(k)}, \dots, \mathbf{s}_N^{(k)} | H_j) = \prod_{n=1}^N f_n(\mathbf{s}_n^{(k)}; \hat{a}_{n|H_j}, \hat{\theta}_n | H_j) \quad (14)$$

Inserting (14) into (13), we obtain

$$p^{(k)}(H_j) = \frac{\prod_{n=1}^N f_n(\mathbf{s}_n^{(k)}; \hat{a}_{n|H_j}, \hat{\theta}_n | H_j) p^{(k-1)}(H_j)}{\sum_{j=1}^M \prod_{n=1}^N f_n(\mathbf{s}_n^{(k)}; \hat{a}_{n|H_j}, \hat{\theta}_n | H_j) p^{(k-1)}(H_j)} \quad (15)$$

The sensor network continuously interrogates the defect target channel and updates the probability of each hypothesis until a hard decision can be made. Let π_{ij} denote the desired probability of accepting H_i when in fact H_j is true. The experiment is terminated and H_i is selected when the condition³⁰

$$L_{i,j}^{(k)} > \frac{1 - \pi_{ij}}{\pi_{ij}}, \quad \forall j \neq i \quad (16)$$

is met for some i , where $L_{i,j}^{(k)}$ is the likelihood ratio of the *posteriori* probability between the hypothesis H_i and H_j , i.e.,

$$L_{i,j}^{(k)} \triangleq \frac{p^{(k)}(H_i)}{p^{(k)}(H_j)}. \quad (17)$$

Note that by (15), (17) can be further written as the updating formula

$$L_{i,j}^{(k)} = \frac{p^{(k-1)}(H_i)}{p^{(k-1)}(H_j)} \cdot \frac{\prod_{n=1}^N f_n(\mathbf{s}_n^{(k)}; \hat{a}_{n|H_i}, \hat{\theta}_n | H_i)}{\prod_{n=1}^N f_n(\mathbf{s}_n^{(k)}; \hat{a}_{n|H_j}, \hat{\theta}_n | H_j)}, \quad (18)$$

or in the logarithmic format

$$\log L_{i,j}^{(k)} = \log L_{i,j}^{(k-1)} + \sum_{n=1}^N \log f_n(\mathbf{s}_n^{(k)}; \hat{a}_{n|H_i}, \hat{\theta}_n | H_i) - \sum_{n=1}^N \log f_n(\mathbf{s}_n^{(k)}; \hat{a}_{n|H_j}, \hat{\theta}_n | H_j). \quad (19)$$

If the condition (16) is not met for any of the hypothesis $H_j, \forall j$, another round of illumination is initiated.

3.3 Waveform design and connection to time reversal

Time reversal is a novel time domain signal processing method.^{18,31,32} In this section, we will establish a connection between the adaptive waveform design strategies based on time reversal and that for the cognitive sensor network sensing systems. For simplicity, we start with two hypotheses $M = 2$. In this case, if the waveform design criterion is to maximize the Euclidean distance between the mean values of the likelihood functions under H_i and H_j , i.e., given the two channel matrix $\mathbf{H}_{\theta_n, H_i}$ and $\mathbf{H}_{\theta_n, H_j}$, i.e.,

$$d^2 = \left(\mathbf{s}_n^{(k)} \right)^H (\mathbf{H}_{\theta_n, H_i} - \mathbf{H}_{\theta_n, H_j})^H \mathbf{R}_w^{-1} (\mathbf{H}_{\theta_n, H_i} - \mathbf{H}_{\theta_n, H_j}) \mathbf{s}_n^{(k)}. \quad (20)$$

the waveform that maximizes the signal-to-noise ratio at the output of the receiver matched filter is the optimal pulse shape.^{33,34} Equation (20) reveals that the optimum transmit signal separates the two signals as far as possible in the whitened received signal space. The solution is the transmission waveform vector that maximizes the distance d^2 , which is the eigenvector corresponding to the largest eigenvalue of

$$\mathbf{\Omega}_n = (\mathbf{H}_{\theta_n, H_i} - \mathbf{H}_{\theta_n, H_j})^H \mathbf{R}_w^{-1} (\mathbf{H}_{\theta_n, H_i} - \mathbf{H}_{\theta_n, H_j}). \quad (21)$$

In particular, if the noise covariance matrix is $\mathbf{R}_n = \sigma_w^2 \mathbf{I}$, where \mathbf{I} is the identity matrix, the optimal waveform for the binary hypothesis case ($M = 2$) is the eigenvector corresponding to the largest eigenvalue of $\mathbf{\Omega}'$ defined as

$$\mathbf{\Omega}'_n = (\mathbf{H}_{\theta_n, H_i} - \mathbf{H}_{\theta_n, H_j})^H (\mathbf{H}_{\theta_n, H_i} - \mathbf{H}_{\theta_n, H_j}). \quad (22)$$

Furthermore, if we allow one of the two hypotheses (H_i, H_j) to be the null hypothesis, say H_j , then $\mathbf{H}_{\theta_n, H_i} = \mathbf{0}$. Hence, (22) reduces to

$$\mathbf{\Omega}''_n = (\mathbf{H}_{\theta_n, H_i})^H (\mathbf{H}_{\theta_n, H_i}). \quad (23)$$

We would like to show that the transmission waveform $s_n^{(k)}$ that maximizes the distance

$$d'^2 = \left(\mathbf{s}_n^{(k)} \right)^H (\mathbf{H}_{\theta_n, H_i})^H (\mathbf{H}_{\theta_n, H_i}) \mathbf{s}_n^{(k)}, \quad (24)$$

is the time reversal waveform. Note that the convolution matrix in (7) describes the time domain linear filtering between the defect channel and the transmitted waveform given in (1). (24) can be re-written as a linear convolution by

$$d'^2 = \|\mathbf{s}_n^{(k)} * \mathbf{h}_{\theta_n, H_i}\|^2, \quad (25)$$

where $\mathbf{h}_{\theta_n, H_i}$ is the vectorized defect channel response for the n -th sensor under hypothesis H_j . To simplify the mathematical expression, we express the convolution as the product in the frequency domain by the Fourier transform, which yields³⁵

$$d'^2 = \frac{1}{L} \|\bar{\mathbf{s}}_n^{(k)} \cdot \bar{\mathbf{h}}_{\theta_n, H_i}\|^2 = \frac{1}{L} |\langle \bar{\mathbf{s}}_n^{(k)}, \bar{\mathbf{h}}_{\theta_n, H_i} \rangle|^2, \quad (26)$$

where $\bar{\mathbf{s}}_n^{(k)}$ and $\bar{\mathbf{h}}_{\theta_n, H_i}$ are the discrete Fourier transform (DFT) of the zero-padded (to L -points) sequences $\mathbf{s}_n^{(k)}$ and $\mathbf{h}_{\theta_n, H_i}$, respectively. The symbol (\cdot) is the dot-product. By the Cauchy-Schwartz inequality, (26) reaches its maximum if the following condition is met:

$$\bar{\mathbf{h}}_{\theta_n, H_i} = \left(\bar{\mathbf{s}}_n^{(k)} \right)^*. \quad (27)$$

Note that the frequency conjugation is equivalent to time-reversal in the time domain. Equation (27) indicates that the optimal transmission waveform under $M = 2$ (i.e., one is the null hypothesis, and the other is an alternative hypothesis for a defect target) is the time-reversal waveform of the defect channel. Readers can refer to other references for more detailed discussions.¹⁸ However, in the case of multiple hypothesis test when $M > 2$, the physical meaning of the optimal transmission waveform is not easy to interpret. Here we adopt the waveform design criterion³⁰

$$\mathbf{\Omega}_n = \sum_{i=1}^{M-1} \sum_{j=i+1}^M w_{ij} (\mathbf{H}_{\theta_n, H_i} - \mathbf{H}_{\theta_n, H_j})^H (\mathbf{H}_{\theta_n, H_i} - \mathbf{H}_{\theta_n, H_j}), \quad (28)$$

where w_{ij} is a weight factor that accounts for the relative importance of discriminating between hypotheses i and j . In this paper, $w_{ij} = p^{(k-1)}(H_i)p^{(k-1)}(H_j)$, where $p^{(k-1)}(H_i)$ is the probability of the hypothesis H_i prior to the k -th waveform transmission. This choice of the weight factor is shown to maximize the average divergence between received signals.³⁶ Due to space limitations, we will defer further discussions on the transmission waveform design problem for multiple sequential hypothesis test in a companion paper.

Table 1. Defect Simulation Model Specifications

	Length x	Width ϕ	Depth r
Hole	0.5 m	0.11 m (60°)	Full-depth (0.008 m)
Interior corrosion	0.5 m	0.11 m (60°)	Half-depth from interior (0.004 m)
Exterior corrosion	0.5 m	0.11 m (60°)	Half-depth from exterior (0.004 m)
Saw cut	0.005 m	0.11 m (60°)	Half-depth from exterior (0.004 m)

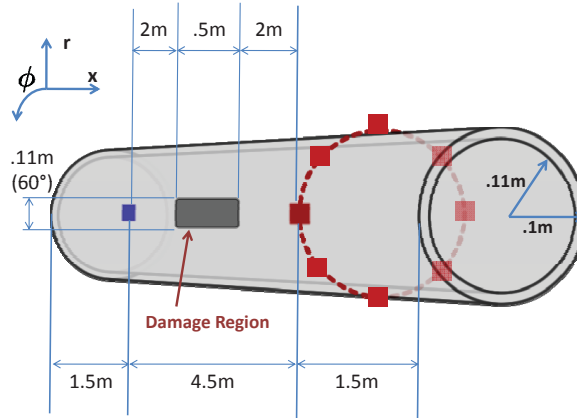


Figure 2. Simulation Geometry. A pipe simulation model with 8 attached transducers.

4. SIMULATION STUDIES AND RESULTS

In this section, we demonstrate the performance of cognitive sensor network for defect target classification using numerical simulations. The benchmark system is the one that does not have the feed-back structure and for which the probing waveform for each illumination remains unchanged. Our simulation study consists of two parts. In the first part, we develop a defect simulation model in the PZflex software environment, simulate the Lamb wave propagation on a pipe, and record the data at transducers. Once the defect model is created, we assume that it is known *a priori*. In the second part, we conduct the sequential probability ratio test to classify the defect targets in Matlab. On each probing, the waveform is adaptively selected and transmitted. The correct probability of classification is calculated. The details of simulation are described below.

4.1 Lamb wave defect simulations

Fig. 2 depicts the pipe model for simulations. The pipe model has length 7.5 m, outer radius 0.11 m, and inner radius 0.102 m. The transmitter sensor and receiver sensor are located at the same circumferential position, $\phi = 0$ and 1.5 m, from their respective ends of the pipe. On the pipe, a total of four defect models are developed (see Table 1 for the four defect model specifications). The damage in all four defect cases is centered in the highlighted region, a patch 0.5 m long by 0.11 m wide (60°). We conducted simulations first on a clean (undamaged) pipe, and then again for each of the four defect scenarios.

4.2 Multi-hypothesis sequential test

To evaluate the performance of the sequential hypothesis test, a total of 600 different sets of targets are generated. Each set consists of $M = 4$ defect hypothesis, which corresponds to $M = 4$ defect impulse response vector $h(t, \theta_n, H_j)$, where $n = 1, \dots, N$, is normalized to unit energy, i.e., $\|\mathbf{h}_{\theta_n, H_j}\|^2 = 1$. The specified error rate in the M-ary sequential hypothesis test is $\pi_{ij} = 0.01$ for all the hypotheses. The initial *a priori* probability $p^{(0)}(H_j) = \frac{1}{M} = 0.25$ for every j . In order to save computational time, we down-sample the defect channel response to the length $L_h = 61$ in our simulation. The length of the waveform signal s_n is $L_s = 61$. Fig. 3 depicts the four defect target spectrum for hole, interior corrosion, exterior

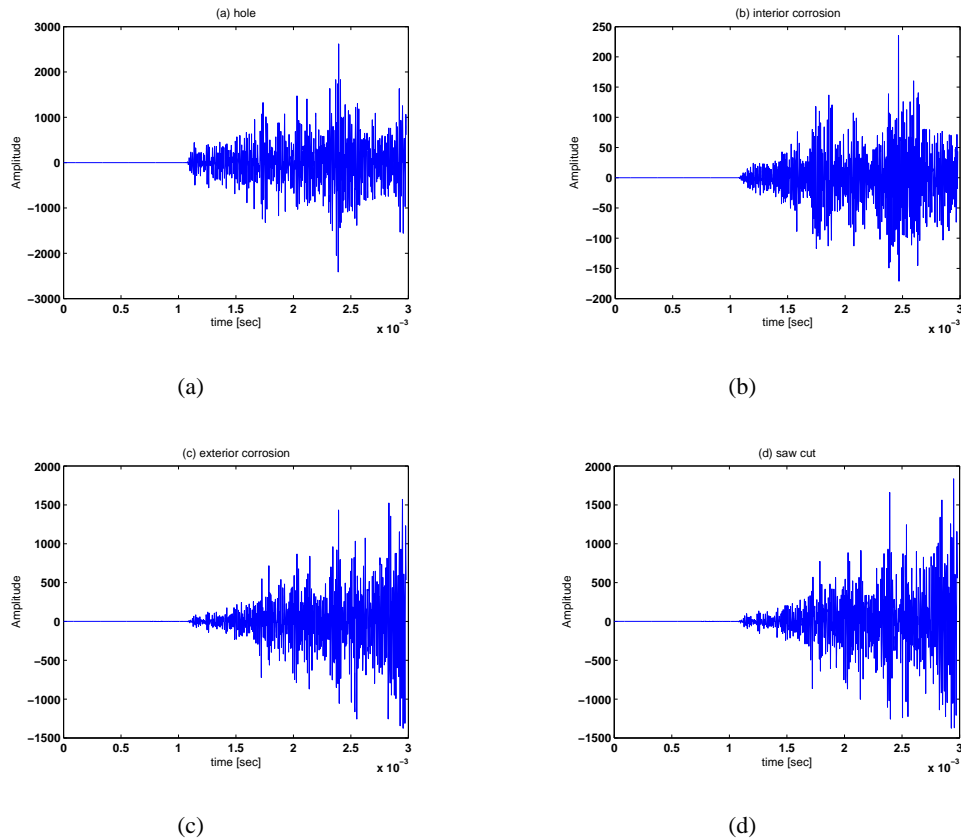


Figure 3. Four defect channel responses obtained from simulations. (a) Hole. (b) Interior corrosion. (c) Exterior corrosion. (d) Sawcut.

corrosion, and saw cut, respectively. Because we consider the defect classification problem, the amplitude coefficient a_n are assumed the same for each of the hypothesis at n -th sensor given one observation. In the sequential test, we assume that $a_n \sim \mathcal{CN}(0, \sigma_a^2)$. The additive noise has the distribution of $\mathbf{w}_n \sim \mathcal{CN}(0, \sigma_w^2 \mathbf{I})$. For simplicity, we set $\sigma_a^2 = \sigma_w^2 = 1$. The number of transducers included in the network is set to be $N = 3$ for simulation purposes. Furthermore, we assume that the aspect angle θ_n is known in order to simply the problem. For each transducer sensor, two types of waveforms are used to detect and classify the defects: a conventional Gaussian modulated sinusoidal waveform and the optimal eigen-waveform. Fig. 5 depicts the real part and the imaginary part of the transmission waveforms. Fig. 5(a) shows the eigen-waveform, while Fig. 5(b) shows the Gaussian modulated sinusoidal waveform.

Fig. 6 shows the classification performance of the cognitive sensor network system. Fig 6(a) shows the correct classification probability versus average number of transmission energy using the eigen-waveform and the conventional Gaussian-modulated sinusoidal pulse. Fig. 6(b) shows the average number of transmission prior to reaching a classification decision. Combining Fig. 6(a) and (b), we conclude that the cognitive system yields higher classification rate than the conventional method with higher efficiency in reaching a decision.

5. CONCLUSION

This paper develops a theoretical framework of cognitive sensor networks for structure defect monitoring and classification using guided wave signals. The cognitive sensor network is characterized by intelligently and adaptively probing and learning from the environment, and transmit waveforms that match the defect target at each illumination. The multiple hypothesis sequential probability test we developed in this paper yields a better correct classification probability while using smaller number of transmissions compared with the fixed length illumination approach in conventional monitoring and classification sensor networks. The proposed method is verified using a PZFlex simulation pipe model with a total of four defect scenarios. The results demonstrate the success of the proposed classification scheme.

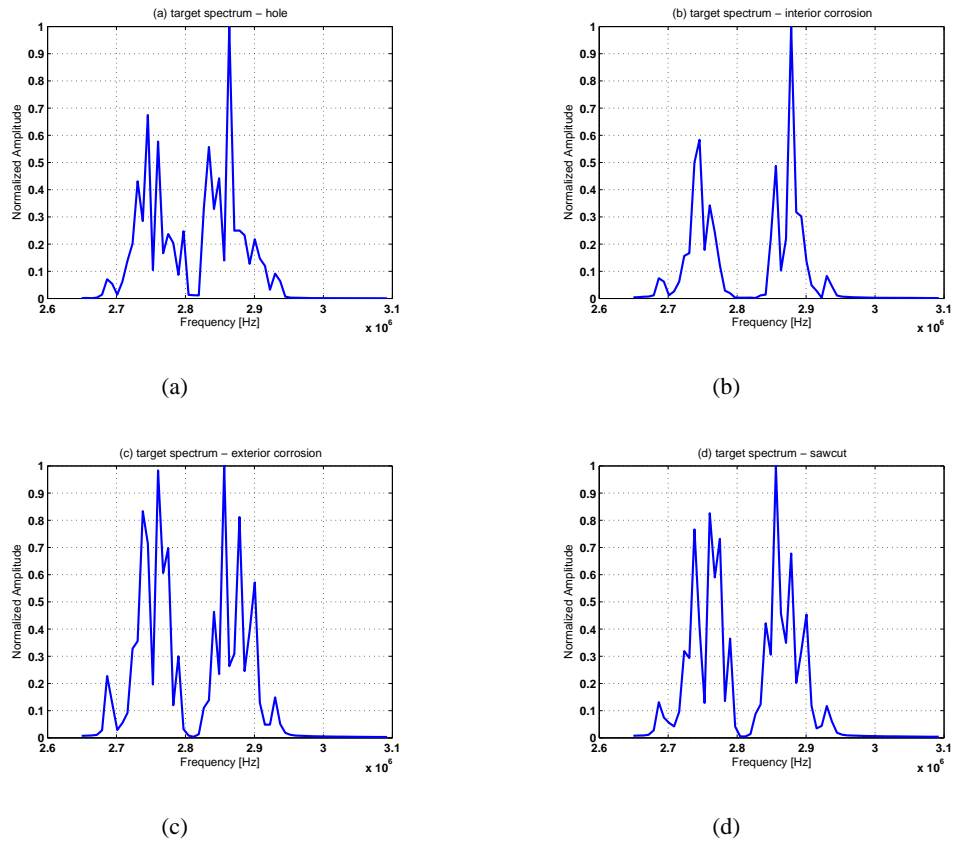


Figure 4. Down-sampled amplitude normalized frequency spectra of four sample defect hypotheses. (a) Hole. (b) Interior corrosion. (c) Exterior corrosion. (d) Sawcut.

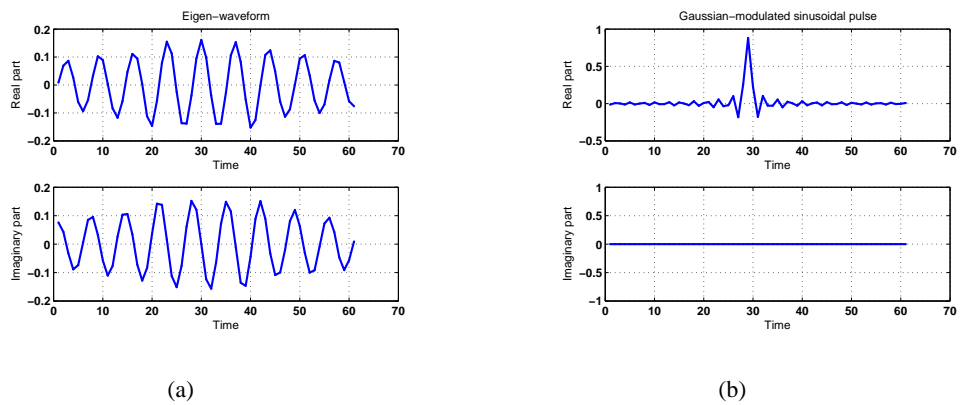


Figure 5. (a) Eigen-waveform. (b) Gaussian modulated sinusoidal pulse.

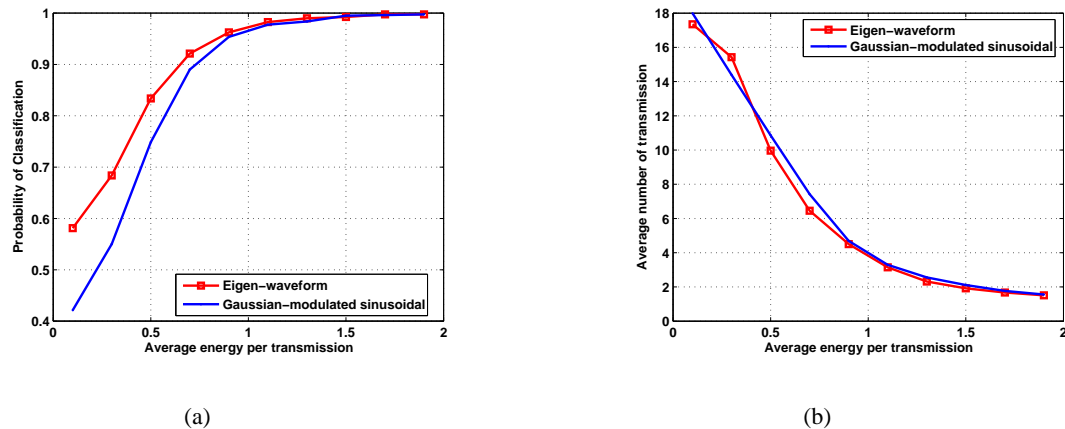


Figure 6. (a) Correct classification probability vs. average transmission energy. (b) Average number of transmission vs. average transmission energy.

6. ACKNOWLEDGEMENT

This work is supported by the Department of Energy under award no. DE-NT-0004654. National Energy Technology Laboratory (NETL) is the funding source for this effort with Cost Share being provided by Carnegie Mellon University (CMU). University of Maryland Eastern Shore (UMES) is funded under a Subcontract Agreement with CMU. CMU is funded under a Subcontract Agreement with Concurrent Technologies Corporation (CTC). CTC is funded under a cooperative agreement with NETL. Joel Harley and Nicholas O'Donoghue are supported by National Defense Science and Engineering Graduate Fellowships, sponsored by the Office of Naval Research and Army Research Office, respectively. L. He was supported by a scholarship from the China Scholarship Council.

REFERENCES

- [1] Glaser, S. D., Li, H., Wang, M. L., Ou, J., and Lynch, J., "Sensor technology innovation for the advancement of structural health monitoring: a strategic program of US-China research for the next decade," *Smart Structures and Systems* **3**(2), 221–244 (2007).
- [2] Lynch, J. P., "An overview of wireless structural health monitoring for civil structures," *Philosophical Transactions of the Royal Society of London. Series A, Mathematical and Physical Sciences* **365**(1851), 345–372 (2007). The Royal Society, London.
- [3] Zimmerman, A. T. and Lynch, J. P., "A parallel simulated annealing architecture for model updating in wireless sensor networks," *IEEE Sensors Journal* **9**, 1503–1510 (November 2009).
- [4] Mitola, J. and Maguire, G. Q., "Cognitive radio," *IEEE Personal Communications* **6**, 13–18 (August 1999).
- [5] Haykin, S., "Cognitive radio: brain-empowered wireless communications," *IEEE Journal on Selected Areas in Communications* **23**, 201–220 (February 2005).
- [6] Haykin, S., "Cognitive radar: A way of the future," *IEEE Signal Processing Magazine* **23**, 30–40 (January 2006).
- [7] Li, J. and Rose, J. L., "Excitation and propagation of non-axisymmetric guided waves in a hollow cylinder," *Journal of Acoustical Society of America* **109**, 457–464 (February 2001).
- [8] Alleyne, D. N., Lowe, M. J. S., and Cawley, P., "The reflection of guided waves from circumferential notches in pipes," *Journal of Applied Mechanics* **65**, 635–641 (September 1998).
- [9] Graff, K. F., [*Wave Motion in Elastic Solids*], Dover Publications, Mineola, NY (1991).
- [10] Rose, J. L., [*Ultrasonic Waves in Solid Media*], Cambridge University Press, New York, NY (1999).
- [11] Gazis, D. C., "Three-dimensional investigation of the propagation of waves in hollow circular cylinders. I. Analytical foundation," *Journal of Acoustical Society of America* **31**, 568–573 (May 1959).
- [12] Demma, A., Cawley, P., Love, M., and Rossenbrand, A. G., "The reflection of the fundamental torsional mode from cracks and notches in pipes," *Journal of Acoustical Society of America* **114**, 611–625 (August 2003).

- [13] Hayashi, T. and Murase, M., "Defect imaging with guided waves in a pipe," *Journal of Acoustical Society of America* **117**, 2134–2140 (April 2005).
- [14] Wilcox, P. D., Lowe, M. J. S., and Cawle, P., "Mode and transducer selection for long range Lamb wave inspection," *Journal of Intelligent Material System and Structure* **12**(8), 553–565 (2001).
- [15] Wang, C. H., Rose, J. T., and Chang, F.-K., "A synthetic time-reversal imaging method for structural health monitoring," *Smart Materials and Structures* **13**(1), 415–423 (2004).
- [16] Xu, B. and Giurgiutiu, V., "Single mode tuning effects on Lamb wave time reversal with piezoelectric wafer active sensors for structural health monitoring," *Journal of Nondestructive Evaluation* **26**, 123–134 (December 2007).
- [17] O'Donoghue, N., Harley, J., Moura, J. M. F., Jin, Y., Oppenheim, I., Ying, Y., States, J., Garrett, J., and Soibelman, L., "Single antenna time reversal of guided waves in pipelines," *Proceedings of Meetings on Acoustics* **6**, 065001–065001–11 (June 2009).
- [18] Jin, Y. and Moura, J. M. F., "Time reversal detection using antenna arrays," *IEEE Transactions on Signal Processing* **57**, 1396–1414 (April 2009).
- [19] Wald, A., "Sequential tests of statistical hypotheses," *Annals of Mathematical Statistics* **16**, 117–186 (June 1945).
- [20] Wooh, S.-C. and Shi, Y., "Optimum beam steering of linear phased arrays," *Wave Motion* **29**, 245–265 (April 1999).
- [21] Oralkan, O., Ergun, A. S., Johnson, J. A., Karaman, M., Demirci, U., Kaviani, K., Lee, T. H., and Khuri-Yakub, B. T., "Capacitive micromachined ultrasonic transducers: Next-generation arrays for acoustic imaging?," *IEEE Transactions on Ultrasonics, Ferroelectrics, and Frequency Control* **49**, 245–265 (November 2002).
- [22] Vanik, M. W., Beck, J. L., and Au, S. K., "Bayesian probabilistic approach to structural health monitoring," *Journal of Engineering Mechanics* **126**, 738–745 (July 2000).
- [23] Sohn, H., Allen, D. W., Worden, K., and Farrar, C. R., "Statistical damage classification using sequential probability ratio tests," *International Journal of Structural Health Monitoring* **2**(1), 57–74 (2003).
- [24] Allen, D. W., Sohn, H., Worden, K., and Farrar, C. R., "Utilizing the sequential probability ratio test for building joint monitoring," in [*SPIE's 7th Annual International Symposium on NDE for Health Monitoring and Diagnostics*], **4707**, 1–11 (2002). March 18–19.
- [25] Baum, C. W. and Veeravalli, V. V., "A sequential procedure for multihypothesis testing," *IEEE Transactions on Information Theory* **40**, 1994–2007 (November 1994).
- [26] Armitage, P., "Sequential analysis with more than two alternative hypotheses, and its relation to discriminant function analysis," *Journal of the Royal Statistical Society. Series B (Methodological)* **12**, 137–144 (November 1950).
- [27] Marcust, M. B. and Swerling, P., "Sequential detection in Radar with multiple resolution elements," *IRE Transactions On Information Theory* **8**, 237–245 (April 1962).
- [28] Bussgang, J. J., "Sequential methods in radar detection," *Proceedings of the IEEE* **58**, 731–245 (May 1970).
- [29] Scharf, L. L., [*Statistical Signal Processing: Detection, Estimation, and Time Series Analysis*], Addison-Wesley Publishing Company, Reading, MA (1991).
- [30] Goodman, N. A., Venkata, P. R., and Neifeld, M. A., "Adaptive waveform design and sequential hypothesis testing for target recognition with active sensors," *IEEE Journal of Selected Topics in Signal Processing* **1**, 105–113 (June 2007).
- [31] Moura, J. M. F. and Jin, Y., "Detection by time reversal: single antenna," *IEEE Transactions on Signal Processing* **55**, 187–201 (January 2007).
- [32] Jin, Y., Moura, J. M. F., and O'Donoghue, N., "Time reversal in multiple-input multiple-output radar," *IEEE Journal of Selected Topics in Signal Processing* **4**, 210–225 (February 2010).
- [33] Bell, M. R., "Information theory and radar waveform design," *IEEE Transactions on Information Theory* **39**, 1578–1597 (September 1993).
- [34] Garren, D. A., Osborn, M. K., Odom, A. C., Osborn, M. K., Goldstein, J. S., Pillai, S. U., and Guerci, J. R., "Full-polarization matched-illumination for target detection and identification," *IEEE Transactions on Aerospace and Electronic Systems* **38**, 824–837 (July 2002).
- [35] Proakis, J. G. and Manolakis, D. G., [*Digital Signal Processing: Principles, Algorithms, and Applications*], Prentice Hall, Upper Saddle River, NJ (1996).
- [36] Mosca, E., "Probing signal design for linear channel identification," *IEEE Transactions on Information Theory* **18**, 481–487 (July 1972).

A Data Mining Framework for Pipeline Monitoring Using Time Reversal

Yujie Ying^{a*}, Lucio Soibelman^a, Joel Harley^a, Nicholas O'Donoghue^a, James H. Garrett, Jr.^a,
Yuanwei Jin^b, José M.F. Moura^a, and Irving J. Oppenheim^a

Abstract

This paper presents a data mining framework under development based on Time Reversal for continuous monitoring of natural gas pipelines. Our goal is to extract damage information from complex guided wave patterns in pipes. We first review Time Reversal methods, and discuss their effectiveness and limitation for defect detection. Then, we describe our experimental results with Time Reversal change detection which show that it is able to detect small defects through its focusing effect. However, Time Reversal is sensitive to changing environmental and operational conditions, which may increase the false alarm rate. To reduce the number of false positives, we propose a data mining framework that integrates Time Reversal with data mining tools. The data mining framework consists of three modules: defect detection, defect localization, and defect classification. We explore the potential use of Time Reversal in each work module. This paper highlights these tasks and provides a clear work flow to further our pipeline monitoring research.

Keywords: data mining, Time Reversal, defect detection, guided waves, and pipeline monitoring.

1 Introduction

Ultrasonic guided wave technology has been extensively investigated for Structural Health Monitoring (SHM) and Nondestructive Evaluation (NDE) applications. Guided waves are sensitive to damage in structures and able to propagate over long distances [1,2]. However, the characteristics of wave propagation in pipes are complicated due to the presence of multiple modes, multiple paths, and dispersion. There are three fundamental classes of wave modes: longitudinal, torsional and flexural modes [1]. As an illustration, Figure 1a shows a 400 kHz Gaussian pulse, and Figure 1b gives the complex wave pattern received after propagating 1.8 meters in a pipe [3]. This dispersive waveform contains a large amount of wave modes that make the data interpretation very difficult.

In order to reduce the effects of dispersion and multiple modes, we apply Time Reversal to spatially and temporally compress the received waves, which compensates for the multi-modal and dispersive pipe environment, as well as enhances signal-to-noise ratio (SNR) [5]. After Time Reversal, a significant peak is produced at the center of the plot as shown in Figure 1c. This focusing feature allows to effectively detect even small defects induced in the pipe. These preliminary results with Time Reversal are encouraging. Our experimental work also shows that Time Reversal is very sensitive to various “changes” in the pipes, not only flaws, but also environmental and operational variations, which increases the rate of false alarms. We extend Time Reversal to defect localization and classification by combining with other methods, in order to more effectively extract useful information from the large number of wave modes and from the large amount of data that we can acquire from pipes.

Data mining is an important technique for extracting or mining knowledge from large amounts of data. It has a broad range of practical uses, including marketing management, risk analysis, and fraud detection [6]. Recently, it has been shown that data mining technology can provide a novel approach for infrastructure inspection and monitoring [7]. For pipeline monitoring, we combine data mining with Time Reversal for uncovering useful information from the complex wave patterns observed.

In Section 2, we describe Time Reversal and its application in change detection of defects. We provide experimental results of the Time Reversal change detection in pipes and discuss its effectiveness and limitation for detecting damage. In Section 3, we introduce a data mining framework under development based on the existing Time Reversal methods as a more comprehensive and systematic solution for pipeline monitoring.

^a Carnegie Mellon University, Pittsburgh

^b University of Maryland Eastern Shore, Princess Anne

* Contact author: yying@cmu.edu

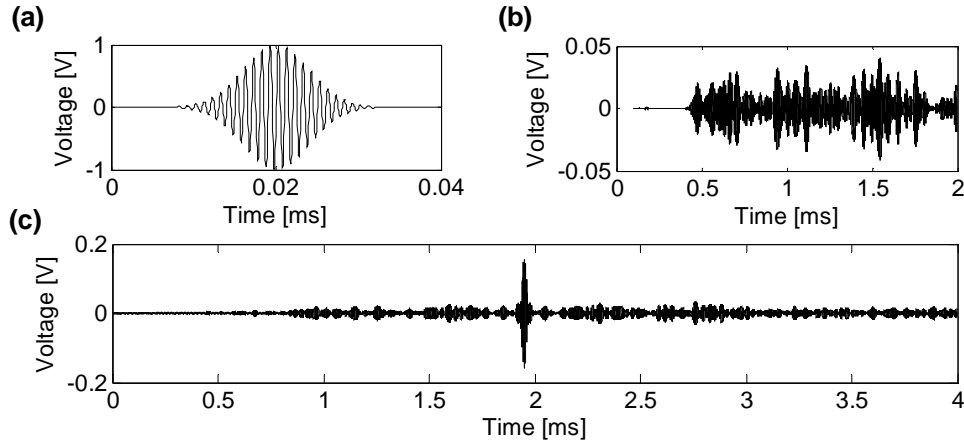


Figure 1. (a) 400 kHz Gaussian windowed excitation, (b) Received signal, (c) Time Reversal focused signal [3]

2 Time Reversal for defect detection

2.1 Time Reversal Focusing

Time Reversal is based on the assumption that the waveguide (pipe) is reciprocal and stationary [5]. Reciprocity ensures the same signals are received when the transmitter and receiver are reversed; stationary means the results do not vary over time. The implementation of Time Reversal Focusing is illustrated in Figure 2, and detailed mathematical description can be found in [3]. In general, Time Reversal is performed in three stages. First, we excite a pulse at the transmitter, and receive the signal response at the receiver. Second, we time-reverse and energy-normalize the received waveform. At the last step, we send the time-reversed and energy-normalized signal backwards, from the receiver to the transmitter, expecting to receive a highly focused signal at the original source. Therefore, we obtain a compressed and significant peak instead of the original complex and dispersive data.

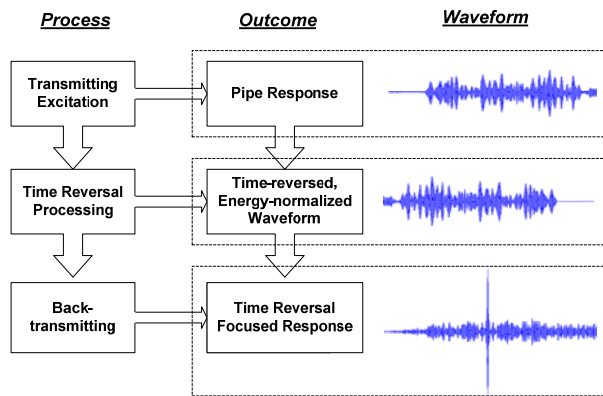


Figure 2. Time Reversal Focusing process

2.2 Time Reversal Change Focusing

Change detection is a popular technique for flaw detection. Test signals are compared to a reference measurement on a known reference pipe. However, the changes often exhibit indistinguishable patterns, especially in a complex pipe environment, and sometimes because they are so small and are masked by noise. In Time Reversal Change Focusing, we apply Time Reversal techniques to those changes, with the process shown in Figure 3. The response component due to the changes is obtained by background subtraction. This waveform is then time-reversed and the change response is retransmitted through the pipe. As a result, the change response becomes focused. In other words, the presence of damage will be evidenced by a significant peak at the center of the Time Reversal. We have shown that Time Reversal Change Focusing increases the SNR and exposes the hidden defect pattern [8-10].

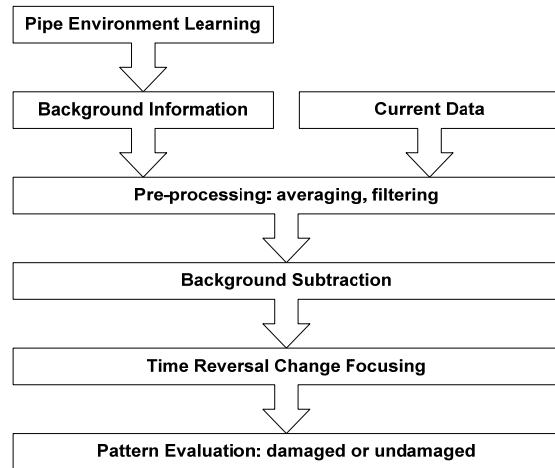


Figure 3. Time Reversal Change Focusing process

2.3 Experimental results

Our first experiment demonstrates the effectiveness of Time Reversal for damage detection in a pipe, which has been discussed in our earlier paper [3]. The test was performed on a steel pipe specimen with length 3050 mm, outside diameter 60.3 mm and wall thickness 3.6 mm. Two piezoelectric wafer transducers (Lead Zirconate Titanate, PZT) were mounted 1.8 m apart on the surface of the pipe, operated as one transmitter and one receiver, respectively. Each wafer was 10 mm long and 5 mm wide. The transmitter was excited by a 300 kHz sinc pulse. We induced a small and partial-thickness sawcut at the lateral direction, 1 mm wide, 1 mm deep and 25 mm in arc dimension, 1095mm from the transmitter.

Figure 4 shows the received patterns of changes by background subtraction. Those changes are very weak and indistinguishable. However, by performing Time Reversal Change Focusing on Figure 4e and Figure 4f, we observe a very significant difference between these two cases, with and without the defect present. As shown in Figure 5, the peak level of the change focused signal increases from 1.05 mV to 29.3 mV, a difference of nearly 30 times or 29.5 dB. Therefore, the defect pattern, with a noticeable peak shown in Figure 5b is easy to indentify.

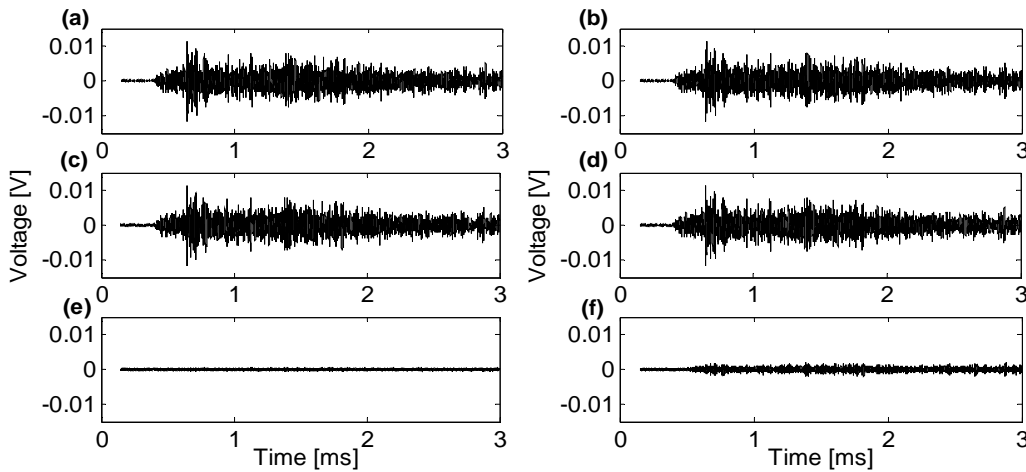


Figure 4. (a) Background information, (b) Background information, (c) Received signal with no damage present, (d) Received signal with damage present, (e) Difference of (a) and (c), (f) Difference of (b) and (d) [3]

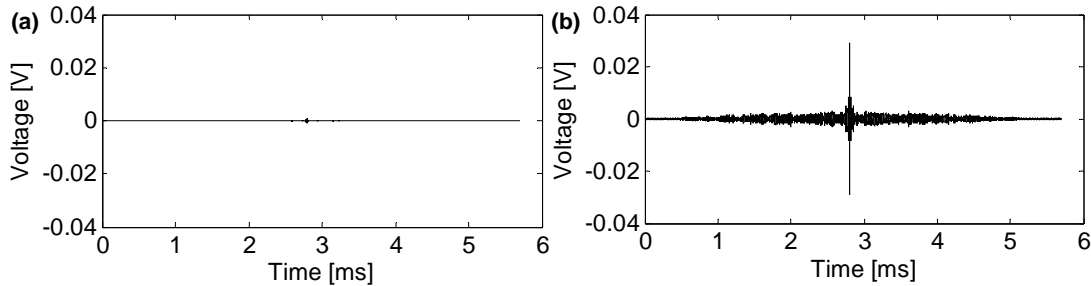


Figure 5. (a) Time Reversal Change Focusing with no damage present, (b) Time Reversal Change Focusing with damage present [3]

We conducted a second test to examine the sensitivity of Time Reversal Change Focusing to other varying factors rather than defects, such as a changing internal atmospheric pressure. The pipe specimen, with length 1833 mm, outer diameter 70 mm and wall thickness 4 mm, has a welded cap and a pressure gauge at each end to control the internal pressure. A pair of PZT wafers, 20

mm long, 8 mm wide, was mounted 1200 mm apart on the pipe. A sinc pulse centered at 200 kHz was chosen as the input signal.

Similar to the damage detection result, Figure 6 also shows that a distinguishable peak is formed after Time Reversal Change Focusing is applied to the response difference at different internal pressures, 0 psi and 83.7

psi. The peak value grows from 0.005 mV to 4.4 mV, a 58.8 dB increase, when the pipe is pressurized up to 83.7 psi. Therefore, Time Reversal Change Focusing is also sensitive to other changes caused by non-defect factors. Admittedly, this phenomenon can be useful in certain

engineering control circumstances where stable internal pressure is required to be monitored. However, for defect detection, it leads to false alarms.

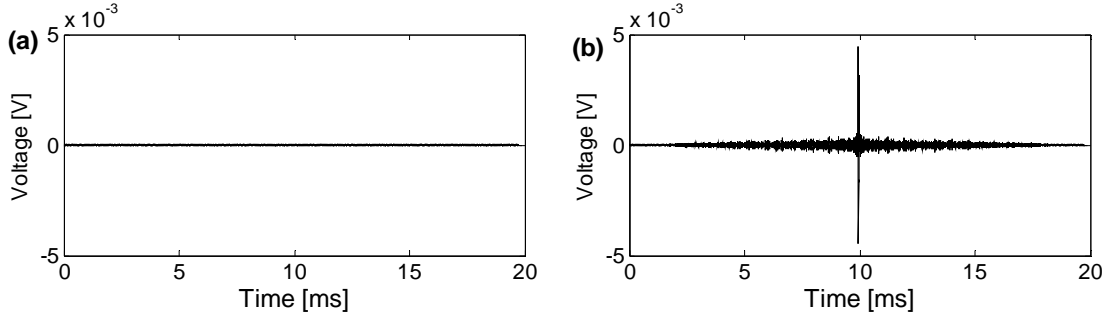


Figure 6. (a) Time Reversal Change Focusing with no internal pressure, (b) Time Reversal Change Focusing with 83.7 psi internal pressure

3 A time-reversal-based data mining framework

Our previous work has shown that Time Reversal can compensate for multiple modes and dispersive behaviors in pipes with an increased peak level of received response, and effectively detect changes in the pipe due to even small flaws. However, Time Reversal Change Focusing is also sensitive to changes caused by

environmental or operational conditions, which can cause false positives in defect detection. A preferred solution for pipeline monitoring utilizes Time Reversal's advantages, high SNR and sensitivity to damage, while combining with other techniques to identify false alarms, as well as to further classify damage types and determine defect locations. We are developing a data mining system based on Time Reversal's benefits that also includes a variety of data mining tools.

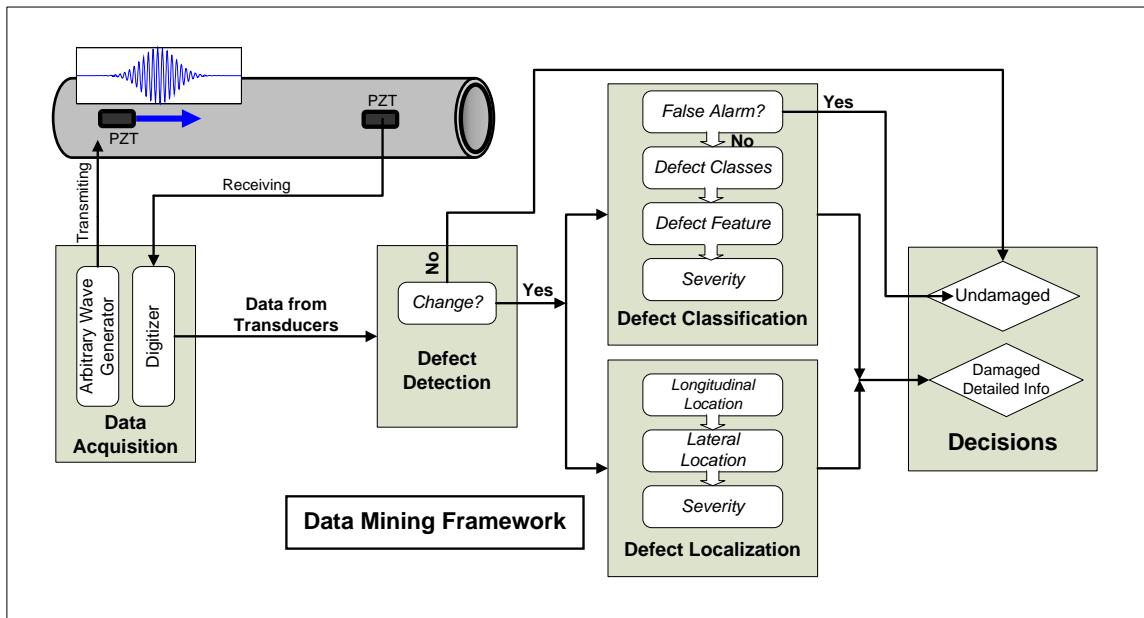


Figure 7. A data mining framework for pipeline monitoring

Figure 7 shows the proposed data mining system for pipeline monitoring. We first perform a pitch-catch method with two PZT transducers attached to the surface of a pipe, one operating as a transmitter and the other as a receiver. Data acquisition equipment is used to excite the transmitter and record the response at the receiver. A tremendous amount of data can be collected through this process, mixed with both wanted information, such as damage features, and unwanted information, such as noise and nondestructive environmental interferences. In order to extract defect-related knowledge from the received complex signal responses, the data stream then flows into the data mining framework for data processing and interpretation. This framework consists of three modules: defect detection, defect location and defect classification.

In the defect detection module, Time Reversal Change Focusing works as the detector and requires data collected by only a pair of transducers to preliminarily evaluate the damage condition in a pipe. This process has been described and demonstrated in Section 2. If an outcome with no “change” is received, a final decision “undamaged” will be made; if change is observed, more data from multiple transducers will be acquired and then transmitted into the classification and location modules for further processing.

The defect classification is still a currently ongoing research task. The major challenge lies in utilizing Time Reversal’s benefits to extract appropriate features as signatures for distinguishing among different damage categories. These features need to be sensitive to defects, but insensitive or orthogonal to environmental and operational variations. Time Reversal techniques have been shown to be very sensitive to defects as well as other changing conditions; however, the sensitivity and dimensionality to environmental effects have not been fully investigated at the current stage of our research.

After the feature selection, the next step is to develop efficient algorithms for classifying defects. Various data mining techniques have been intensely exploited in previous research for damage classification, such as Genetic Algorithms[11,12], Artificial Neural Networks[13,14], statistical analysis [15], Support Vector Machines [16] and computer vision [17]. We will compare, combine, and improve upon these classification methods to obtain the optimal approach. Moreover, we propose a multilayer defect classification model for this task, based on a sewer pipe inspection project done by some members in our research group. When a change has been inspected by the detector, the data corresponding to the change becomes input to a first level classifier that recognizes the change as a real flaw or a false alarm. The defect data is then transmitted to a

second level classifier where the defect is classified as one of the different damage classes, such as cracks, corruptions, and pittings. Next, a third level classifier is used to identify more specific features of the defects, such as direction of a crack, size of a corrosion area, etc. Finally, the data streams down into a fourth level classifier to determine the degree of severity of the defects [17].

Defect localization is another ongoing research task. We have previously used Time Reversal for localizing targets in rich scattering environments for radar (electromagnetic) data. Different algorithms have been developed and compared in [18]. At present, we are analyzing and extending appropriate algorithms of Time Reversal for damage localization in pipes, with sparse distributed transducer arrays. Time Reversal is applied due to its higher detection probability and increased resolution when compared to conventional change detection based on simple background subtraction [19]. Therefore, higher accuracy can be achieved when we locate the defects. Multiple transducers are considered for localization, which provide a rich data source and allow for increased fidelity in visualization and localization of defect. The location information in the defect localization module includes both the longitudinal and circumferential, or lateral coordinates of the pipe. Next, the system determines the severity of the defect according to its location, for example, whether the defect is located at a vital section of a pipe.

After data flows through the classification and localization modules, a “damaged” decision is generated, and appended with detailed damage information, such as the defect type and location. It should be noted that a real-world implementation may not need to implement every stage of our framework; which stage to use may depend on the requirements of the decision makers and resolution of specific tasks. For instance, the estimation of lateral location is not required for pipes with small diameter, as manual inspection is trivial once the longitudinal location has been estimated by the framework.

4 Conclusion

Time Reversal has been shown to be a useful tool for revealing damage information from complex pipe wave patterns, due to its compensation for multiple modes and dispersion, with an enhanced signal-to-noise ratio. Time Reversal Change Focusing has experimentally demonstrated its effectiveness as a defect detector; however, it suffers from false alarms induced by changing environmental conditions. Data mining techniques are promising tools to overcome this problem. Integration with Time Reversal promises Time

Reversal's benefits and a more comprehensive and reliable solution for pipeline monitoring. We will further investigate Time Reversal's application in our framework for the defect localization and classification, including how to further illuminate changes in the environment, and how to project and visualize the locations and characteristics of the defects.

Acknowledgements

National Energy Technology Laboratory (NETL) is the funding source for this effort with Cost Share being provided by Carnegie Mellon University (CMU). Concurrent Technologies Corporation (CTC) is funded under a cooperative agreement with NETL. CMU is funded under a Subcontract Agreement with CTC. Joel Harley and Nicholas O'Donoghue are supported by National Defense Science and Engineering Graduate Fellowships, sponsored by the Office of Naval Research and the Army Research Office, respectively.

References

- [1] J.L. Rose, *Ultrasonic Waves in Solid Media*, Cambridge: Cambridge University Press, 1999.
- [2] M.J.S. Lowe, D.N. Alleyne, and P. Cawley, "Defect detection in pipes using guided waves," *Ultrasonics*, vol. 36, 1998, pp. 147–154.
- [3] J. Harley, N. O'Donoghue, Y. Ying, J.H. Garrett, Y. Jin, J.M.F. Moura, I. J. Oppenheim, and L. Soibelman, "Focusing of ultrasonic waves in cylindrical shells using time reversal," in *Proceedings of the 7th International Workshop on Structural Health Monitoring*, Stanford, CA: September 2009.
- [4] P. Cawley, "Practical long range guided wave inspection—managing complexity," *AIP Conference Proceedings*, 2003, pp. 22–40.
- [5] M. Fink, "Time reversal of ultrasonic fields—Part I: Basic principles," *IEEE Trans. Ultrason. Ferroelectr. Freq. Control*, vol. 39, 1992, pp. 555–566.
- [6] J. Han and M. Kamber, *Data mining*, Morgan Kaufmann, 2006, pp.1-9.
- [7] J.M. Ko and Y.Q. Ni, "Technology developments in structural health monitoring of large-scale bridges," *Engineering structures*, vol. 27, 2005, pp. 1715–1725.
- [8] N. O'Donoghue, J. Harley, J.M. Moura, and Y. Jin, "Detection of structural defects in pipes using Time Reversal of guided waves," in *Proceeding 41st Annual Asilomar Conference on Signals, Systems, and Computers*, Pacific Grove, CA: November 2009.
- [9] J.M.F. Moura and Y. Jin, "Detection by time reversal: single antenna," *IEEE Transactions on Signal Processing*, vol. 55, no.1, January 2007, pp. 187–201.
- [10] Y. Jin and J.M.F. Moura, "Time-reversal detection using antenna arrays," *IEEE Transactions on Signal Processing*, vol. 57, no.4, April 2009, pp. 1396–1414.
- [11] J.H. Chou and J. Ghaboussi, "Genetic algorithm in structural damage detection," *Computers and Structures*, vol. 79, 2001, pp. 1335–1353.
- [12] Y. Xia, "Vibration-based damage detection of structures by genetic algorithm," *Journal of Computing in Civil Engineering*, vol. 16, 2002, pp. 222–229.
- [13] A.L. Avilés, L.H. Hernández-Gómez, J.F. Durodola, G. Urriolagoitia-Calderón, and G. Urriolagoitia-Sosa, "Locating and classifying defects with Artificial Neural Networks," *Applied Mechanics and Materials*, Vols. 13-14, 2008, pp. 117-123.
- [14] S.K. Sinha and P.W. Fieguth, "Neuro-fuzzy network for the classification of buried pipe defects," *Automation in Construction*, vol. 15, 2006, pp. 73–83.
- [15] H. Sohn, K. Worden, and C.R. Farrar, "Statistical damage classification under changing environmental and operational conditions," *Journal of Intelligent Material Systems and Structures*, vol. 13, Sep. 2002, pp. 561–574.
- [16] K. Worden and A.J. Lane, "Damage identification using support vector machines," *Smart Materials and Structures*, vol. 10, 2001, pp. 540–547.
- [17] W. Guo, L. Soibelman, and J.H. Garrett, "Automated defect detection for sewer pipeline inspection and condition assessment," *Automation in Construction*, vol. 18, 2009, pp. 587–596.
- [18] J.M.F. Moura and Y. Jin, "Time reversal imaging by adaptive interference canceling," *IEEE Transactions on Signal Processing*, vol. 56, no.1, 2008, pp. 233–247.
- [19] Y. Jin, J.M.F. Moura, N. O'Donoghue, M.T. Mulford, and A.A. Samuel, "Time reversal synthetic aperture radar imaging in multipath," *Proceeding 41st Annual Asilomar Conference on Signals, Systems, and Computers*, Pacific Grove, CA: November 2007, pp. 1812–1816.

Time Reversal for Damage Detection in Pipes

Yujie Ying^{a*}, Joel Harley^b, James H. Garrett, Jr.^a, Yuanwei Jin^c, José M.F. Moura^b, Nicholas O'Donoghue^b, Irving J. Oppenheim^a, and Lucio Soibelman^a

^aDept. of Civil and Environmental Engineering, Carnegie Mellon University, Pittsburgh, PA 15213

^bDept. of Electrical and Computer Engineering, Carnegie Mellon University, Pittsburgh, PA 15213

^cDept. of Engineering and Aviation Sciences, University of Maryland Eastern Shore, Princess Anne, MD 21853

ABSTRACT

Monitoring the structural integrity of vast natural gas pipeline networks requires continuous and economical inspection technology. Current approaches for inspecting buried pipelines require periodic excavation of sections of pipe to assess only a couple of hundred meters at a time. These inspection systems for pipelines are temporary and expensive. We propose to use guided-wave ultrasonics with Time Reversal techniques to develop an active sensing and continuous monitoring system.

Pipe environments are complex due to the presence of multiple modes and high dispersion. These are treated as adverse effects by most conventional ultrasonic techniques. However, Time Reversal takes advantage of the multi-modal and dispersive behaviors to improve the spatial and temporal wave focusing. In this paper, Time Reversal process is mathematically described and experimentally demonstrated through six laboratory experiments, providing comprehensive and promising results on guided wave focusing in a pipe with/without welded joint, with/without internal pressure, and detection of three defects: lateral, longitudinal and corrosion-like. The experimental results show that Time Reversal can effectively compensate for multiple modes and dispersion in pipes, resulting in an enhanced signal-to-noise ratio and effective damage detection ability. As a consequence, Time Reversal shows benefits in long-distance and low-power pipeline monitoring, as well as potential for applications in other infrastructures.

Keywords: Time Reversal, guided waves, damage detection, pipeline, ultrasonics, Structural Health Monitoring (SHM), and Nondestructive Evaluation (NDE).

1. INTRODUCTION

Ultrasonic guided wave technology has provided a useful tool for Structural Health Monitoring (SHM) and Nondestructive Evaluation (NDE) applications over decades. Guided waves are sensitive to surface and internal damage in structures and are able to propagate over long distances¹⁻³. However, guided wave propagation in pipes is complicated due to the presence of multiple modes at each frequency and its dispersion characteristics^{3,4}. Current pipeline inspection approaches often choose narrowband and low frequency excitation to selectively exploit a single mode for inspection, so as to suppress unwanted modes and to reduce the dispersive effects^{5,6}. Those conventional approaches usually involve periodic excavation of a section of pipe and attachment of large rings of transducers. The systems are temporary, bulky and require high transmission powers to inspect over long distances. Therefore, the technology and process is very expensive and not efficient for guided wave propagation in a pipe.

Time Reversal is a signal processing technique to increase the spatial and temporal wave focusing⁷. Time Reversal techniques have been exploited for Lamb waves in thin plates, leading to an enhanced signal level and compensation for multiple modes and dispersion⁸⁻¹¹. Previous research has also shown Time Reversal focusing is beneficial from highly dispersive environment^{8,12-14}. Therefore, we have developed Time Reversal focusing technique for the complex pipe environment by taking advantage of the multimodal, dispersive guided waves in pipes.

* Contact author: yying@cmu.edu.

In this paper, we first briefly present the characteristics of guided waves in pipes, followed by a mathematical description of the Time Reversal focusing process. We then provide comprehensive laboratory test results to examine Time Reversal's applications to focus ultrasonic waves in pipes, and to demonstrate the capability of Time Reversal change focusing to illuminate different types of defects.

2. GUIDED WAVES IN PIPES

Guided waves are ultrasonic waves propagating through a medium with geometric boundaries⁴. The boundaries form a waveguide such as a plate, rod, or pipe. Guided waves are multi-modal and dispersive in nature: multiple wave modes can be generated at different frequencies; dispersion is the phenomenon that the velocity of different modes depends on the frequency.

Guided waves in pipes or hollow cylinders contain three fundamental classes of wave modes, i.e. an infinite number of longitudinal modes, an infinite number of torsional modes, and a doubly infinite number of flexural modes. Longitudinal modes and torsional modes are axisymmetric, while flexural modes are non-axisymmetric¹⁵. We use two indices M and N to denote the fields of the guided wave modes. The index N, named circumferential order, gives the order of symmetry around the axes of the cylinder, so that for axisymmetric modes, N equals 0; the index M, named family order, sorts the modes for a given family. Therefore, longitudinal modes, torsional modes, and flexural modes are often written as L (0, M), T (0, M) and F (N, M)¹⁶.

In a cylindrical coordinate system of a pipe, $\mathbf{x} = (r; \theta; z)$, we define $r(\mathbf{x}, t)$ as the superposition of each mode at a given location \mathbf{x} at a given time t, obtained from¹⁷

$$r(\mathbf{x}, t) = \sum_{M=0}^{\infty} a_M e^{j(\omega t - \beta_M z)} + \sum_{N=0}^{\infty} \sum_{M=0}^{\infty} a_M^N e^{j(\omega t - \beta_M^N z)} \quad (1)$$

where ω is the angular frequency, a_M^N and β_M^N are the amplitude and wave number due to the Mth mode of the Nth family, respectively, and denoted as a_M and β_M when N=0, i.e. for axisymmetric modes.

Note that $r(\mathbf{x}, t)$ is also a received response produced by an excitation $s(t)$, i.e. the different guided wave modes are excited by $s(t)$. Therefore, in the frequency domain, the input excitation and the response are related through a pipe transfer function $H(\mathbf{x}, \omega)$, as expressed in the following:

$$R(\mathbf{x}, \omega) = S(\omega) H(\mathbf{x}, \omega) \quad (2)$$

where $R(\mathbf{x}, \omega)$ and $S(\omega)$ are the Fourier Transform of $r(\mathbf{x}, t)$ and $s(t)$, respectively.

3. TIME REVERSAL FOCUSING

In Time Reversal processing, we assume the waveguide is reciprocal and stationary⁷. Reciprocity ensures the same signals are received when the waves propagate backward; stationary means the results do not vary over time. Section 3.1 and 3.2 mathematically describe the Time Reversal process of guided waves in a pipe.

3.1 Time Reversal focusing of guided waves

We consider performing pitch-catch method using two in-line transducers attached on the surface a pipe, one as a transmitter and the other as a receiver, so that Eq.(2) can be simplified as¹⁷⁻¹⁹

$$R(\omega) = S(\omega) H(\omega) \quad (3)$$

The received signal is then time-reversed and energy-normalized, before travelling back through the pipe. We note that in the frequency domain, time reversal is equivalent to the negation of angular frequency ω , thus the time-reversed and energy-normalized signal becomes

$$S^{TR}(\omega) = kR(-\omega) = kS(-\omega)H(-\omega) \quad (4)$$

where k is the energy normalization term, ensuring the time reversed signal has the same energy as the original input, expressed as

$$k = \sqrt{\frac{\int_{-\infty}^{\infty} |S(\omega)|^2 d\omega}{\int_{-\infty}^{\infty} |R(\omega)|^2 d\omega}}. \quad (5)$$

When the new input signal is transmitted back through the pipe, the received signal can now be written as

$$\begin{aligned} Y(\omega) &= S^{TR}(\omega)H(\omega) \\ &= kS(-\omega)H(-\omega)H(\omega) \end{aligned} \quad (6)$$

If we assume that phase velocity $v_m(\omega)$ is even symmetric with respect to ω such that $v_m(\omega) = v_m(-\omega)$, then

$$\beta_M^N(-\omega) = \frac{-\omega}{v_m(-\omega)} = -\frac{\omega}{v_m(\omega)} = -\beta_M^N(\omega). \quad (7)$$

Therefore, we have $R(-\omega) = R^*(\omega)$. Since $S(-\omega) = S^*(\omega)$ due to the conjugate symmetric Fourier Transform of the driven signal $S(\omega)$, it results in

$$H(-\omega) = H^*(\omega) \quad (8)$$

Therefore, Eq. (6) can be rewritten as

$$\begin{aligned} Y(\omega) &= kS^*(\omega)H^*(\omega)H(\omega) \\ &= kS^*(\omega)|H(\omega)|^2 \end{aligned} \quad (9)$$

Eq. (9) shows the received signal has the same phase-profile as the conjugate or time-reversed excitation signal. This is an indication of a large reduction in dispersion and multi-modal effects after Time Reversal is applied. The guided wave modes focus at the original source at a single point in time, leading to an enhanced signal level and compensation for multiple modes and dispersion in pipe environment. As a result, we expect the time domain signal to be symmetric with a large peak at the center.

3.2 Time Reversal change focusing

The above section has shown Time Reversal leads to focusing of various guided wave modes at the original source. Here, we describe a similar Time Reversal process, but for focusing at “changes” caused by damage in a pipe. The basic idea is to obtain the response component due to the changes by background subtraction and then time-reverse and retransmit the response due to the changes through the pipe. Those changes are also focused, Time Reversal change focusing. In other words, the presence of damage can be present as a significant peak at the center of the Time Reversal focused signal.

We assume we are able to measure the response of the pipe before any damage occurs and this response is stationary over time, thus the received response due to the background “clutter” is given by¹⁸

$$R_C(\omega) = S(\omega)H_C(\omega). \quad (10)$$

$S(\omega)$ is known, and $R_C(\omega)$ can be measured, so Eq.(10) gives $H_C(\omega)$, the clutter transfer function.

When the damage is induced, the received signal becomes

$$R(\omega) = S(\omega)H(\omega) = S(\omega)(H_C(\omega) + H_T(\omega)). \quad (11)$$

where $H_T(\omega)$ is the transfer function of the “target” referring to damage or “change” in the pipe.

The response due to the “target” is the difference between the received signal and the response due to the “clutter”, therefore

$$\begin{aligned} R_T(\omega) &= R(\omega) - R_C(\omega) \\ &= S(\omega)H_T(\omega) \end{aligned} \quad (12)$$

We then time-reverse and energy-normalize the response due to the “target” or the “change” in the pipe, and obtain a new excitation which will be sent backward through the pipe. This time-reversed and energy-normalized signal can be expressed as

$$\begin{aligned} S_T^{TR}(\omega) &= kR_T(-\omega) \\ &= kS(-\omega)H_T(-\omega) \\ &= kS^*(\omega)H_T^*(\omega) \end{aligned} \quad (13)$$

where k is the energy normalization term given by Eq. (5).

When the new input signal is transmitted back in the pipe, the received signal is

$$\begin{aligned} Y(\omega) &= S_T^{TR}(\omega)H(\omega) \\ &= kS^*(\omega)H_T^*(\omega)(H_C(\omega) + H_T(\omega)) \\ &= kR_T^*(\omega)H_C(\omega) + kS^*(\omega)|H_T(\omega)|^2 \end{aligned} \quad (14)$$

After Time Reversal process, this received signal also consists of two components, the response due to the “clutter” and the response due to the “target”. The “clutter” response can be determined, since $H_C(\omega)$ is known from Eq. (10) and $R_T(\omega)$ is measured according to Eq. (12). As a result, we subtract the “clutter” component from Eq.(14) and obtain the equation of the change in the pipe as

$$\begin{aligned} Y_T(\omega) &= Y(\omega) - kR_T^*(\omega)H_C(\omega) \\ &= kS^*(\omega)|H_T(\omega)|^2 \end{aligned} \quad (15)$$

We can see Eq. (15) is similar to Eq.(9), but the focused signal is now caused by damage in the pipe. We expect to see a large peak at the center of the time domain signal as an indication of the defects' existence. Therefore, Time Reversal change focusing provides an easy-implemented metric for damage detection in a pipe, without any interpretation of wave modes as done by many conventional methods.

4. EXPERIMENTAL RESULTS

In this section, we present experimental results of Time Reversal focusing technique applied to six different laboratory scenarios. The first three subsections discuss Time Reversal focusing of guided waves in a pipe with/without welded joint, with/without internal pressure; the next three demonstrate Time Reversal change focusing for detection of three different defects: lateral, longitudinal and corrosion-like.

All the experiments were conducted on steel pipe specimens with two piezoelectric wafer transducers (Lead Zirconate Titanate, PZT 5A4E) mounted on the surface of each pipe using cyanoacrylate adhesive. One PZT transducer functioned as a transmitter and the other as a receiver, performing in pitch-catch method. A National Instruments PXI system was used to drive the transmitter and to record waveforms at the receiver. A sinc pulse was chosen as the input signal (Figure 2a), because it resulted in more modes and more dispersion (as compared to narrowband excitation), which are beneficial for Time Reversal^{12,17}. Note that all the following Time Reversal focused signals were generated mathematically using the measured received responses by Eq. (9) or (15). The scheme of the experiments is shown in Figure 1. The specifications of the experimental specimens are given in Table 1. The experimental results are summarized in Table 2 and Table 3.

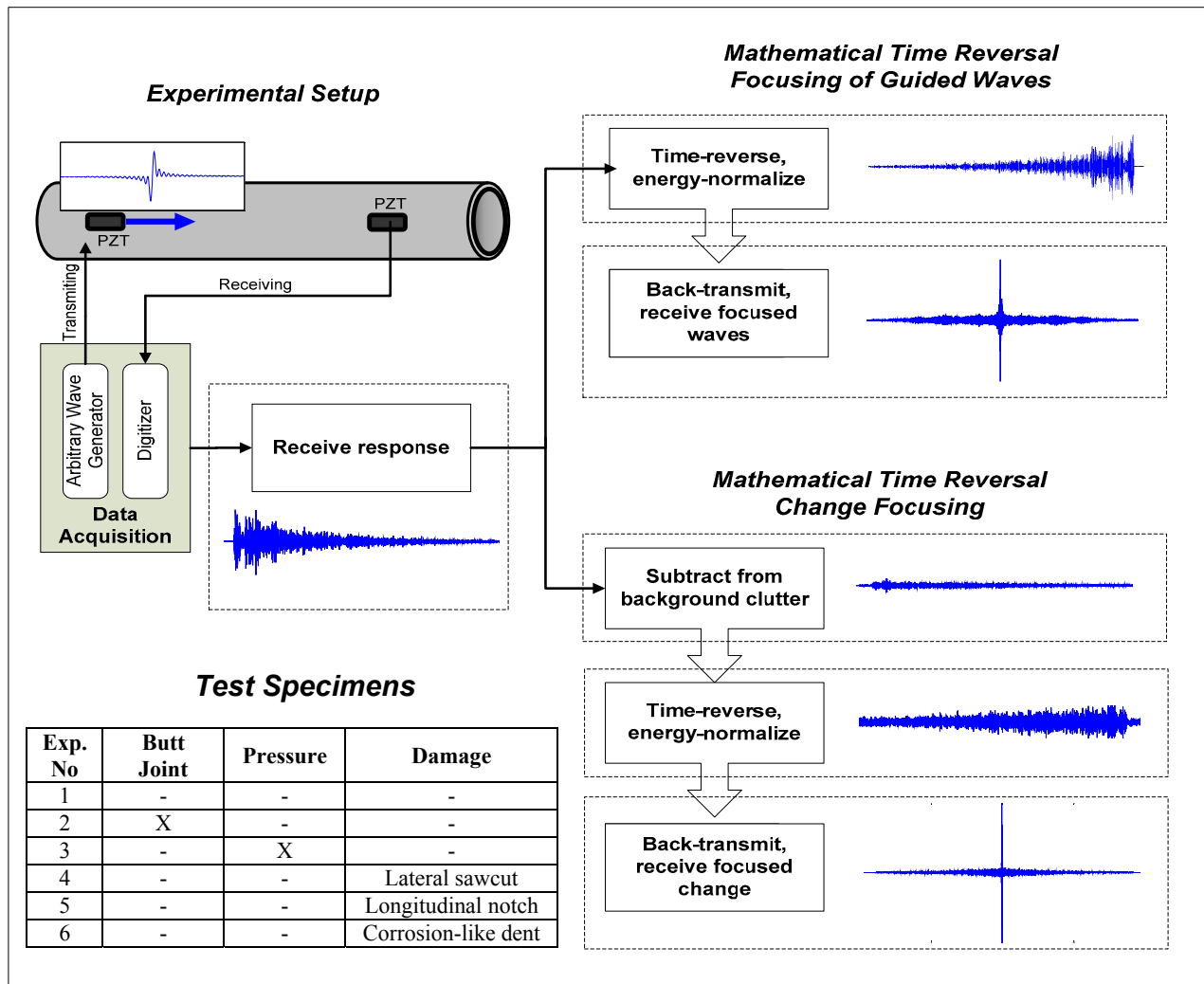


Figure 1. Scheme of the experiments.

Table 1. Specifications of the experimental specimens

Exp. No	Steel Pipe Specimens			Transducers		
	Dimensions [mm]			Specifications	Size [mm*mm]	Dist. ^c [mm]
	Length	OD ^a	WT ^b			
1	1833	70	4	-	20*8	1200
2	1833	70	4	10-mm-wide welded butt joint, 900 mm from one end of the pipe.	20*8	1200
3	1833	70	4	83.7 psi internal pressure.	20*8	1200
4	3050	60.3	3.6	Lateral sawcut: 1 mm wide, 1 mm deep and 25 mm in arc dimension, 590 mm from the transmitter.	10*5	3050
5	1730	74	5	Longitudinal defect: 220 mm long, 3 mm wide and 1 mm deep, 450 mm from the transmitter.	12*6	1000
6	1730	74	5	Corrosion-like defect: major axes 20 mm, minor axes 15 mm, 1 mm deep, 300 mm from the transmitter.	12*6	1000

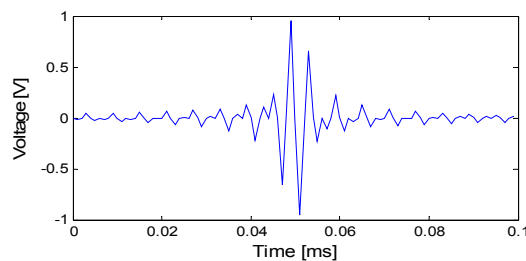
(^aOD: outside diameter; ^bWT: wall-thickness; ^cDist: distance between the transmitter and the receiver).

4.1 Guided waves focusing in a pipe

The experiment was performed on a pipe with length 1833 mm, outside diameter 70 mm and wall thickness 4 mm. Two PZT wafer transducers were located 1200 mm apart on the pipe. Each wafer was 20 mm long, and 8 mm wide.

When the transmitter is excited by a sinc pulse centered at 250 kHz shown in Figure 2a, the received response appears to contain a large amount of guided wave modes which are very complex and difficult to be separated or interpreted, as shown in Figure 2b. However, after performing the Time Reversal focusing process, different wave modes are compressed, presenting as a large peak at the center of the plot shown in Figure 2c. This peak is formed as a consequence of focusing wave modes as explained by Eq.(9). Moreover, we can see a significant increase in the maximum amplitude of the received signal, from 41.0 mV to 103.9 mV, an 8.1 dB increase after Time Reversal is applied.

The following experiments will discuss the effectiveness of Time Reversal focusing technique in some more complicated scenarios rather than in the seamless, non-pressurized and undamaged pipe that we used for this experiment.



(a)

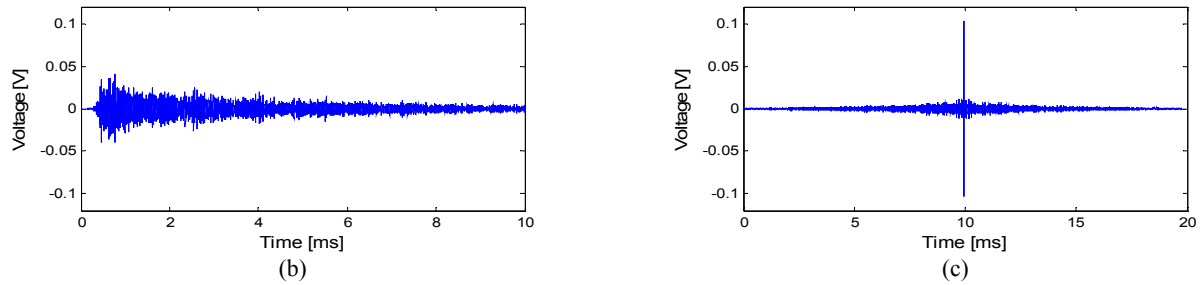


Figure 2. (a) 250 kHz sinc pulse excitation, (b) received signal, and (c) Time Reversal focused signal.

4.2 Pipe with a welded butt joint

The pipe specimen was nominally identical as the one we used in the previous experiment, but with a 10-mm-wide welded butt joint located 900 mm from one end of the pipe. The size and location of the two PZTs as well as the excitation signal, a 250 kHz sinc pulse shown in Figure 2a, were the same as with the jointless pipe.

We can see from Figure 3 a 6.2 dB increase in the maximum received amplitude, from 18.2 mV to 37.2 mV, after Time Reversal is applied. The experimental results in Figure 2 and Figure 3 show in parallel that Time Reversal can effectively compress waves temporally and spatially in both cases, with and without a welded butt joint. However, it is noted that the maximum received amplitude in the pipe with the welded butt joint is less, by 7.1 dB, than the amplitude compared with the strength of the received signals in the jointless pipe.

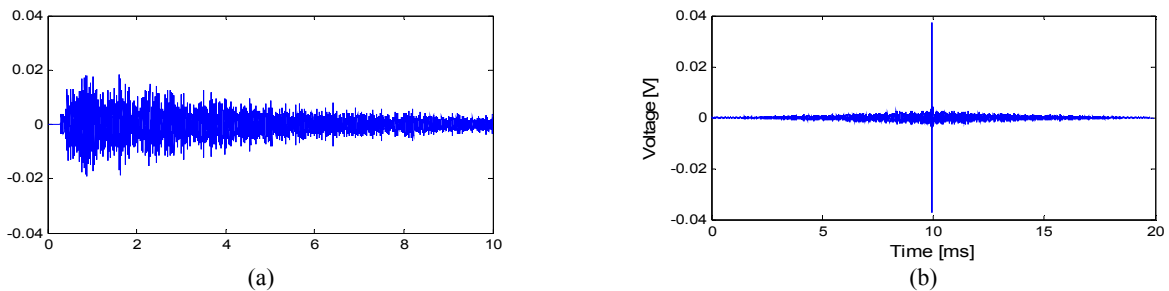


Figure 3. (a) Received signal, and (b) Time Reversal focused signal in the pipe with a welded butt joint.

We hypothesize that the welded butt joint reflects a significant portion of the ultrasonic waves, resulting in an energy loss in the pipe. To study the hypothesis we performed supplementary experiments on the pipe with a welded butt joint using a Krautkramer USPC 2100 system and angle beam/wedge transducers. Those transducers were sequentially positioned at different locations to capture guided wave behaviors along different paths in the pipe. The received signals were displayed in strip-chart format with an adjustable amplifier. To compare the strength of the signals, we fixed the maximum amplitudes at the same level and recorded the required gain (dB) of the amplifier, so that less gain indicated stronger signals. Figure 4 is a snapshot showing a received waveform in pulse-echo mode with a signal wedge transducer placed 300 mm from the welded butt joint. An evident echo is received at about 120 μ s, which is consistent with the path length 600 mm and the longitudinal wave velocity roughly 5 km/s. In pitch-catch method, Figure 5 shows a 10 dB energy loss when a welded butt joint is between two wedge transducers, compared to the received signal when the two transducers are located at different section of the pipe with no weld in between. These experimental results are consistent with the previous experiments performed with PZT wafers on two pipes, with/without a welded butt joint. We can safely conclude that welded joint causes a considerable portion of the waves to be reflected back from the weld without reaching the receiver.

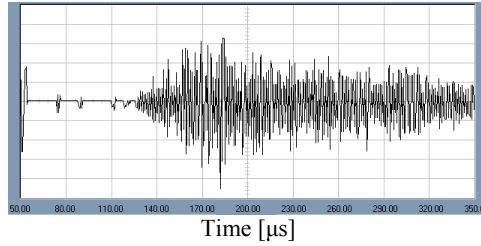


Figure 4. Pulse-echo method: reflection waves from the welded butt joint with gain 95.3 dB.

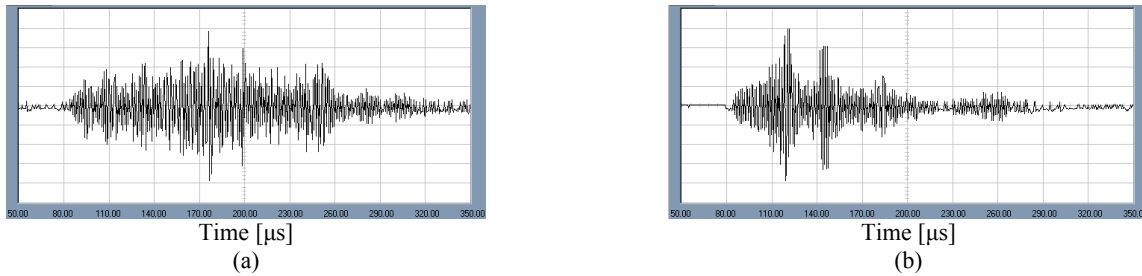


Figure 5. Pitch-catch method: received signals when (a) the joint is between the two transducers with gain 95.1 dB, and (b) no weld is in between with gain 85 dB.

Figure 4 and Figure 5 also show a pronounced waveform difference among reflection waves, transmission waves from the joint, and waves propagating without encountering the joint. The discrepancy indicates a large difference of the joint influence on different wave modes. This joint effect makes the wave modes even more difficult to be distinguished for some conventional detection methods that are based on mode selection and interpretation. However, Time Reversal provides an enhanced peak value despite the fact that the weld causes energy loss in the pipe. Moreover, the results are specific to the experimental configuration, and there exist several engineering choices to limit or overcome this effect, which is not discussed in this paper.

4.3 Pipe with internal pressure

The test specimen for this experiment has a welded-on cap and a pressure gauge at the two ends of the pipe to control the internal atmospheric pressure, with length 1833 mm, outer diameter 70 mm and wall thickness 4 mm. Two PZT wafers, sized at 20 mm x 8 mm, were mounted 1200 mm apart on the pipe. A sinc pulse centered at 250 kHz was chosen as the input signal (Figure 2a).

Similar to the experimental results in the pipe with a welded butt joint, Time Reversal presents a significant spatial and temporal focusing of guided waves in the pipe. Figure 6 shows Time Reversal amplifies the peak value of the received signal from 33.8 mV to 97.5 mV, a 9.2 dB increase, when the pipe is not pressurized. Figure 7 shows the maximum received amplitude increases from 23.2 mV to 33.7 mV, a difference of 3.3 dB, when the pipe is pressurized to 83.7 psi. It should be noted that the high air pressure inside the pipe not only affects the amplitude of the ultrasonic waves, leading to a 3.3 dB drop in the maximum received amplitude when the internal pressure is increased by 83.7 psi, but also restricts Time Reversal's ability of enhancing the peak level, jumping down to a 3.3 dB increase from a 9.2 dB augment.

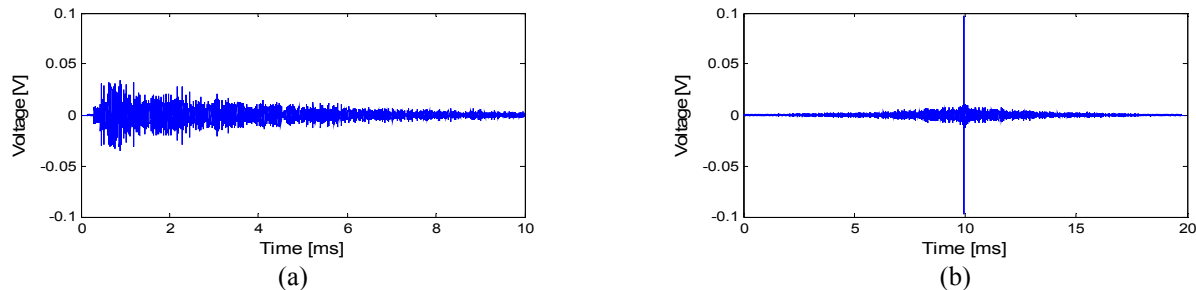


Figure 6. (a) Received signal, and (b) Time Reversal focused signal with 0 psi internal pressure.

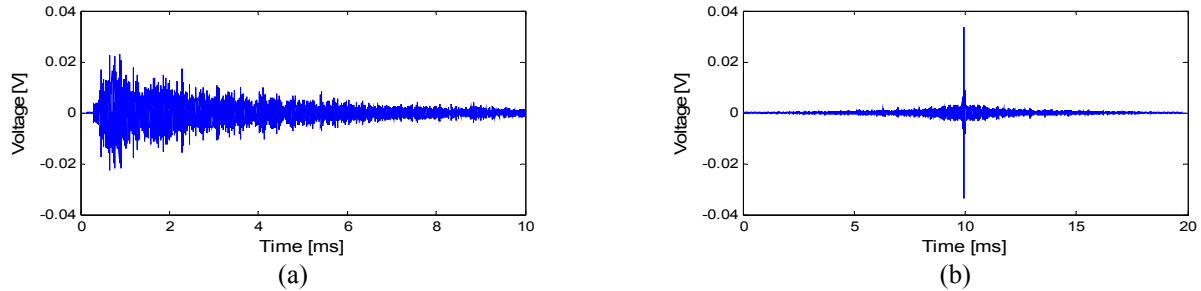


Figure 7. (a) Received signal, and (b) Time Reversal focused signal with 83.7 psi internal pressure.

4.4 Pipe with a lateral defect

This experiment was performed on a pipe specimen with length 3050 mm, outside diameter 60.3 mm and wall thickness 3.6 mm. A PZT wafer transmitter and receiver pair was mounted at the two ends of the pipe. Each wafer was 10 mm long and 5 mm wide. The transmitter was excited by a 200 kHz sinc pulse. We induced a small and partial-thickness sawcut at the lateral direction, 1 mm wide, 1 mm deep and 25 mm in arc dimension, 590 mm from one end of the pipe.

Figure 8(a)-(c) shows the received signals before and after the lateral cut was created; Figure 8(d) and (e) gives the changes of the responses after background subtraction. Those changes are very weak and indistinguishable. However, by performing Time Reversal change focusing on Figure 8(d) and (e), we obtain a very significant difference between these two cases, with and without the lateral defect present. As shown in Figure 9, the peak level of the change focused signal increases from 0.0037 mV to 0.1243 mV, a difference of nearly 34 times or 30.6 dB. The noticeable peak shown in Figure 9b is produced as an outcome of illuminating the change in the pipe specimen due to the sawcut. The result shows that Time Reversal change focusing is effective at identifying defects in the lateral direction of a pipe.

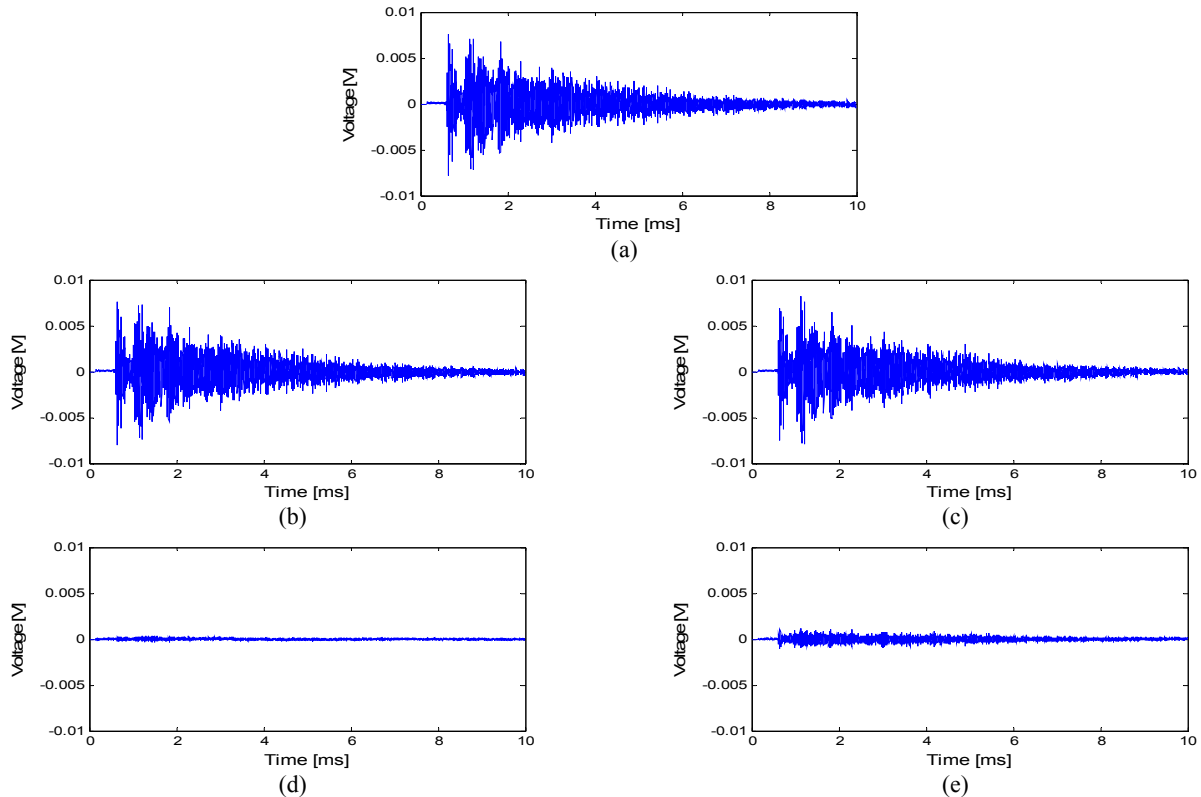


Figure 8. (a) Background clutter, (b) received signal before a lateral defect is induced, (c) received signal after a lateral defect is induced, (d) difference of (a) and (b), and (e) difference of (a) and (c).

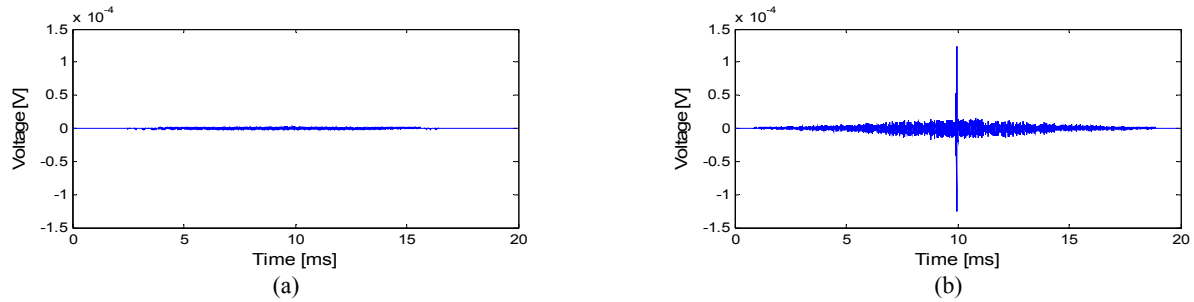


Figure 9. Time Reversal change focusing (a) before and (b) after a lateral defect is induced.

4.5 Pipe with a longitudinal defect

This experiment was conducted on a pipe specimen with length 1730 mm, outside diameter 74 mm and wall thickness 5 mm. A pair of PZT wafer transmitter and receiver was mounted 1000 mm apart on the pipe. Each wafer was 12 mm long and 6 mm wide. The input signal at the transmitter was a 200 kHz sinc pulse. A longitudinal notch, 220 mm long, 3 mm wide and 1 mm deep, was grinded into the pipe 450 mm from the transmitter.

After Time Reversal change focusing is applied, an evident peak is observed at the center of the plot shown in Figure 10b, as an indication of the change in the pipe caused by the longitudinal defect. The increase of the maximum amplitude is nearly 192 times or 45.7 dB, from 0.0146 mV to 2.8 mV (see Figure 10). The result shows that Time Reversal change focusing can effectively recognize defects in the longitudinal direction of a pipe. This observation is consistent with our expectation of scattering of pipe waves by such longitudinal defects.

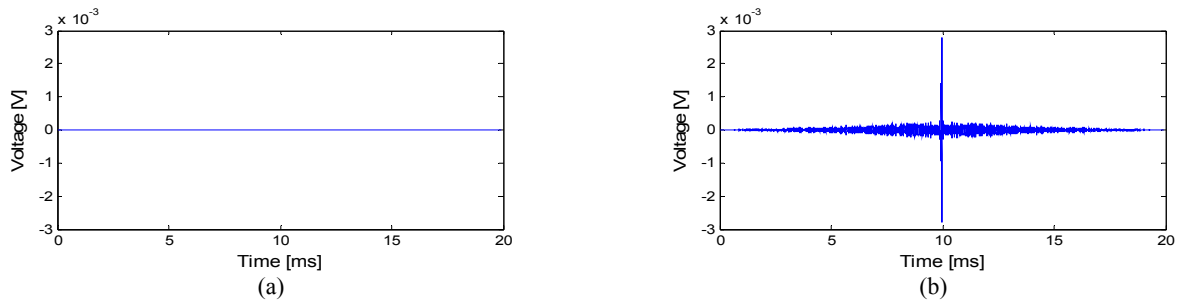


Figure 10. Time Reversal change focusing (a) before and (b) after a longitudinal defect is induced.

4.6 Pipe with a corrosion-like defect

A similar experiment was performed on a specimen with length 1730 mm, outside diameter 74 mm and wall thickness 5 mm, except for a corrosion-like defect over a small area on the surface of the pipe. The dent was 1 mm deep, with major axes 20 mm and minor axes 15 mm. A PZT wafer transmitter and a receiver were mounted 1000 mm apart on the pipe, 12 mm in length and 6 mm in width. The distance between the dent and the PZT transmitter was 300 mm. A sinc pulse center at 200 kHz was chosen as the excitation signal.

Figure 11 shows that Time Reversal change focusing can illuminate the corrosion-like defect by presenting a distinguishable peak in the received signal. The amplitude of the peak is about 14 times or 23.1 dB higher than the one before the dent is created, from 0.0425 mV to 0.6093 mV. Therefore, Time Reversal change focusing is also effective at identifying small corrosion-like defects in a pipe. This observation is consistent with our expectation of scattering of pipe waves by such corrosion-like defects.

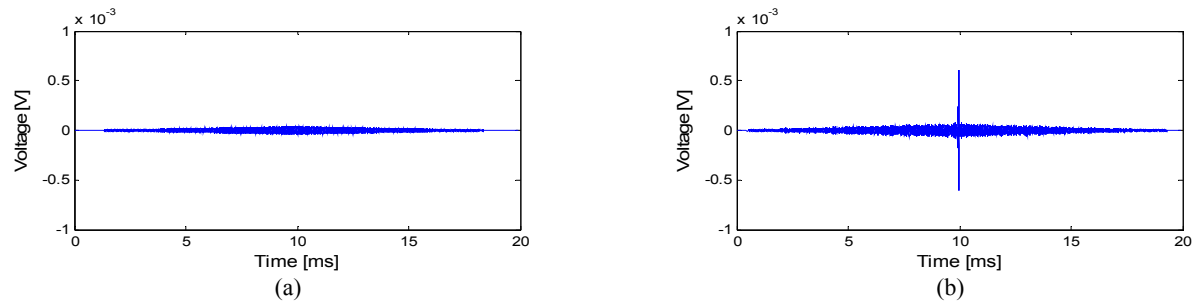


Figure 11. Time Reversal change focusing (a) before and (b) after a corrosion-like defect is induced.

Table 2. Experimental results of Time Reversal focusing of guided waves.

Exp. No	Pipe	Peak Level			Plots
		Received Signal	Time Reversal Focused Signal	Difference	
1	Simple pipe	41.0 mV	103.9 mV	8.1 dB	Figure 2
2	Pipe with welded butt joint	18.2 mV	37.2 mV	6.2 dB	Figure 3
3	Simple pipe with internal pressure	23.2 mV	33.7 mV	3.3 dB	Figure 7

Table 3. Experimental results of Time Reversal change focusing.

Exp. No	Defect Type	Peak Level after Time Reversal Change Focusing			Plots
		Before Defect Induced	After Defect Induced	Difference	
4	Lateral	0.0037 mV	0.1243 mV	30.6 dB	Figure 9
5	Longitudinal	0.0146 mV	2.8 mV	45.7 dB	Figure 10
6	Corrosion-like	0.0425 mV	0.6093 mV	23.1 dB	Figure 11

5. CONCLUSIONS

Time Reversal focusing has been shown to compensate for multiple modes and dispersion in pipe environment, resulting in an enhanced signal-to-noise ratio and effective change detection by presenting a distinguishable peak. This technique has been effectively demonstrated in six laboratory circumstances, providing with comprehensive and promising results on guided wave focusing in a pipe with/without welded joint, with/without internal pressure, and detection of three different defects: lateral, longitudinal and corrosion-like. The focusing feature allows Time Reversal to benefit long-distance and low-power pipeline monitoring, and also shows enormous prospective for Structural Health Monitoring and Nondestructive Evaluation applications in other infrastructures. It is noted that Time Reversal change focusing leads to different amplification factors of the received peak levels among various types of defects with different sizes. This phenomenon reflects Time Reversal's potential as a metric for evaluating the magnitude of damage in the pipe, which is envisioned as a part of our future work. Another challenging research topic would be how to distinguish and classify "changes" caused by different damage types as well as some operational and environmental variations.

ACKNOWLEDGMENTS

National Energy Technology Laboratory (NETL) is the funding source for this effort with Cost Share being provided by Carnegie Mellon University (CMU). Concurrent Technologies Corporation (CTC) is funded under a cooperative agreement with NETL. CMU is funded under a Subcontract Agreement with CTC. Joel Harley and Nicholas O'Donoghue are supported by National Defense Science and Engineering Graduate Fellowships, sponsored by the Office of Naval Research and the Army Research Office, respectively.

REFERENCES

- [1] Demma, A., Cawley, P., Lowe, M., and Roosenbrand, A.G., "The reflection of the fundamental torsional mode from cracks and notches in pipes," *The Journal of the Acoustical Society of America* 114 (2), 611-625 (2003).
- [2] Lowe, M.J.S., Alleyne, D.N., and Cawley, P., "Defect detection in pipes using guided waves," *Ultrasonics* 36(1-5), 147-154 (1998).
- [3] Rose, J.L., [Ultrasonic Waves in Solid Media], Cambridge University Press, Cambridge, (1999).
- [4] Shull, P.J., [Nondestructive evaluation: theory, techniques, and applications], Marcel Dekker, Inc., New York, (2002).
- [5] Cawley, P., "Practical Long Range Guided Wave Inspection—Managing Complexity," in *AIP Conference Proceedings* 657, 22-40 (2003).
- [6] Lowe, M.J.S., and Cawley, P., "Long Range Guided Wave Inspection Usage—Current Commercial Capabilities and Research Directions." Department of Mechanical Engineering, Imperial College London, London, (2006).
- [7] Fink, M., "Time reversal of ultrasonic fields—Part I: Basic principles," *IEEE Trans. Ultrason. Ferroelectr. Freq. Control* 39(5), 555-566 (1992).
- [8] Prada, C., and Fink, M., "Separation of interfering acoustic scattered signals using the invariants of the time-reversal operator. Application to Lamb waves characterization," *The Journal of the Acoustical Society of America* 104, 801-807 (1998).
- [9] Ing, R.K., and Fink, M., "Time-reversed Lamb waves," *IEEE Transactions on Ultrasonics, Ferroelectrics, and Frequency Control* 45(4), 1032-1043 (1998).
- [10] Sohn, H., Park, H.W., Law, K.H., and Farrar, C.R., "Damage Detection in Composite Plates by Using an Enhanced Time Reversal Method," *Journal of Aerospace Engineering* 20(3), 141-151 (2007).
- [11] Park, H.W., Sohn, H., Law, K.H., and Farrar, C.R., "Time reversal active sensing for health monitoring of a composite plate," *Journal of Sound and Vibration* 302(1-2), 50-66 (2007).
- [12] Nunez, I., and Negreira, C., "Efficiency parameters in time reversal acoustics: Applications to dispersive media and multimode wave propagation," *The Journal of the Acoustical Society of America* 117(3), 1202-1209 (2005).
- [13] Moura, J.M.F., and Jin, Y., "Detection by time reversal: single antenna," *IEEE Transactions on Signal processing* 55(1), 187-201(2007).
- [14] Jin, Y., and Moura, J.M.F., "Time-Reversal Detection Using Antenna Arrays," *IEEE Transactions on Signal Processing* 57(4), 1396-1414 (2009).
- [15] Li, J., and Rose, J.L., "Excitation and propagation of non-axisymmetric guided waves in a hollow cylinder," *The Journal of the Acoustical Society of America* 109, 457-464 (2001).
- [16] Seco, F., Martín, J.M., Jiménez, A., Pons, J.L., Calderón, L., and Ceres, R., "PCDISP: a tool for the simulation of wave propagation in cylindrical waveguides," in *Proceedings of the 9th International Congress on Sound and Vibration*, 23-29(2002).
- [17] O'Donoghue, N., Harley, J., Moura, J.M.F., Jin, Y., Oppenheim, I.J., Ying, Y., States, J., Garrett, J.H., and Soibelman, L., "Single Antenna Time Reversal of Guided Waves in Pipelines," in *Proceedings of Meetings on Acoustics* 6(1), 065001-11 (2009).
- [18] Harley, J., O'Donoghue, N., States, J., Ying, Y., Garrett, J.H., Jin, Y., Moura, J.M.F., Oppenheim, I.J., and Soibelman, L., "Focusing of Ultrasonic Waves in Cylindrical Shells using Time Reversal," in *Proceedings of the 7th International Workshop on Structural Health Monitoring*, (2009).
- [19] Prada, C., Manneville, S., Spoliansky, D., and Fink, M., "Decomposition of the time reversal operator: Detection and selective focusing on two scatterers," *The Journal of the Acoustical Society of America* 99(4), 2067-2076 (1996).

National Energy Technology Laboratory

626 Cochran Mill Road
P. O. Box 10940
Pittsburgh, PA 15236-0940

3610 Collins Ferry Road
P. O. Box 880
Morgantown, WV 26507-0880

13131 Dairy Ashford, Suite 225
Sugarland, TX 77478

1450 Queen Avenue S
Albany, GA 31707-2198

2175 University Ave. South
Suite 201
Fairbanks, AK 99709

Visit the ETL website at:
www.netl.doe.gov

Customer Service:
1-800-553-7681

